INVESTIGATIONS OF THE COMPOSITION-FUNCTION RELATIONSHIPS IN NORMAL, DEGRADED, AND ENGINEERED ARTICULAR CARTILAGE USING EPIC-MICROCOMPUTED TOMOGRAPHY

A Dissertation
Presented to
The Academic Faculty

by

Ashley Wells Palmer

In Partial Fulfillment
of the Requirements for the Degree
Doctor of Philosophy in the
School of Mechanical Engineering

Georgia Institute of Technology

May 2007

INVESTIGATIONS OF THE COMPOSITION-FUNCTION RELATIONSHIPS IN NORMAL, DEGRADED, AND ENGINEERED ARTICULAR CARTILAGE USING EPIC-MICROCOMPUTED TOMOGRAPHY

Approved by:

Dr. Marc E. Levenston, Advisor
School of Mechanical Engineering
Georgia Institute of Technology

Dr. Robert L. Sah
Department of Bioengineering
University of California, San Diego

Dr. Ravi V. Bellamkonda
Department of Biomedical Engineering
Georgia Institute of Technology

Dr. Raymond P. Vito
School of Mechanical Engineering
Georgia Institute of Technology

Dr. Robert E. Guldberg
School of Mechanical Engineering
Georgia Institute of Technology

Date Approved: February 20, 2007

ACKNOWLEDGEMENTS

While a PhD is an individual effort in its purest form, I know that the quality of my work, my sanity, and my physical well being would have suffered were it not for the unwavering support and assistance of those around me. Some of these contributions were more direct than others just as some were more sustained. Nevertheless, they all played a role in the completion of this work and I wish to acknowledge my appreciation here.

One of the most significant figures in this journey has been my PhD advisor, Marc Levenston. Marc helped convince me to leave the cushy world of industry to join his lab at Georgia Tech. The experience was invaluable, both for the intellectual and personal development it provided, and Marc played a key part in that growth. Marc provided me with the intellectual freedom to stumble, rebound, stumble again, and eventually develop competency as a researcher. Though this process often frustrated me, I feel it ultimately resulted in a more challenging and productive environment and taught me important lessons about myself for which I will always be indebted to Marc.

I also wish to thank the members of my PhD dissertation committee: Drs. Ravi Bellamkonda, Robert Guldberg, Robert Sah, and Raymond Vito. Despite demanding schedules, each made time for quick and informal research updates and offered balanced and objective debate. In particular, I would like to recognize Bob Guldberg for his patience and support throughout the EPIC-μCT studies, and Bob Sah and his laboratory at the University of California San Diego for their assistance with the strain study in Chapter 5. Additionally, I would also like to acknowledge funding support provided by Roche Palo-Alto, the Arthritis Foundation, the NIH, the Georgia Tech/Emory Center for

the Engineering of Living Tissues (GTEC) as part of the National Science Foundation ERC Program, and the NSF-sponsored TI:GER IGERT program via a graduate fellowship.

The administrative and support staff at Georgia Tech made my experience at the Institute undoubtedly more productive and efficient. In my work with the GTEC Education and Outreach committee, Shawna Young-Garcia and Sally Gerrish were a constant source of support and always pitched in to ensure our projects were a success. Johnafel Crowe displayed endless patience in instructing me on the use of the confocal microscope, and Tracey Couse and Sha'Aqua Asberry were both excellent resources in experimenting with different histology techniques and processing. I would also like to thank John Graham of the ME machine shop for his help with the design and manufacturing of CT sample tubes and the microindentation device of Appendix A. Kyle French of the ME electronics lab was also instrumental in the design and construction of circuitry for the load cell in the microindentation device.

At Georgia Tech, I was fortunate to be surrounded not only by a brilliant group of researchers but also by a fun group of individuals. My elders in the Levenston lab, particularly Stacy Imler, Janna Mouw, and Eric Vanderploeg, were a wealth of knowledge and fun. Stacy was a constant source of energy and spontaneity and always kept a smile on her face, even while teaching me sterile culture technique for the millionth time. Janna Kay and I quickly discovered that we share competing personalities but eventually learned that "two alpha females can coexist" and develop a great friendship. I had the opportunity to know Eric as a teacher, as a researcher, as an office mate, and as a friend and have met no one that equals his kindness and intelligence. After

the elders, Onyinyechi Irrechukwu and I were the next pairing. Onyi was always there to bring a lighter side to the lab, keeping us entertained with her endless A capella performances and stories of her escapades with European men. John Connelly (JC), Chris Wilson (CW, pronounced "C Dub"), and I formed the trifecta in the lab. JC and CW had the unfortunate pleasure of sitting next to me for the majority of their time at Tech. Whether we were touring Europe together, living it up at the Northside Tavern, going for All-Conference at ORS, or just hanging out in Atlanta, their presence made every experience, as they would say, "wicked awesome." I look forward to regular reunions with the boys and will treasure their friendship always. My time with Sarah West and James Nishimuta, though short lived, was also a lot of fun.

One of the greatest strengths of Georgia Tech's program is the interaction of students in different labs. There was no better example than in Wing 2D. In particular, I would like to single out Galen "G-Rob" Robertson, Chris Gemmiti, Megan Oest, Srinidhi Nagaraja, Angela Lin, Blaise Porter, and Craig Duvall. You all made my time inside the lab, outside the lab, and in the air an absolute blast. Outside the wing, I also enjoyed many Halloweens and great house parties with the crew of 1510 (Adam Higgins, Chris Lessing, Matt Rhyner, and John Wilson) and the fabulous ladies that kept them in line (Nimisha Gupta, Hillary Irons, Mary Millner, Sarah Stabenfeldt). Though he had published in Nature while most of us were still in graduate school diapers, Bryan Marshall may be remembered most for introducing me to the delicacy of easy cheese and cheese puffs. In short, I cannot (and probably should not) say enough about these individuals.

Outside of Georgia Tech, I was blessed with a network of friends who helped remind me there were people smart enough to avoid engineering and graduate school all together. One of my greatest joys in Atlanta was playing tennis through ALTA, the Atlanta Lawn Tennis Association. I was introduced to ALTA by Bridget Szymanski, who I met through our mutual friend Srin. During many hours on the courts and over a few pints of cider and pizza at Fellini's, Bridget and I became best friends. Even after she left Atlanta for bigger and better things, Bridget remained a constant source of support, sending cards and care packages when I needed them most. I hope I can be as good of a friend to her as she has been to me. Joining a mixed doubles team was one of the best decisions I made while in Atlanta. There, I met an amazing group of people, including David Carico, Drew Seibert, Jorge Fuenzalida, Anthony Russo, Chris Herrin, Christine Falluco, Kim Morgan, Karin Krug, and Sandy Strippoli. They are not only fabulous tennis players but also some of the kindest people I know. Through tennis, I also met Will Thistle. Will taught me a lot about myself and life's simplicities, and I will always cherish the many good times we shared together. The move to Atlanta also allowed me to reconnect with Grace Prakalapakorn, a fellow Dukie and Chi Omega. Though our schedules limited our visits, Grace was always up for a quick dinner, a movie, and endless girl talk. I will miss the good times with all of you!

Finally, I would like to thank my family for their unwavering support. My mom Marjorie and my paternal grandmother Nannie instilled in me at an early age the importance of education. In many ways, this achievement is as much theirs as it is mine. While my father Ken was not able to see me finish college or graduate school, his zest for life provided me with an appropriate perspective on work and school and helped me

maintain balance in my life. I would also like to thank my cousin Ron for his friendship and unbridled advice over the years. I love you all and am blessed to have you in my life.

TABLE OF CONTENTS

LIST OF TABLES

LIST OF FIGURES

LIST OF ABBREVIATIONS

2D	Two Dimensional
3D	Three Dimensional
AC	Articular Chondrocytes
ANOVA	Analysis of Variance
dGEMRIC	Delayed Gadolinium-Enhanced MRI of Cartilage
DMEM	Dulbecco's Modified Eagle's Medium
DMMB	Dimethylmethylene Blue
ECM	Extracellular Matrix
EPIC-μCT	Equilibrium Partitioning of an Ionic Contrast Agent-μCT
FCD	Fixed Charge Density
FT-IRIS	Fourier Transform-Infrared Imaging Spectroscopy
IL-1	Interleukin-1
MFC	Meniscal Fibrochondrocytes
MMP	Matrix Metalloproteinase
MRI	Magnetic Resonance Imaging
PG	Proteoglycan
OA	Osteoarthritis
OCT	Optical Coherence Tomography
PBS	Phosphate Buffered Saline
sGAG	Sulfated Glycosaminoglycan
TGF-β	Transforming Growth Factor-Beta
μCT	Microcomputed Tomography

LIST OF SYMBOLS

E_{equil}	Equilibrium Modulus in Unconfined Compression
$\|E^*_{dyn}\|$	Dynamic Modulus in Unconfined Compression
$\|G^*_{dyn}\|$	Dynamic Shear Modulus

SUMMARY

Articular cartilage provides a low-friction surface during normal joint motion and distributes forces to the underlying bone. The extracellular matrix composition (ECM) of healthy cartilage has previously been shown to be an excellent predictor of its mechanical properties. Changes in ECM composition and loss of mechanical function are known to occur with degenerative conditions such as osteoarthritis. Identifying differences in the composition-function relationships of articular cartilage under different anabolic, catabolic, and homeostatic conditions may therefore be a useful approach for identifying factors (e.g. ECM content, distribution, and structure) which are critical to mechanical function. In addition, diagnostic tools capable of monitoring changes in the articular cartilage ECM may increase our understanding of the effects of ECM changes on composition-functions relationships.

The goals of this work were to investigate composition-function relationships in healthy, degraded, and engineered articular cartilage and to develop a μCT-based approach to analyze changes in matrix composition and morphology in articular cartilage. In healthy cartilage explants, compressive and shear properties were dependent on both sGAG and collagen content. In contrast, the compressive properties of IL-1-stimulated cartilage were dependent on sGAG but not collagen content. To assess changes in sGAG content, EPIC-μCT, a 3D contrast-enhanced microcomputed tomography technique was developed. EPIC-μCT attenuation was found to be an excellent predictor of sGAG content in IL-1-stimulated cartilage explants and engineered cartilage. In addition, analytical approaches were developed to use EPIC-μCT for the *in situ* analysis of

cartilage morphology. EPIC-μCT was also used to analyze spatial differences in sGAG accumulation in bilayer engineered cartilage for comparison with the local strain profile. This work underscores the significance of ECM composition and structure in regulating cartilage mechanical properties and validates the use of EPIC-μCT as a diagnostic for monitoring sGAG content and potentially for assessing mechanical function in models of degeneration and regeneration.

CHAPTER 1

INTRODUCTION

1.1 Motivation

Diarthroidal joints experience a complex combination of motion and mechanical forces during normal activity. The role of articular cartilage is to provide a low-friction surface during motion and to distribute forces to the underlying bone. The unique function of articular cartilage, in particular, is closely linked to its extracellular matrix (ECM) composition and organization[1]. Proteoglycans (PGs), collagen, and interstitial water within the ECM are regarded as the major regulators of articular cartilage mechanical function, with an osmotic swelling pressure generated by PG and water interactions and balanced by the collagen network providing resistance to applied loads. Supporting the role of the ECM in cartilage function, strong relationships have been reported between mechanical stiffness and proteoglycan and collagen content in healthy human articular cartilage[2,3]. Alterations in ECM composition and mechanical loading occur during development, in response to physical trauma, and during degenerative conditions including osteoarthritis (OA)[4-9]. Thus, the ability to noninvasively monitor changes in cartilage matrix composition, which may be reflective of changes in cartilage mechanical properties, could provide an alternate means of assessing function. Microcomputed tomography (μCT), a three-dimensional (3D) X-ray imaging technique, offers micron-level resolution, *in vivo* monitoring potential, and versatile spatial and morphological analysis but has seen little application in soft tissues due to their poor radiopacity. The development of a μCT-based approach for the monitoring of changes in

cartilage matrix composition would be useful both as a clinical diagnostic and as a research tool for improving our understanding of composition-function relationships in healthy, degraded, and engineered cartilage tissues.

1.2 Research Objectives

The overall goals of this work were to investigate composition-function relationships in healthy, degraded, and engineered articular cartilage and to develop a μCT-based approach to analyze changes in matrix composition and morphology in articular cartilage. Characterization of composition-function relationships in healthy, degraded, and engineered cartilage was of interest to identify any fundamental differences in the response of articular cartilage due to its local ECM composition. The development of a μCT-based approach for the analysis of cartilage ECM composition and morphology was designed to complement the composition-function investigations and to investigate its use as a surrogate for direct biochemical and mechanical assessment. Common to both pursuits was the goal of increasing our understanding and assessment of composition-function relationships in articular cartilage. Three specific aims were designed to investigate the research objectives, using both a model of cartilage degeneration and tissue engineering strategies.

SPECIFIC AIM I: Characterize the composition-function relationships of healthy and degraded articular cartilage using interleukin-1 (IL-1) stimulation to induce cell-mediated degradation.

To investigate the composition-function relationships of healthy and degraded articular cartilage, articular cartilage explants were cultured in either control or IL-1-

supplemented media for up to 32 days. At regular intervals, matrix composition and mechanical properties of both treatments were characterized. Sulfated glycosaminoglycan (sGAG) and collagen contents in both the media and explants were assessed by biochemical assays. The complex shear modulus and the equilibrium and dynamic unconfined compression moduli were measured by mechanical testing at corresponding time points. Correlation and linear regression analyses were performed to determine relationships among ECM components, among mechanical properties, and between ECM components and mechanical properties.

HYPOTHESIS I: IL-1-stimulated degradation of articular cartilage will alter the composition-function relationships reported for healthy articular cartilage. Specifically, composition-function relationships in degraded articular cartilage will be more dependent on sGAG content than in healthy articular cartilage.

SPECIFIC AIM II: Develop and validate a μCT-based technique for the imaging of ECM composition and morphology in articular cartilage.

The approach taken in developing the μCT imaging technique was to use an ionic contrast agent to increase the radiopacity of the cartilage matrix while exploiting the interaction with the negative fixed charge density (FCD) primarily associated with the sGAGs attached to PGs within the ECM. With its reliance on the **E**quilibrium **P**artitioning of an **I**onic **C**ontrast agent to relate differences in FCD, the technique was dubbed EPIC-μCT. Initial work focused on the selection of a contrast agent with a high X-ray attenuation signal and an osmolality similar to that of cartilage, as well as

characterization of the time needed to reach chemical equilibrium within cartilage explants. Subsequent studies examined the relationship between EPIC-μCT X-ray attenuation and sGAG content in control and IL-1-stimulated cartilage explants. Additional studies developed approaches to isolating cartilage from surrounding tissues *in situ* in an intact rabbit joint.

HYPOTHESIS II: The X-ray attenuation of articular cartilage equilibrated in a negatively-charged, radiopaque contrast agent will be inversely correlated with its sGAG content, providing a nondestructive and accurate predictor of sGAG content.

SPECIFIC AIM III: Explore the use of EPIC-μCT in monitoring sGAG accumulation in tissue engineered constructs and characterize the composition-function relationships of tissue engineered constructs.

Two studies were conducted using 3% agarose gels seeded with either articular chondrocytes (AC) or a co-culture of AC and meniscal fibrochondrocytes (MFC). The first study examined the effects of the EPIC-μCT protocol (e.g. contrast agent exposure, X-ray scanning, both) on matrix composition, proliferation, and cell viability at regular intervals during development in longitudinally-monitored constructs. A second study was conducted to monitor the temporal and spatial development of a bilayer agarose construct using both EPIC-μCT and two-dimensional (2D) strain microscopy (in collaboration with Dr. Robert Sah's lab at UCSD).

HYPOTHESIS IIIa: Repeated application of the EPIC-μCT protocol will not negatively affect cell viability or sGAG production in tissue engineered cartilage constructs and will be sensitive enough to quantify sGAG accumulation during construct development.

HYPOTHESIS IIIb: EPIC-μCT will be sensitive to spatial patterns of sGAG accumulation in constructs and a strong indicator of the mechanical properties in tissue-engineered constructs.

1.3 Significance and Contribution

The studies performed reveal differences in composition-function relationships in healthy, degraded, and engineered articular cartilage and validate EPIC-μCT as a novel, noninvasive 3D imaging technique for the assessment of articular cartilage composition and morphology. The use of IL-1 to stimulate degradation in cartilage explants provided insights into the altered composition-function relationships that occur during degenerative conditions. This information may be useful in developing interventional strategies aimed at reversing or halting degradation *in vivo*. The development of EPIC-μCT represents a promising contribution to the area of cartilage diagnostics. The technique's ability to accurately monitor changes in sGAG content in cartilage explants, intact joints, and engineered constructs illustrates its sensitivity over a wide range of sGAG contents and its ability to isolate and analyze distinct spatial regions of interest. The initial investigations into the ability of EPIC-μCT sGAG measurements to predict mechanical properties suggests the technique may be a useful surrogate to mechanical testing in assessing the function of articular cartilage. Finally, the spatial resolution of EPIC-μCT makes the technique particularly attractive for studying matrix changes in

small animal models of degeneration and regeneration, where the limited thickness of articular cartilage prohibits accurate assessment of composition and direct measurement of material properties by existing approaches.

CHAPTER 2

BACKGROUND

2.1 Articular Cartilage

2.1.1 Composition and Organization

Articular cartilage is a type of hyaline cartilage that lines the bony surfaces of diarthrodial joints (Figure 2.1). While its primary function lies in lubrication, articular cartilage also plays a role in load distribution and shock absorption. The functionality of articular cartilage arises from a complex ECM that is secreted and remodeled by entrapped chondrocytes and is characterized by a heterogeneous, zonal organization of type II collagen, proteoglycans, and water[1,10-12].

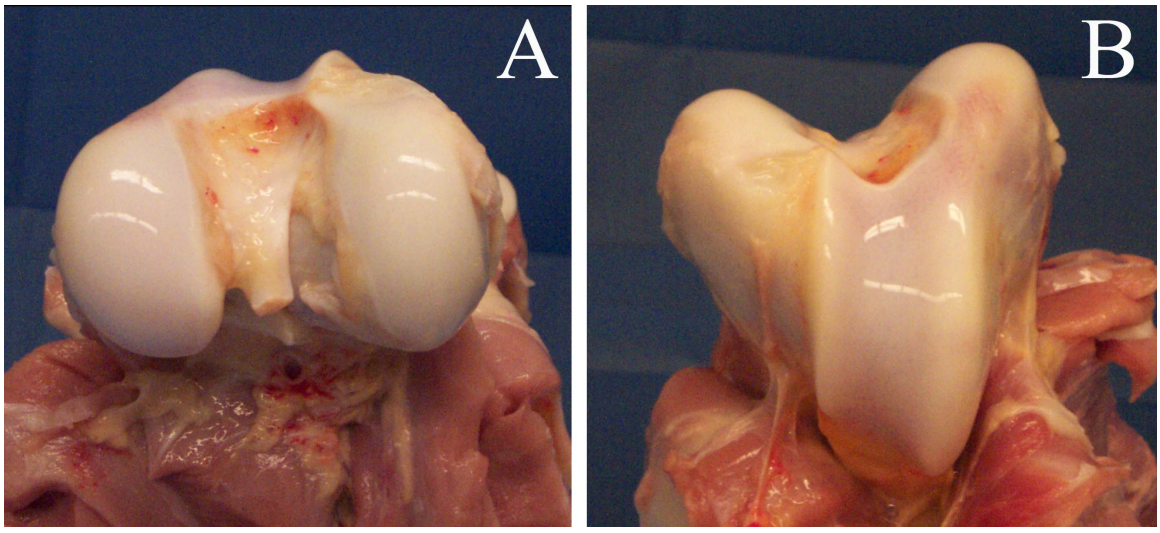

Figure 2.1: Color photographs of a dissected 1-2 week-old bovine femur. Articular cartilage is the glossy, white tissue covering the ends of the condyles (A) and femoral groove (B).

The molecular structure and organization of the matrix constituents of articular cartilage contribute to its range of properties. Type II collagen, a fibrillar protein that carries a nearly neutral charge, represents 10-20% of the wet mass and provides the primary tensile strength and tensile stiffness. PGs comprise 5-10% of articular cartilage by wet mass and consist of a varying number and type of negatively-charged sGAG chains covalently attached to a core protein. The large aggregating PG aggrecan represents 50-85% of the total PG content and has up to 50 keratin sulfate and 100 chondroitin sulfate side chains (Figure 2.2). Interactions between sGAGs and ionic interstitial fluid create an osmotic swelling pressure that is balanced by fibers in the surrounding collagen network, offering resistance to applied loading.

Cartilage is often divided into distinct zones, as the organization of collagen, PGs and water varies significantly throughout the depth of the tissue (Figure 2.3). The superficial zone (10-20% of total thickness) is characterized by the lowest PG density and flattened chondrocytes interspersed in a dense network of collagen fibers that run parallel to the articular surface. In the middle zone (40-60%), the chondrocytes have a more spherical morphology, the collagen density decreases, the PG density reaches a maximum, and the collagen fibers appear randomly oriented about a preferred 45° angle. In the deep zone (lower 30%), collagen fibers are oriented perpendicular to the subchondral bone and cell density is at its lowest. Water content is highest in the superficial zone and begins a gradual decrease with depth in the middle zone[1,12,13]. Mature tissue has been shown to exhibit a significantly higher collagen fiber and collagen crosslink density[9,14], decreased PG content[14], and smaller length sGAGs[5,15-17] than immature cartilage.

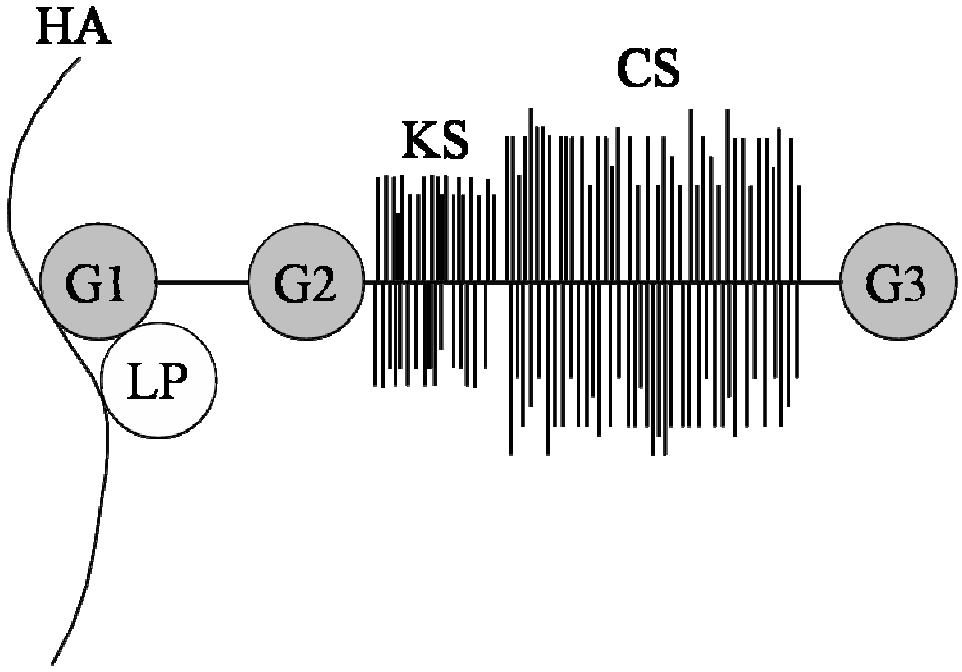

Figure 2.2: The molecular representation of the PG aggrecan, illustrating the location of keratin sulfate (KS) and chondroitin sulfate (CS) side chains relative to the three globular domains (G1, G2, G3) on the aggrecan core protein. Aggrecan associates with hyaluronic acid (HA) through the link protein (LP).

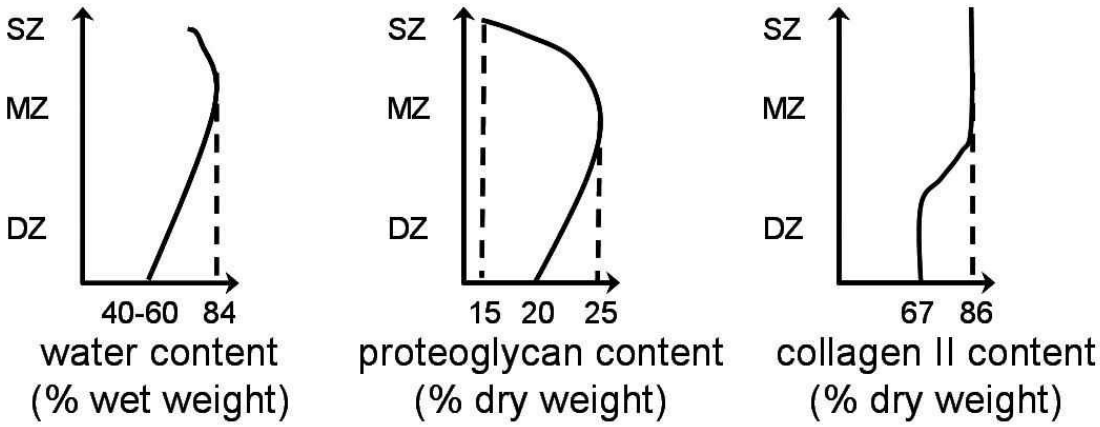

Figure 2.3: The relative distribution of ECM water, PGs, and type II collagen throughout the depth of articular cartilage (SZ=superficial zone, MZ=middle zone, DZ=deep zone). Adapted from Mow VC and Wang CC. *Clin Orthop Relat Res (367 Suppl): S204-223.*

2.1.2 Mechanical Properties

The mechanical properties of articular cartilage have been extensively characterized and have been shown to vary with species[1,3,18], loading mode[1,19,20], disease state[6,13,21], age[22-25], topographical location[18,26,27], and depth within the tissue[20,25,26,28]. Commonly reported values of tissue moduli for healthy bovine articular cartilage are presented in Table 2.1. The aggregate and unconfined compression moduli are measured by application of a compressive displacement through a rigid platen and provide an indication of the equilibrium stiffness of the tissue with or without radial confinement, respectively. As the aggregate modulus restricts lateral expansion of the collagen network, the measurement characterizes primarily the interactions of the negatively-charged PGs and interstitial fluid. By allowing lateral expansion of the collagen network, the unconfined compressive modulus evaluates the contribution of the collagen network as well as PG-fluid interactions. The dynamic compressive modulus is frequency and offset dependent, with higher loading frequencies and compressive offsets producing a stronger resistance to deformation. The shear modulus, which reflects the resistance to distortion in the absence of volumetric changes, is also offset dependent and may be measured under equilibrium or dynamic conditions.

2.1.3 Composition-Function Relationships

Additional studies have examined composition-function relationships in fetal[9,29], immature[9,29], mature[20,29], and tissue-engineered[30] cartilage under either compressive, tensile or shear loading conditions. In general, the mechanical properties of healthy bovine articular cartilage have been found to depend on both collagen and sGAG contents.

Table 2.1: Mechanical properties of bovine articular cartilage compiled from references [4,20,26]. Dynamic compression modulus is reported for 3mm diameter full thickness explants tested in unconfined compression at 10% strain and a rate of 2mm/s. Dynamic shear modulus is reported for 0.01-20Hz at 5-16% compressive strain.

Mechanical Property	MPa
Equilibrium Tensile Modulus	4-7.79
Compression Moduli	
– Aggregate (Confined)	0.47-0.89
– Unconfined	0.2-5.5
– Dynamic (magnitude)	5.0-16.0
Dynamic Shear Modulus (magnitude)	0.2-2.5

2.2 Articular Cartilage Pathology

2.2.1 Osteoarthritis

OA generally refers to a set or subset of clinical symptoms associated with the degeneration of articular cartilage, including patient pain, joint space narrowing by conventional X-ray or MRI, and joint instability. Pathologically, OA is characterized by loss of PGs, fibrillation and fissuring of the articular surface, decreases in modulus and ultimate tensile strength and elevated levels of matrix-degrading enzymes including aggrecanases and matrix metalloproteinases (MMPs)[1,4,13,31]. The precise etiology of OA is poorly understood but its incidence is increased with aging and it may be accelerated by mechanical trauma. The problem is compounded by the poor repair capacity of mature articular cartilage. Current OA treatments are focused on preserving existing cartilage function and managing patient pain. Clinical interventions include drug treatments to inhibit matrix enzyme activity, osteochondral transplantation, debridement, and in

extreme cases, total joint replacement. These treatments are met with varied success, suggesting that a better understanding of cartilage biology and OA development is needed to improve patient outcomes.

2.2.2 Aging

In addition to the reduced capacity for self-repair that accompanies tissue maturation, a number of changes occur in the ECM composition and organization of cartilage. The accumulation of non-enzymatic glycation products with age has been shown to increase collagen network stiffness, potentially making it more brittle and susceptible to fatigue-induced damage[32]. In addition, changes in the sulfation patterns of sGAGs have been reported[15], which may alter the osmotic swelling properties of the tissue. Cell metabolic activity has also been shown to vary with age, with mature chondrocytes synthesizing less collagen and PGs of smaller size and shorter sGAGs[5]. Age-related differences in the response of cells to growth factors have also been observed[33,34].

2.2.3 Mechanical Injury

Meniscectomies and anterior cruciate ligament transections have resulted in decreased ECM content, altered ECM organization and decreased mechanical properties of articular cartilage in canine models[6,35]. Models examining blunt trauma to the knee (e.g. automobile accident) have also indicated softening and fissuring of articular cartilage[36,37]. Mechanical injury models have been shown to decrease matrix synthesis[38-40] and elevate MMP levels[41], in addition to causing physical disruption of the matrix[39-42]. The extent of the injury is dependent on loading rate[39,41,43], strain[41], peak stress[43,44], and loading duration[43].

2.3 Effects of Cytokines on Articular Cartilage

2.3.1 Degradation Models

To study the development and progression of OA and to characterize events following articular cartilage injury and their relationship to OA, a variety of models have been developed. Among the biochemical stimulation models, the most commonly cited are the *in vivo* introduction of fibronectin[45-48], *in vitro* stimulation of chondrocyte-mediated catabolism using factors such as retinoic acid[49-51], tissue necrosis factor-α[52,53] or IL-1[49,52,53], and direct ECM digestion via addition of exogenous proteolytic enzymes[20,54].

IL-1α and IL-1β have received particular focus both *in vitro* and *in vivo* as regulatory and inflammatory cytokines implicated in the progression of OA. Within hours of exposure to exogenous IL-1, upregulation in transcription and activation of aggrecanases occurs in monolayer cultures of chondrocytes and tissue explants, leading to early breakdown and release of PGs[21,49,53]. Following degradation of the PGs, activation of MMPs leads to enzyme-mediated degradation of the collagen network[21,49,55]. Furthermore, IL-1 induced degradation is dose-dependent[56-59] and IL-1 exposure has also been shown to decrease sGAG[49,57,59,60] and protein synthesis[49,58,61,62]. Depletion of PGs and collagen network degradation are accompanied by increases in osmotic swelling and permeability and decreases in equilibrium and dynamic compressive moduli and compression-induced streaming potential[21,49].

2.3.2 Stimulation Models

Anabolic cytokines or growth factors have been shown to be potent stimulators of ECM synthesis. In particular, transforming growth factor-β (TGF-β) has been shown to stimulate PG synthesis up to seven times over untreated, serum-free bovine articular

cartilage explants. This stimulation appears to be dose-dependent, with maximal PG synthesis in explant culture achieved at a concentration of 10ng/mL[63]. TGF-β has also been shown to stimulate protein synthesis over 0.1-10ng/mL in primary rabbit articular chondrocytes[64]. TGF-β has exhibited stimulatory effects in the recovery of PG synthesis following IL-1 treatment of articular cartilage explants[65,66]. The stimulatory effect of TGF-β on PG synthesis appears to decline with age in both human and bovine articular cartilage[33,34].

2.4 Imaging Techniques

2.4.1 Cartilage-specific

Several nondestructive imaging techniques have been used to examine the composition and structure of cartilage and surrounding tissues, with the spatial resolution of the imaging application often dictating the technique used. Traditional x-ray and computed tomography (CT) are commonly used in evaluating joint space narrowing and changes in the adjacent bone structure (e.g. osteophytes). Unaided magnetic resonance imaging (MRI) extends these capabilities to the 3D visualization of fissures and tears of the articular surface[67]. The emergence of contrast-based MRI techniques including delayed gadolinium-enhanced MRI of cartilage (dGEMRIC) have provided accurate, 3D regional profiles of sGAG concentration in both developing and degrading matrices[56,68]. Similarly, optical coherence tomography (OCT), a light-based technique analogous to the application of sound waves in ultrasound, has shown promise in monitoring the fibrillar organization of collagen in normal and osteoarthritic cartilage[69,70]. Fourier Transform Infrared Imaging Spectroscopy (FT-IRIS) has been shown to detect changes in sGAG

content and collagen content and fiber orientation by monitoring changes in frequency absorbance spectrums[71].

2.4.2 Microcomputed Tomography

As with conventional CT, μCT has been widely used in the imaging of bone and is the standard method for quantifying trabecular bone architecture[72-76]. The high spatial resolution, fast scan times, quantitative morphology analysis, and 3D reconstruction capabilities provided by μCT have recently led investigators to explore its potential in non-traditional applications such as the characterization of porous biomaterials and soft tissues. For example, the use of a perfused contrast agent with μCT has provided quantitative analysis of the 3D morphology of vascular networks[77]. μCT has not generally been used to analyze cartilaginous tissues due to the inability of soft tissues to attenuate x-rays, but a recent study using the paramagnetic probe Gd-DTPA^{2-} demonstrated the potential use of μCT for the imaging of cartilage[78].

CHAPTER 3

ALTERED COMPOSITION-FUNCTION RELATIONSHIPS IN INTERLEUKIN-1-STIMULATED ARTICULAR CARTILAGE

3.1 Introduction

Articular cartilage, a hyaline cartilage that lines the bony surfaces of diarthrodial joints, provides joint lubrication and load distribution to the underlying bone. The tissue is comprised of chondrocytes embedded within a dense ECM consisting primarily of the large, aggregating PG aggrecan, type II collagen, and water. The high density of negatively-charged sGAG chains attached to the aggrecan core protein gives rise to an osmotic swelling pressure that resists compression and is balanced by tensile stresses carried by the collagen fiber network. Due to low tissue permeability, dynamic loads produced by functional activity are carried primarily through pressurization of entrapped fluid[79]. The resident chondrocytes synthesize and remodel the ECM[1,12,80,81] but can also contribute to tissue destruction in various degenerative conditions.

Relationships between ECM composition and mechanical properties have been studied to elucidate the contributions of PGs and collagen to macroscopic mechanical behaviors in healthy, developing and degenerating articular cartilage[2,4,9,29-31,82]. Previous studies have probed collagen network integrity by characterizing swelling-induced changes in geometry or stress created by hypotonic conditions[49,83,84]. Explant stiffness arising from the interactions of the PGs and collagen network under both cyclic and steady-state loads have been extensively characterized by the dynamic and equilibrium moduli in compression, shear and tension[20,26,85,86]. Indentation studies, performed either

in vitro or *in situ*, provide yet another assessment of the composition-function relationships present in articular cartilage[87,88].

Characterizing the composition-function relationships of articular cartilage during degeneration may elucidate the contributions of matrix constituents to altered cartilage function. As the regulatory and inflammatory cytokine IL-1 has been implicated in the progression of OA, stimulation of articular cartilage with IL-1 provides an appropriate model for investigating these relationships. Within hours of exposure to exogenous IL-1, upregulation in transcription and activation of aggrecanases occurs in monolayer cultures of chondrocytes and tissue explants, leading to early breakdown and release of PGs[21,49,53]. Following release of the PGs, the collagen network in cartilage explants undergoes MMP-mediated degradation[21,49,55]. Furthermore, IL-1-induced degradation is dose-dependent[56-59] and IL-1 exposure has also been shown to decrease sGAG[49,57,59,60] and protein synthesis[49,58,61,62]. Depletion of PGs and collagen network degradation are accompanied by increases in permeability and decreases in equilibrium and dynamic compressive moduli and compression-induced streaming potential[21,49].

The cell-mediated destruction of PGs and collagen and loss of mechanical properties that are observed with IL-1 stimulation suggest the utility of this model in examining composition-function relationships in degenerating articular cartilage. To that end, this study presents a detailed time course of the biochemical and biophysical changes associated with IL-1-stimulated cartilage degradation and then examines the relationships between biochemical composition and functional properties. In addition to furthering our understanding of the importance of PGs and collagen to normal mechanical function, this study also contributes to our knowledge of cartilage

degeneration by identifying changes in composition-function relationships associated with IL-1-mediated catabolism.

3.2 Materials and Methods

3.2.1 Tissue Explant Preparation and Culture

Under aseptic conditions, 3mm diameter full thickness cartilage explants were harvested with a dermal biopsy punch (Miltex; York, PA) from the femoral condyles and patellar grooves of both stifle joints of a 1-2 week old bovine calf (Research 87; Boylston, MA). A custom cutting block was used to remove the most superficial ~300μm and the deep zone tissue, resulting in middle zone explants with a thickness of 1.78 ± 0.020mm as measured with digital calipers (Mitutoyo USA; Aurora, IL). Forty explants were randomly assigned to either control or IL-1 stimulation. To allow for equilibration to culture conditions, explants were precultured for 72 hours at 37°C and 5% CO_2 in serum-free control medium consisting of high glucose Dulbecco's Modified Eagle's Medium (DMEM) supplemented with 50μg/mL gentamicin, 0.1mM non-essential amino acids (Invitrogen; Carlsbad, CA) and 50μg/mL ascorbate (Sigma; St. Louis, MO). Explants were placed two per well in 48 well plates (Becton Dickinson; Franklin Lakes, NJ) in 0.5mL of either control medium or control medium supplemented with 20ng/mL recombinant human IL-1α (Peprotech; Rocky Hill, NJ). This IL-1 dosage has previously been shown to induce aggressive cell-mediated degradation, with complete depletion of sGAGs within two weeks[21,89]. Samples were cultured for up to 32 additional days, with media changed and collected every 48 hours. Four explants per group were removed from culture at 4, 8, 12, 16, 24, and 32 days following pre culture and stored in 0.15M PBS

(Invitrogen) with protease inhibitors (PI Cocktail Set I, Calbiochem; San Diego, CA) at -20°C for subsequent compression testing and biochemical analysis.

A second degradation study was conducted specifically to examine changes in shear properties due to IL-1 stimulation. Sixty-five explants (4mm diameter x 2mm thick) were isolated as described above from middle zone cartilage of a second 1-2 week old calf. Following a 3-day preculture, explants were cultured in individual wells for up to 24 additional days in 0.5mL of control medium or control medium supplemented with 20ng/mL IL-1α. Five explants per group were removed from culture at days 0, 4, 8, 12, 16, 20, and 24 and stored in 0.15M PBS with protease inhibitors at -20°C for subsequent dynamic shear testing and biochemical analysis.

3.2.2 Mechanical Testing

Prior to mechanical testing, explants were thawed at room temperature. Thicknesses were measured with digital calipers and wet masses were also determined. Compression testing of tissue explants was performed using a SMT-S 5.6lbf load cell (Interface; Scottsdale, AZ) and an ELF 3230 testing frame (Enduratec; Minnetonka, MN) at room temperature in 0.15M PBS with protease inhibitors, with displacements corrected for load cell compliance. Torsional shear testing was performed using a CVO 120HR stress-controlled rheometer with strain feedback (Bohlin; East Brunswick, NJ).

Samples were tested in unconfined compression by applying a 0.1N tare load followed by four steps (5% each, 1mm/s ramp rate) of stress relaxation with a 10 minute relaxation after each strain step. As 10 minutes may not reflect complete relaxation, the force vs. time data, F(t), for each step were fit to an analytical solution for the unconfined

compression stress relaxation of a linear biphasic material described by Armstrong *et al*[85]:

$$F(t) = F_\infty \left[1 + \sum_{n=1}^{\infty} A_n \exp\left(-\frac{\alpha_n^2 H_A k t}{a^2} \right) \right], \qquad 3.1$$

where F_∞ is the equilibrium (relaxed) force, $A_n = 1/\left[(1-\upsilon)^2 \alpha_n^2 - (1-2\upsilon) \right]$, α_n are the roots to the characteristic Bessel function equation $J_1(x) - (1-\nu) x J_o(x)/(1-2\nu) = 0$, a is the sample radius, H_A is the aggregate modulus and k is the linear permeability. For each relaxation step, a three parameter least squares fit was performed using Matlab 7.1 (Mathworks; Natick, MA) to determine the value of the step offset, $F_{\infty,}$ and the product $H_A k$ assuming a Poisson's ratio of 0.1 and using the first five terms of the analytical solution. A linear regression of the equilibrium stresses ($F_\infty/(\pi a^2)$) against the applied strain over the range of 10-20% was used to determine E_{equil}, the unconfined compression equilibrium modulus of each sample.

After relaxation at the 10% compression step, sinusoidal compression (±1.5% strain) was applied at 0.005, 0.05, 0.5, and 5Hz. For each frequency, the magnitude of the dynamic compressive modulus, $|E^*_{dyn}|$, was calculated by WinTest DMA software (Enduratec) as the ratio of the fundamental stress and strain magnitudes determined using a Fast Fourier Transform.

Samples were tested in torsional shear by applying a 10% compressive offset and, after a 12 minute relaxation, applying a nominal sinusoidal shear strain of 0.5% amplitude over a range of frequencies (0.01, 0.1, 1, and 10Hz). The magnitude of the complex shear modulus $|G^*_{dyn}|$ was determined by the rheometer software from the ratio of the measured stress to the applied strain.

3.2.3 Biochemical Analysis

Following mechanical testing, explants were lyophilized overnight and dry masses were determined. Explants were then solubilized with 4 mg/mL proteinase K (Calbiochem) in 100mM ammonium acetate (pH 7.0) (Sigma). The digested explants and conditioned media were assayed for sGAGs via the dimethylmethylene blue (DMMB) assay[90], using shark chondroitin sulfate (Calbiochem) as a standard. Collagen was assayed via the pDAB/chloramine-T assay for hydroxyproline, using trans-4-hydroxy-L-proline (Sigma) as a standard and assuming a 1:8 mass ratio of hydroxyproline:collagen[91]. As the compressive properties were expected to be related to the matrix fixed charge density (FCD, or charge per unit interstitial fluid volume), the sGAG and (for consistency) collagen contents were normalized by water volume in the composition-function analyses.

3.2.4 Statistical Analyses

All statistical analyses were performed using Minitab Release 14 (Minitab; State College, PA) with significance at $p<0.05$. Interdependence among matrix components or among mechanical properties was determined via linear correlation analyses. Differences among time points in a given treatment group or between treatments at a given time point were examined via one-way ANOVA with Tukey's test for posthoc pairwise comparisons. To compensate for heteroscedasticity, the equilibrium modulus and dynamic shear modulus data were log transformed prior to ANOVA. Due to loss of sample integrity for IL-1 treated explants, sample sizes were insufficient to perform some comparisons at later time points. Regressions of mechanical parameters against matrix constituents were compared between treatment groups as described by Zar[92] using

custom Minitab macros. Briefly, the groups were first compared to test the null hypothesis of equal regression slopes. In the case of a common slope, the groups were then compared to test the null hypothesis of equal intercepts. A common regression was used if neither null hypothesis was rejected.

3.3 Results

3.3.1 Explant and Media Biochemistry

As previously demonstrated[21,49,53,55,93,94], treatment with 20ng/mL IL-1α resulted in substantial matrix depletion over the 32 day culture period. sGAG release for IL-1-stimulated samples peaked at day 8 with 59% of total sGAG released (Figure 3.1A) and was essentially complete by day 14. Collagen release to the media by IL-1 samples became significantly elevated over controls at day 6 ($p<0.05$), peaked near day 14, and remained essentially constant through day 24, at which point 74% of the total collagen release had occurred (Figure 3.1B). Control samples displayed a steady increase in sGAG content over the culture period, indicating a basal level of proteoglycan synthesis (Figure 3.2A). Consistent with the sGAG release data, the residual sGAG content of IL-1-stimulated explants decreased relative to control explants during the first 16 days in culture and reached the detection limit of the DMMB assay by day 24. The residual collagen content of control explants did not significantly vary during the culture period, while the collagen content of the IL-1-stimulated explants gradually decreased following day 8 (Figure 3.2B). Explant water content showed little variation with culture in either control or IL-1 groups (Figure 3.2C). A steady increase in the thickness of control explants accompanied the increased sGAG, with no further increase for the duration of

culture (Figure 3.2D). In contrast, the thickness of IL-1 treated explants did not significantly change during culture.

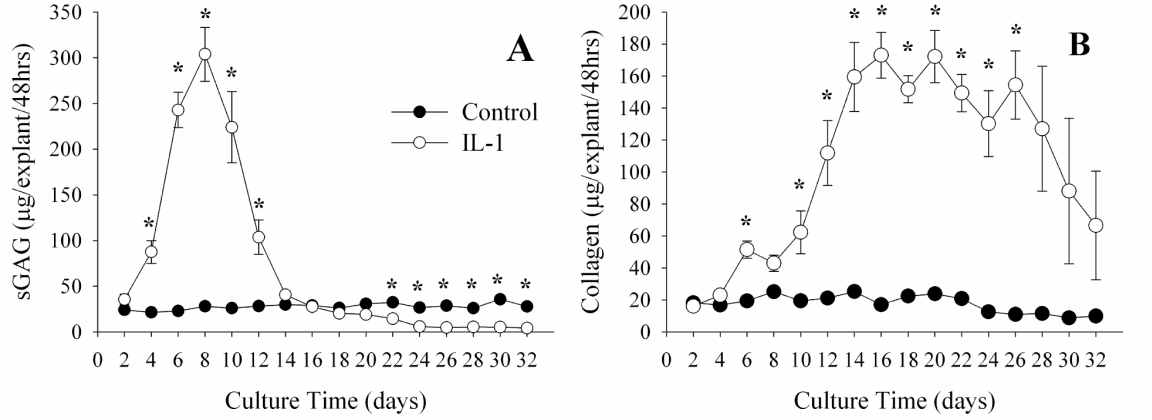

Figure 3.1: sGAG (**A**) and collagen (**B**) release to the media over 48 hour period for control (●) and IL-1 treated (○) explants. * denotes $p<0.05$ between control and IL-1-stimulated explants (n=4, mean±SEM).

3.3.2 Explant Mechanical Properties

ANOVA indicated no significant effect of culture time on the control equilibrium modulus ($p=0.076$) or dynamic modulus ($p=0.063$) (Figures 3.3A-3B). In contrast, IL-1-stimulated explants exhibited substantial changes in mechanical properties reflecting the ECM degradation kinetics. Both the equilibrium modulus and dynamic compression modulus decreased as the sGAG release progressed, with the equilibrium modulus reaching detection limits by day 16. The dynamic modulus remained measurable through day 24, indicating sensitivity to relatively small levels of residual matrix. Treatment with IL-1 for 32 days resulted in sufficient matrix loss that explants could not sustain handling for mechanical testing. The dynamic compressive modulus exhibited similar frequency

dependence across time points and treatment groups, with consistent differences between treatment groups at all frequencies (Figure 3.4).

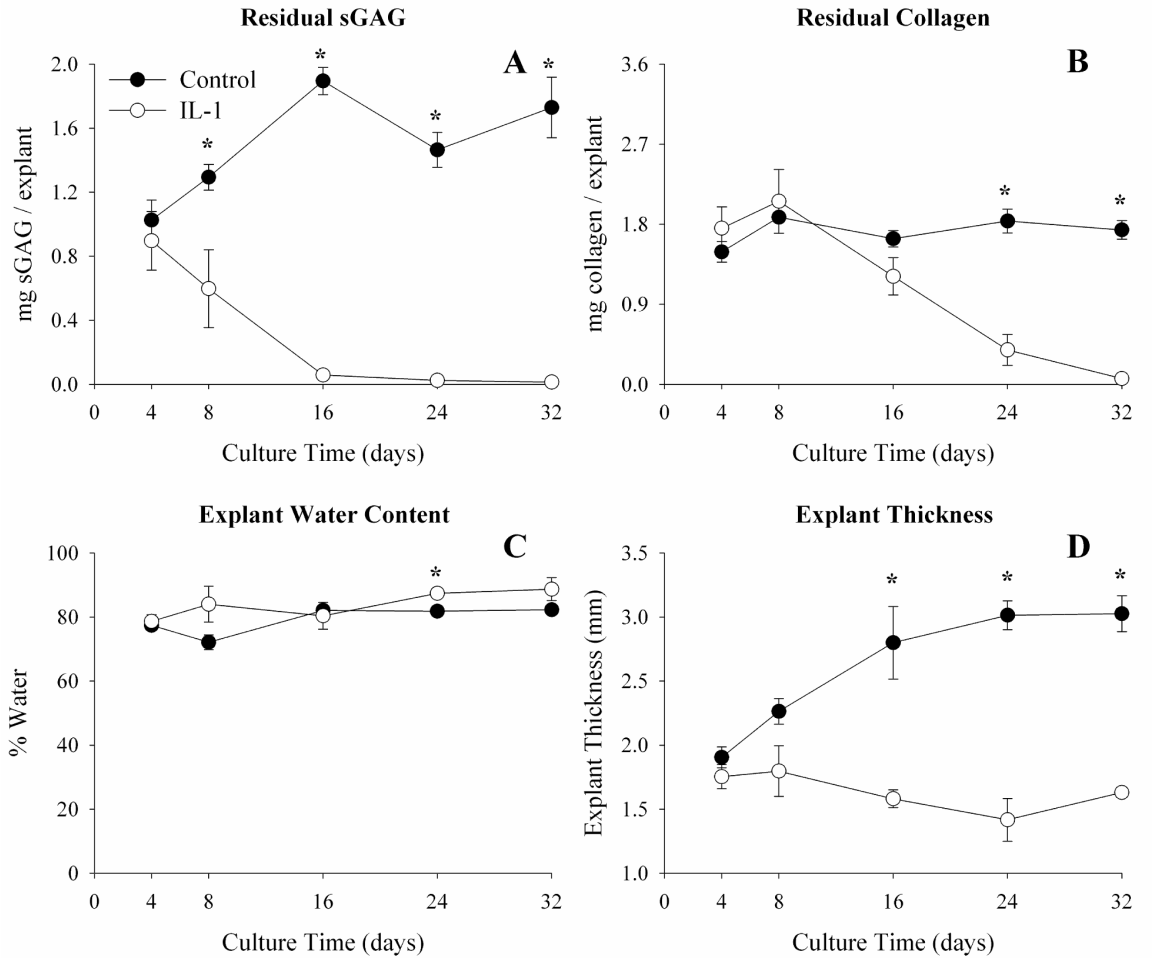

Figure 3.2: Residual sGAG content (**A**), collagen content (**B**), water content (**C**), and explant thickness (**D**) as a function of culture time for control (●) and IL-1-stimulated (○) explants. * denotes $p<0.05$ between control and IL-1-stimulated explants (n=4, mean±SEM).

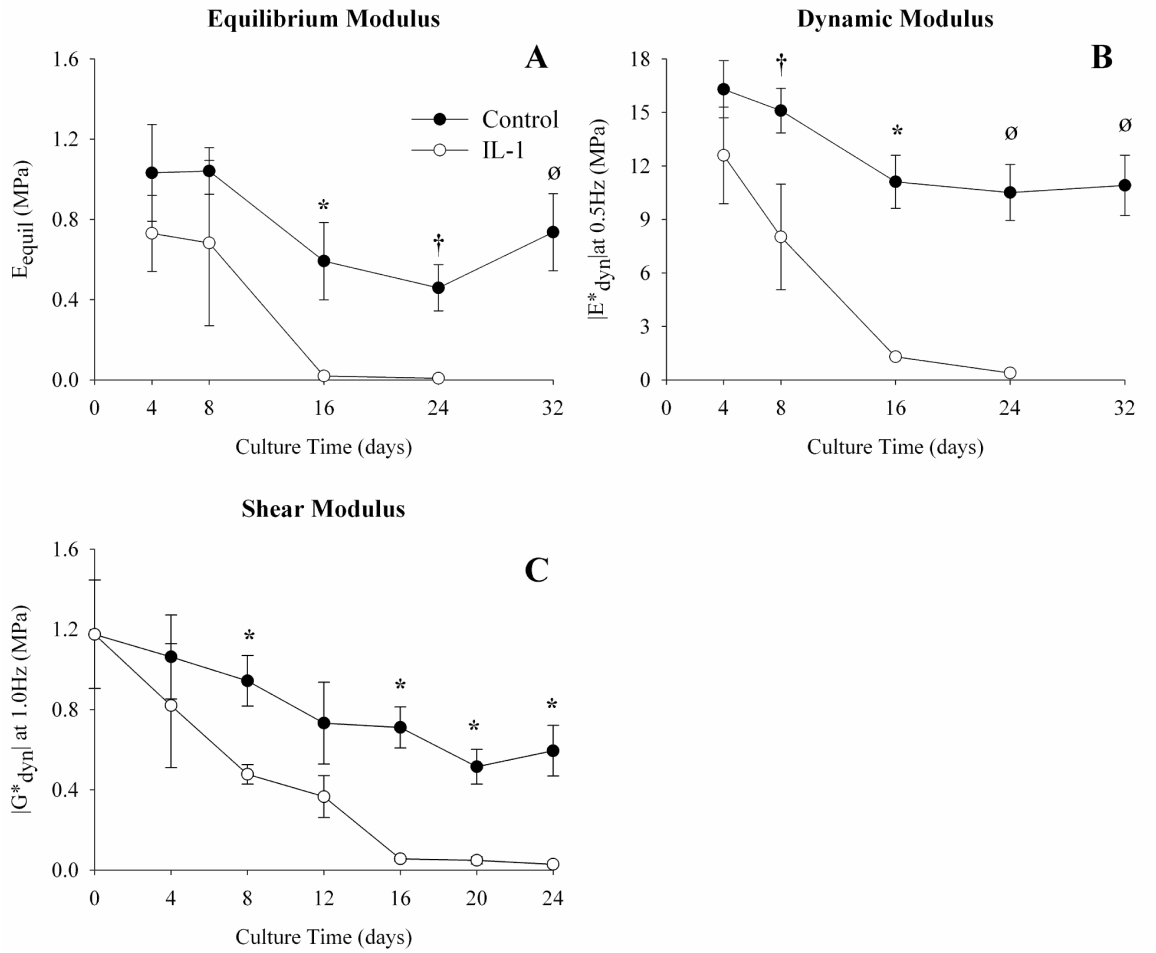

Figure 3.3: Compressive and shear properties as a function of culture time for control (●) and IL-1-stimulated (○) explants: (**A**) Equilibrium unconfined compression modulus; (**B**) Dynamic unconfined compression modulus at 0.5Hz; (**C**) Dynamic shear modulus at 1Hz. * denotes $p<0.05$ and † denotes $p=0.06$ between control and IL-1-stimulated explants (n=4-5, mean±SEM). Ø denotes an insufficient number ($n\leq2$) of IL-1-stimulated explants to perform the statistical analysis.

ANOVA indicated that the dynamic shear modulus of control explants did not vary with culture time ($p=0.130$) (Figure 3.3C). In contrast, the dynamic shear modulus of IL-1-stimulated explants exhibited an initial rapid decrease through day 8 and continued to decrease until it reached detection limits at day 20. The dynamic shear modulus appeared to stabilize in the period between peak sGAG release and substantial collagen release (days 8 and 12), suggesting that $|G^*_{dyn}|$ is sensitive to changes in both

sGAG and collagen content. As with the dynamic compression modulus, the dynamic shear modulus exhibited similar frequency dependence across time points and treatment groups, with consistent differences between treatment groups at all frequencies (Figure 3.5).

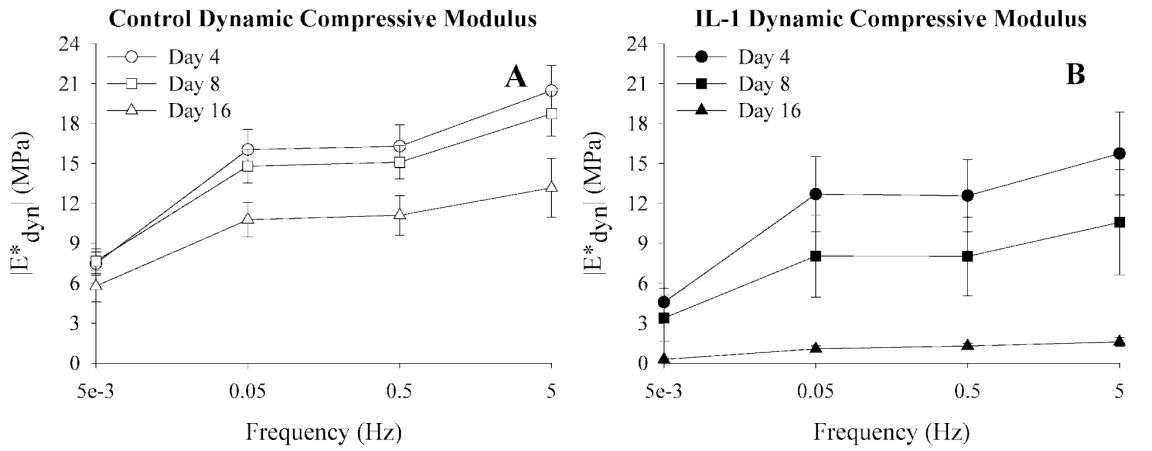

Figure 3.4: Dynamic unconfined compression modulus as a function of frequency and culture time for control (**A**) and IL-1-stimulated (**B**) explants (n=4, mean±SEM).

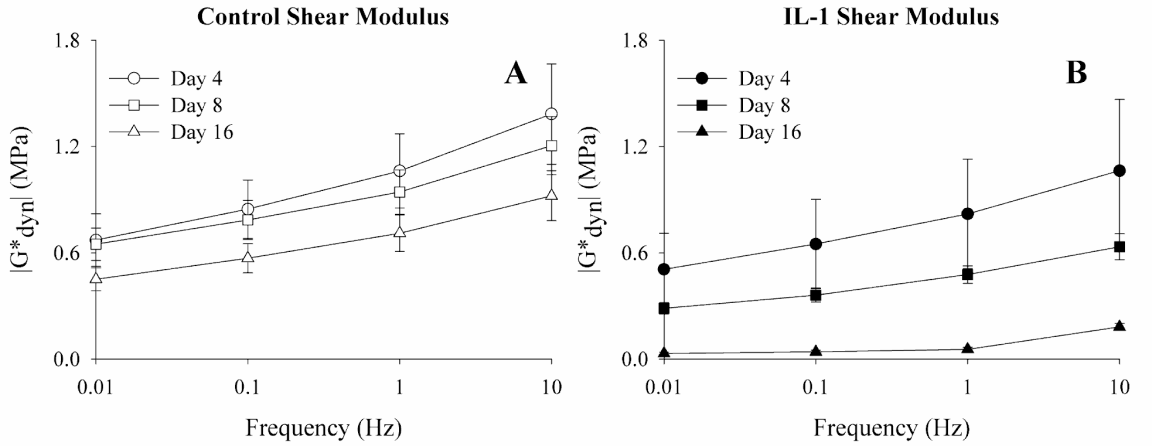

Figure 3.5: Dynamic shear modulus as a function of frequency and culture time for control (**A**) and IL-1-stimulated (**B**) explants (n=4, mean±SEM).

3.3.3 Composition-Function Relationships

Regression analyses indicated substantial differences between control and IL-1-simulated explants in the dependence of mechanical properties on tissue composition (Table 3.1). The dependence of E_{equil} on sGAG concentration was not significantly different for control and IL-1-stimulated explants, but the regressions were significantly different between treatment groups for all other mechanical properties. The compressive properties of control explants were significantly dependent on sGAG concentration (Figures 3.6A-3.6B) and collagen concentration (Figures 3.6D-3.6E). In contrast, for IL-1-stimulated explants, all compressive properties were strongly dependent on sGAG concentration (Figures 3.6A-3.6B) but none were significantly dependent on collagen concentration (Figures 3.6D-6E). Both for control and IL-1-stimulated explants, $|G^*_{dyn}|$ was strongly dependent on sGAG concentration (Figure 3.6C) and weakly dependent on collagen concentration (Figure 3.6F). Note that the regression analyses of the unconfined dynamic compression modulus $|E^*_{dyn}|$ and dynamic shear modulus $|G^*_{dyn}|$ are reported for data obtained at 0.5Hz and 1.0Hz, respectively, although the trends remained consistent for the other frequencies examined.

Table 3.1: Linear regressions of physical properties as a function of biochemical composition in control and IL-1-stimulated explants. Linear regression coefficients are significant at $p<0.05$ (NS=non-significant). Common regression coefficients are indicated by a box that spans the two groups. Units of all mechanical properties are in MPa (E_{equil} = Equilibrium Unconfined Compression Modulus, $|E^*_{dyn}|$ = Magnitude of Dynamic Compression Modulus at 0.5Hz, $|G^*_{dyn}|$ = Magnitude of Dynamic Shear Modulus at 1Hz).

y = a*x + b							
y		x = sGAG /H_2O (mg/mL)			x = Collagen /H_2O (mg/mL)		
		R^2	A	b	R^2	a	b
E_{equil}	Control	0.66	9.03E-03	-5.76E-02	0.48	6.19E-03	5.54E-03
	IL-1 treated				NS	--	--
$\|E^*_{dyn}\|$	Control	0.27	6.88E-02	6.47E+00	0.51	5.77E-02	6.03E+00
	IL-1 treated	0.96	1.53E-01	-3.12E-01	NS	--	--
$\|G^*_{dyn}\|$	Control	0.53	1.874E+04	-2.77E+05	0.26	4.15E+03	3.76E+05
	IL-1 treated			1.28E+05			-2.49E+05

Table 3.2: Correlations between biochemical constituents for control and IL-1-stimulated cartilage explants. Correlation coefficients are significant at $p<0.05$ (NS=non-significant).

	Control		IL-1-stimulated	
	collagen/H_2O	sGAG/H_2O	collagen/H_2O	sGAG/H_2O
sGAG/H_2O	+0.780		NS	
% H_2O	-0.915	-0.687	-0.775	-0.630

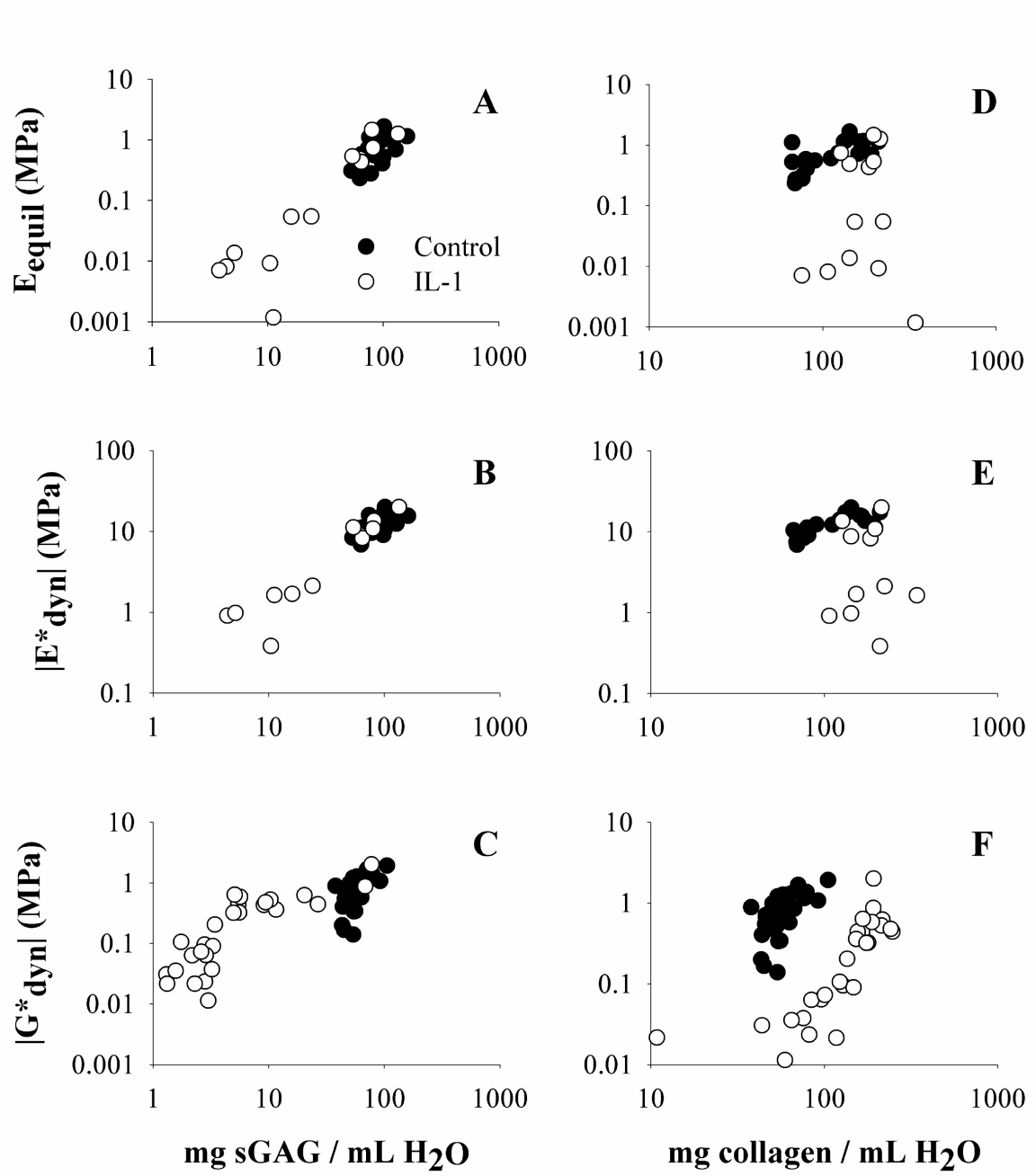

Figure 3.6: Physical properties plotted against sGAG concentration (A-C) and collagen concentration (D-F) for control (●) and IL-1-stimulated (○) explants. Data are presented on logarithmic scales.

Table 3.3: Correlations between compressive properties of control and IL-1-stimulated explants. Correlation coefficients are significant at $p<0.05$ (E_{equil} = Equilibrium Unconfined Compression Modulus, $|E^*_{dyn}|$ = Magnitude of Dynamic Compression Modulus at 0.5Hz).

p<0.05	Control		IL-1-stimulated	
	E_{equil}	$\|E^*_{dyn}\|$	E_{equil}	$\|E^*_{dyn}\|$
$\|E^*_{dyn}\|$	+0.929		+0.877	

Interdependences among ECM components and among the measured mechanical properties were examined to aid in interpreting the dependences indicated by the regression analyses. Data from all time points were pooled for control and IL-1-stimulated explants. Significant, negative correlations were found between percent water and both collagen and sGAG concentrations for both the control and IL-1 treatments (Table 3.2). A significant, positive correlation was found between collagen and sGAG concentrations for control explants but not for IL-1-stimulated explants, reflecting the decoupled sGAG and collagen release profiles. Significant, positive correlation coefficients were found among all compressive mechanical properties for both the control and IL-1 treatments (Table 3.3). In control and IL-1-stimulated explants, high correlations ($0.877<R<0.929$) were found between the equilibrium compressive modulus and the dynamic compressive modulus, suggesting that the measurements offer similar predictions of the mechanical integrity of the ECM. As with the regression analyses, correlations are presented for the unconfined dynamic compression modulus $|E^*_{dyn}|$ at

0.5Hz and the dynamic shear modulus $|G^*_{dyn}|$ at 1.0Hz, although the reported trends were consistent at all other frequencies.

3.4 Discussion

Composition-function relationships of bovine articular cartilage were investigated in immature explants during IL-1-induced catabolism. These studies provide detailed time courses of the biochemical and biophysical changes associated with IL-1-induced catabolism and examine the relationships between ECM constituents and compressive and shear properties. The loss of ECM and compressive mechanical properties reported during IL-1 stimulation is consistent with previous studies using IL-1[21,49,53,55,93-95]. The compressive and shear moduli of control explants were found to be dependent on PG and collagen content, which is consistent with previous reports for untreated cartilage[1,9,20,54,80,96]. In contrast, IL-1 stimulation altered composition-function relationships, generally indicating a significant dependence of mechanical properties on sGAGs but not collagen.

The composition-function relationships presented indicate a preferential dependence of mechanical properties on sGAG content following IL-1 stimulation, which may be reflective of the studies design or the degradation characteristics of the IL-1 model. In particular, the early, rapid depletion of sGAGs following IL-1 stimulation and the associated decay in mechanical properties may account for the strong dependence on sGAG concentration, since nearly all of the decay in properties occurs prior to significant collagen depletion. Due to the characteristics of IL-1-induced cartilage degeneration, a comparable examination of the effects of depleting collagen while holding the PG content fairly constant is not possible with this model system. Direct enzymatic digestion of

collagen with collagenases has been used to investigate the specific dependence of mechanical properties on collagen[54], but the results of this experimental system are difficult to interpret as passive PG release often occurs as a secondary effect of collagen cleavage. Recovery experiments that promote significant regeneration of collagen following matrix degradation could further clarify these relationships, but significant collagen accumulation remains a challenge in cartilage tissue engineering efforts.

Analysis of the temporal changes in biophysical properties following IL-1 stimulation suggests that some measurements may be more sensitive to patterns of ECM loss caused by IL-1 stimulation. For the IL-1 group, E_{equil} reached the detection limit of the test at day 16 ($p<0.05$) while $|E^*_{dyn}|$ and $|G^*_{dyn}|$ were still measurable at days 24 and 20 ($p=0.052$), respectively. Through day 16, sGAG and collagen content in IL-1 stimulated explants decreased relative to controls by 96.8% and 26.2%, respectively. Since collagen degradation follows PG degradation in IL-1-induced cartilage degradation, the time course data presented here suggest that $|E^*_{dyn}|$ and $|G^*_{dyn}|$ may be sensitive to changes in collagen as well as proteoglycan content.

While IL-1 stimulation resulted in altered composition-function relationships in immature articular cartilage, the reported trends may be model specific and not applicable to systems with different ECM composition, organization and mechanical properties. In particular, mature articular cartilage contains a significantly higher collagen fiber and collagen crosslink density[9,14], lower PG content[14], smaller length sGAGs[5,15-17], and decreased cellularity[97] relative to immature cartilage. Additionally, the cell-mediated activity of IL-1 may be more aggressive in immature than mature cartilage due to its higher cell density, though little age-related sensitivity to IL-1 has been reported in

human articular cartilage[33]. In addition to potential age-related differences in composition-function relationships, regional variations in ECM composition and mechanical properties have also been reported both with tissue depth[28,98] and topographical location[29,96]. While the present study did not examine variations in composition-function relationships with topographical location, the use of immature middle zone cartilage minimizes variations due to tissue inhomogeneity through the tissue depth.

While the correlation and regression analyses applied in the present study revealed differences in control and IL-1-stimulated cartilage, the study design and analysis should be considered when interpreting the results. Given the complex ECM organization and nonlinear behavior of articular cartilage, the linear regression analyses used here may incompletely capture the true composition-function relationships. The Donnan and Poisson-Boltzmann models[99,100], which predict osmotic swelling pressures using a nonlinear dependence on PG concentration, support that argument. The composition-function relationships may be further influenced by the choice of biochemical parameters (i.e. collagen, sGAG, water). A number of other studies investigating composition-function relationships have evaluated collagen cleavage[83] and pyridinoline or collagen crosslinks[9,29,83,101]. Collagen crosslinks and collagen cleavage, in particular, may be critical parameters to examine since the integrity of the collagen network cannot be evaluated by the hydroxyproline assay used in the present study. Testing mode[9,29] and compressive offset[20] have also been found to influence composition-function relationships in articular cartilage.

The observed differences in composition-function relationships between control and IL-1-stimulated cartilage explants offer insights into the interacting contributions of proteoglycans and collagen to ECM function and provide a baseline for interpreting effects of specific interventions aimed at slowing or reversing cartilage degradation. Furthermore, the strong dependence of all measured physical properties on sGAG concentration during IL-1-induced degeneration suggests that measurements of sGAG concentration may be a useful surrogate for direct mechanical measurements. For example, imaging techniques such as dGEMRIC (delayed gadolinium-enhanced MRI of cartilage)[102] and EPIC-μCT[103] that produce maps of tissue proteoglycan concentration may provide sufficient information to noninvasively estimate functional properties of cartilage in animal models of degeneration and recovery or in clinical practice. Through this and similar approaches, it may be possible to determine which matrix molecules are most critical to proper function or repair capacity and to lend this knowledge to future tissue engineering strategies and OA treatments.

CHAPTER 4

DEVELOPMENT AND VALIDATION OF EQUILIBRIUM PARTITIONING OF AN IONIC CONTRAST AGENT-MICROCOMPUTED TOMOGRAPHY

4.1 Introduction[1]

Analysis of small animal models is limited by the availability of quantitative evaluation techniques for studying the ECM changes associated with OA and cartilage repair. Histology is traditionally used to monitor the spatial distribution of matrix macromolecules but is time consuming, subject to distortion artifacts and tissue damage, and produces only semi-quantitative analysis of 2D sections that may provide inaccurate 3D representations. Biochemical assays are available to quantify the amount and type of matrix macromolecules in cartilage but these assays fail to provide their spatial distributions, particularly in small animals where the limited thickness and volume of cartilage makes it difficult or impossible to extract samples from multiple regions. Additionally, longitudinal monitoring of changes with time are impossible due to the destructive nature of these histological and biochemical techniques.

Proteoglycans are a particularly appropriate target for studying OA and for evaluating the efficacy of cartilage defect repair. PGs comprise 5-10% of articular cartilage by wet mass[1] and are key regulators of its equilibrium and dynamic mechanical

---

[1] Material presented in Chapter 4 was reprinted, with permission, from the Proceedings of the National Academy of Sciences 103(51):19255-19260, Palmer AW, Guldberg RE, Levenston ME, "Analysis of Cartilage Matrix Fixed Charge Density and Three-Dimensional Morphology Via Contrast-Enhanced Microcomputed Tomography", Copyright 2006, National Academy of Sciences.

properties. This regulation is the result of ionic interactions between interstitial fluid and negatively-charged sulfated glycosaminoglycans attached to the PG backbone[104]. The amount and distribution of PGs changes substantially during development[29], during degeneration and repair[56,65], and in response to blunt trauma[41]. Of particular clinical interest, initial stages of OA are marked by aggrecanase-mediated cleavage of PGs[105], resulting in altered sulfation patterns[106] and progressive depletion of PGs from the ECM. Furthermore, changes in the ECM composition of articular cartilage precede and have been linked to changes in mechanical properties[4,9]. Therefore, the ability to noninvasively detect changes in PG content could provide an indirect indication of the integrity of the cartilage matrix and a means to monitor disease progression or reversal.

These studies address the development and validation of a contrast-based microcomputed tomography (μCT) technique for high resolution imaging of PGs in soft tissues. Microcomputed tomography is an X-ray based imaging modality capable of three-dimensional, quantitative morphological analysis, and current systems provide images at micron-level voxel resolutions. μCT imaging has traditionally been applied to hard tissues and is the standard for quantifying trabecular bone microstructural changes associated with aging and osteoporosis[107,108]. However, μCT has not been useful for direct imaging of soft tissues due to the low X-ray absorption of non-mineralized tissues. To compensate for the poor radiopacity of soft tissues, a novel contrast-enhanced μCT technique has been developed in which samples are equilibrated in a solution containing an ionic CT contrast agent prior to μCT scanning, yielding an equilibrium distribution of the ionic contrast agent that is inversely related to the density of the negatively-charged sGAGs. In monitoring PG content, the technique relies on detection of the *E*quilibrium

*P*artitioning of the *I*onic *C*ontrast agent via μCT (EPIC-μCT). The studies presented here used Hexabrix™ 320, a clinically available CT contrast agent containing ioxaglate, a negatively-charged hexa-iodinated dimer.

To demonstrate the potential of this approach to examine the ECM of cartilage, data is first presented validating the ability of EPIC-μCT to monitor PG content and distribution in an *in vitro* model of IL-1-induced cartilage degradation, a common model for studying cell-mediated cartilage catabolism[53,93]. The data indicate consistent agreement with traditional biochemical and histological analysis of PGs and demonstrate a strong correlation between X-ray attenuation and PG content. A second study presents data illustrating the potential of EPIC-μCT for 3D morphometric analyses of articular cartilage *in situ* on a rabbit femur. The EPIC-μCT images reproduce visible features of articular surface topography and ligament insertions, and segmentation of cartilage from the underlying bone allows quantitative analysis of cartilage morphology.

4.2 Materials and Methods

4.2.1 Principle of the Technique

Similar to the dGEMRIC technique[109], EPIC-μCT relies on the partitioning of a charged contrast agent within a charged ECM. In cartilage, type II collagen carries a nearly neutral net charge while the sulfated GAGs primarily associated with the large, aggregating proteoglycan aggrecan confer a highly negative net charge to the ECM. The interstitial fluid carries a corresponding excess of positively charged solutes, resulting in bulk macroscopic electroneutrality. Given these properties, conditions of electrochemical equilibrium predict that a negatively-charged solute capable of permeating the tissue

would distribute inversely to the negatively-charged sGAGs, and therefore spatially target regions of lower sGAG density. For a region of tissue with a fixed charge density (FCD) ρ_m (in Coulombs/L) submerged in a bath containing a single monovalent salt at a concentration C_o, the Gibbs-Donnan theory for an ideal solution predicts the interstitial anion concentration within the tissue C^- as:

$$C^- = \frac{\rho_m + \sqrt{(\rho_m)^2 + (2FC_o)^2}}{2F} \tag{4.1}$$

where F is Faraday's constant. For a tissue such as cartilage, a negatively-charged solute capable of permeating the tissue would distribute inversely to the negatively-charged sGAGs, and therefore spatially target regions of lower sGAG density. If the anion concentration could be noninvasively detected, it would thus provide an indirect measure of the matrix FCD (and therefore the sGAG concentration).

It should be noted that while Equation 4.1 describes the distribution of an ideal anionic solute in a dilute solution, factors including steric interactions between solutes, solvation effects and restricted availability of intrafibrillar water will influence the activity (or effective concentration) of a solute within the tissue, resulting in deviations from the ideal behavior. Furthermore, most commercial contrast agents are multicomponent mixtures, complicating theoretical predictions of solute behavior. Additionally, a macroscopic imaging technique such as EPIC-μCT will actually detect the apparent macroscopic concentration $\overline{C}^-$:

$$\overline{C}^- = \phi^f C^- \tag{4.2}$$

where ϕ^f is the fluid volume fraction (approximately 0.8 for articular cartilage[1]). Consequently, the quantitative relationship between the concentration of the anionic contrast agent and the tissue fixed charge density will not exactly follow Equation 4.1 and must be determined empirically for a given contrast formulation or dilution and tissue type. Serial dilutions of the contrast agent (as in Figure 4.1) could then be used as phantoms to calibrate attenuation as a function of contrast agent concentration, allowing standardization of the quantification to account for different scan parameters or differences between μCT systems.

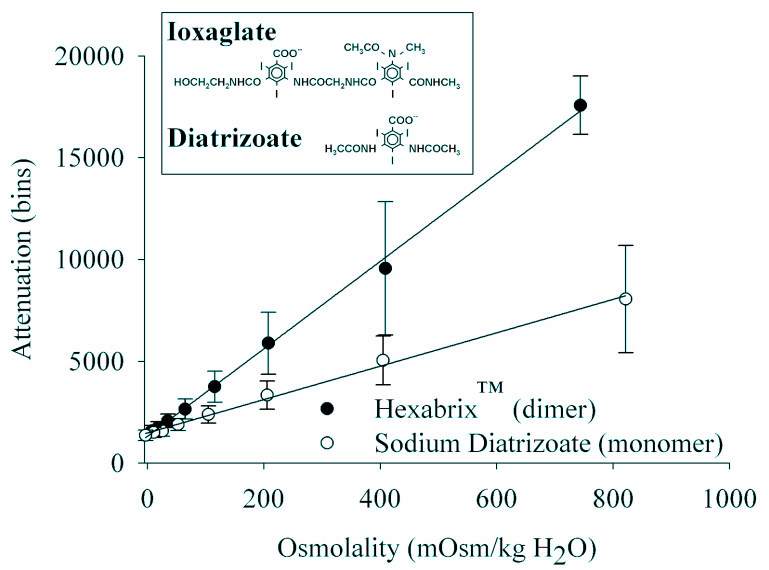

Figure 4.1: Linear decrease of X-ray attenuation with dilution of anionic CT contrast agents. At a given osmolality, attenuation of Hexabrix is higher than that of sodium diatrizoate because of the higher iodine content of the dimeric ioxaglate ion, resulting in a greater sensitivity to changes in matrix FCD.

While this approach would work in theory for any ionic contrast agent, the present study explored contrast-enhanced μCT imaging of cartilage using Hexabrix™ 320

(Mallinckrodt; Hazelwood, MO), an ionic contrast agent labeled for clinical use in contrast-enhanced CT scanning of the head and body and for direct injection in the uterus, fallopian tubes, and joint spaces. Hexabrix™ 320 is a sterile, non-pyrogenic, aqueous solution consisting of 39.3% (w/v) ioxaglate meglumine and 19.6% (w/v) ioxaglate sodium. Dissociated ioxaglate provides six iodine atoms per monovalent anion, resulting in a greater X-ray attenuation at a given osmolality than is achieved with tri-iodinated monomers (Figure 4.1) and thus providing a greater sensitivity to differences in FCD. Considering the important functional contributions of the FCD of cartilage that arise from the interactions of bound sGAGs with mobile ions in the interstitial fluid, the osmolarity of the contrast agent was also a concern, as significant mismatches would yield swelling or shrinkage artifacts. While slightly hypertonic to cartilage (~300-400mOsm/L), Hexabrix™ at 460mOsm/L represents one of the closest matches among ionic iodinated contrast agents. In addition, the commercial formulation of Hexabrix™ is pH balanced to 6-7.6pH, minimizing any concerns of the effect of short-term exposure on cell viability and metabolic activity.

4.2.2 *In Vitro* Evaluation Model

To evaluate the potential for EPIC-μCT to monitor changes in the ECM of cartilage, degradation was produced *in vitro* by incubation of bovine articular cartilage explants with interleukin-1α (IL-1). Briefly, IL-1α and IL-1β are regulatory and proinflammatory cytokines implicated in the progression of OA. Within hours of treatment with IL-1, an upregulation in cell-mediated aggrecanase expression is noted in articular cartilage[21,49,53]. The increased aggrecanase expression leads to progressive degradation of the PG network. Following PG depletion, the collagen network undergoes

matrix metalloproteinase-mediated degradation[21,49,55]. Given the similarities of the IL-1 model kinetics to matrix degradation noted during degenerative conditions, IL-1 stimulation of articular cartilage is a well-suited model for this evaluation study.

4.2.3 Tissue Explant Preparation and Culture

Sixty-six 4mm diameter, full thickness explants were harvested aseptically with a disposable biopsy punch (Miltex; York, PA) from both stifle joints of a 2-4 week old calf (Research 87; Boylston, MA). Using a custom cutting block, explants were trimmed of all visible subchondral bone by cutting parallel to the articular surface. The tallest and shortest heights of each sample were measured with digital calipers and averaged to obtain the explant thickness. The full-thickness explants had an average thickness of 5.00±0.07mm, with a range of 3.85-6.35mm. Sixty explants were assigned to either control or IL-1-treated groups and six explants were designated as Day 0 controls, with particular care taken to ensure a uniform distribution of thicknesses and harvest legs across groups. Explants were cultured in 24 well plates (Becton Dickinson; Franklin Lakes, NJ) in 1mL of either control medium (high glucose Dulbecco's Modified Eagle's Medium (Invitrogen; Carlsbad, CA) supplemented with 50μg/mL ascorbate (Sigma; St. Louis, MO), 0.1mM non-essential amino acids (Invitrogen), and 50μg/mL gentamicin (Invitrogen)) or control medium supplemented with 20ng/mL recombinant human IL-1α (Peprotech; Rocky Hill, NJ). This IL-1 concentration has previously been shown to yield nearly complete depletion of sGAGs from bovine articular cartilage explants within two weeks[21]. The control and IL-1-treated explants were cultured for up to 10 days, with media changed and collected every 48 hours. Six explants per group were removed from

culture at days 0, 2, 4, 6, 8, and 10 for EPIC-μCT scanning and subsequent destructive analysis.

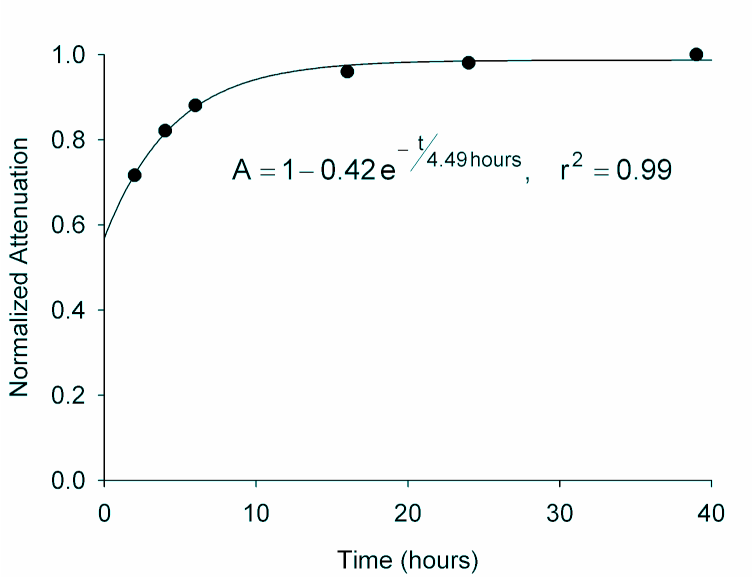

Figure 4.2: Time course of Hexabrix equilibration in full-thickness immature bovine cartilage explants (p=0.0001).

4.2.4 μCT Scanning and Analysis

After removal from culture, each explant was incubated with 1mL full-strength Hexabrix™ supplemented with protease inhibitors at 37°C under gentle agitation for 24hrs, exceeding the time required for full equilibration (Figure 4.2). Explants were then patted to remove excess fluid and loaded 6 per batch into custom μCT chambers. All scanning was performed in air using a VivaCT 40 (Scanco Medical; Switzerland) at 45kVa, 133mA, 200ms integration time, and a voxel size of 21μm. Though scan time varied with the thickness of the explant, two explants were scanned in parallel in an average of 15 minutes. After scanning, explants were immersed in 2mL of 0.15M PBS

supplemented with protease inhibitors for 24 hours at 4°C to allow for desorption of the Hexabrix™. One explant per condition per time point was reserved for subsequent histological analysis. The remaining explants were placed in fresh PBS and protease inhibitors and stored at -20°C until further biochemical analysis.

Using Scanco software, a histogram of the X-ray attenuation readings was generated and used to determine an appropriate threshold for image processing. The average X-ray attenuation was than calculated for the thresholded volume of each full-thickness explant. To visualize the spatial variation in sGAG content, 3D color images representing the range of X-ray attenuation values within a sample were generated using Scanco image processing software. Note that valid comparisons between samples and accurate quantification of FCD require that consistent scan and threshold parameters be used for all samples and standards.

4.2.5 Biochemical Analysis

Following EPIC-μCT scanning, explants reserved for biochemical analysis were lyophilized for 18 hours and solubilized with 1mg/mL proteinase K (EMD Biosciences; San Diego, CA) in 100mM ammonium acetate (pH 7.0). The digested explants and conditioned media were then assayed for sGAGs via the 1,9-dimethylmethylene blue (DMMB) colorimetric assay with shark chondroitin sulfate (Sigma; St. Louis, MO) as a standard[90].

4.2.6 Histology

For comparison with the 3D spatial images generated by EPIC-μCT, a subset of full thickness explants was stained for sGAGs by safranin-O. Explants reserved for

histology were placed in 10% neutral buffered formalin for 72 hrs at 4°C before being transferred to 70% ethanol at 4°C until paraffin embedding and processing. Explants were cut down the longitudinal axis, creating two cylindrical halves. After paraffin embedding, 5μm-thick sections through the entire explant thickness were removed using a rotary microtome. Sections were stained for sGAGs using a 0.1% safranin-O solution with a 0.2% aqueous solution of fast green used as a counter stain.

4.2.7 *In Situ* Imaging of Rabbit Femur

A femur was obtained post-mortem from a ~3 month old rabbit from an unrelated study and dissected free of surrounding tissue (Figure 4.3A). In preliminary experiments, the ability to visualize soft tissue during *in situ* imaging of an immature rabbit femur was highly dependent on the concentration of the Hexabrix™ equilibration solution. Use of the full strength Hexabrix™ solution (100%) provided excellent visualization of surface topology but the enhanced radiopacity of the soft tissue proved too similar to that of bone to allow reproducible identification of the tissue interface. As the Hexabrix™ solution was diluted with 0.15M PBS, the radiopacity of the soft tissue linearly decreased and the cartilage could be more readily distinguished from the underlying bone (Figure 4.4 inset). Note that dilution of the Hexabrix™ solution also decreases the sensitivity of the attenuation to differences in tissue FCD, and additional analyses are required to determine whether an intermediate contrast agent concentration will allow the cartilage to be distinguished from the bone while simultaneously facilitating accurate quantification of the FCD. Based on results of dilution studies, the femur was immersed for 1 hour in 40/60% (v/v) Hexabrix™/0.15M PBS at 37°C under gentle agitation. The femur was scanned at a 21μm voxel resolution in a VivaCT 40 and evaluated after selecting an

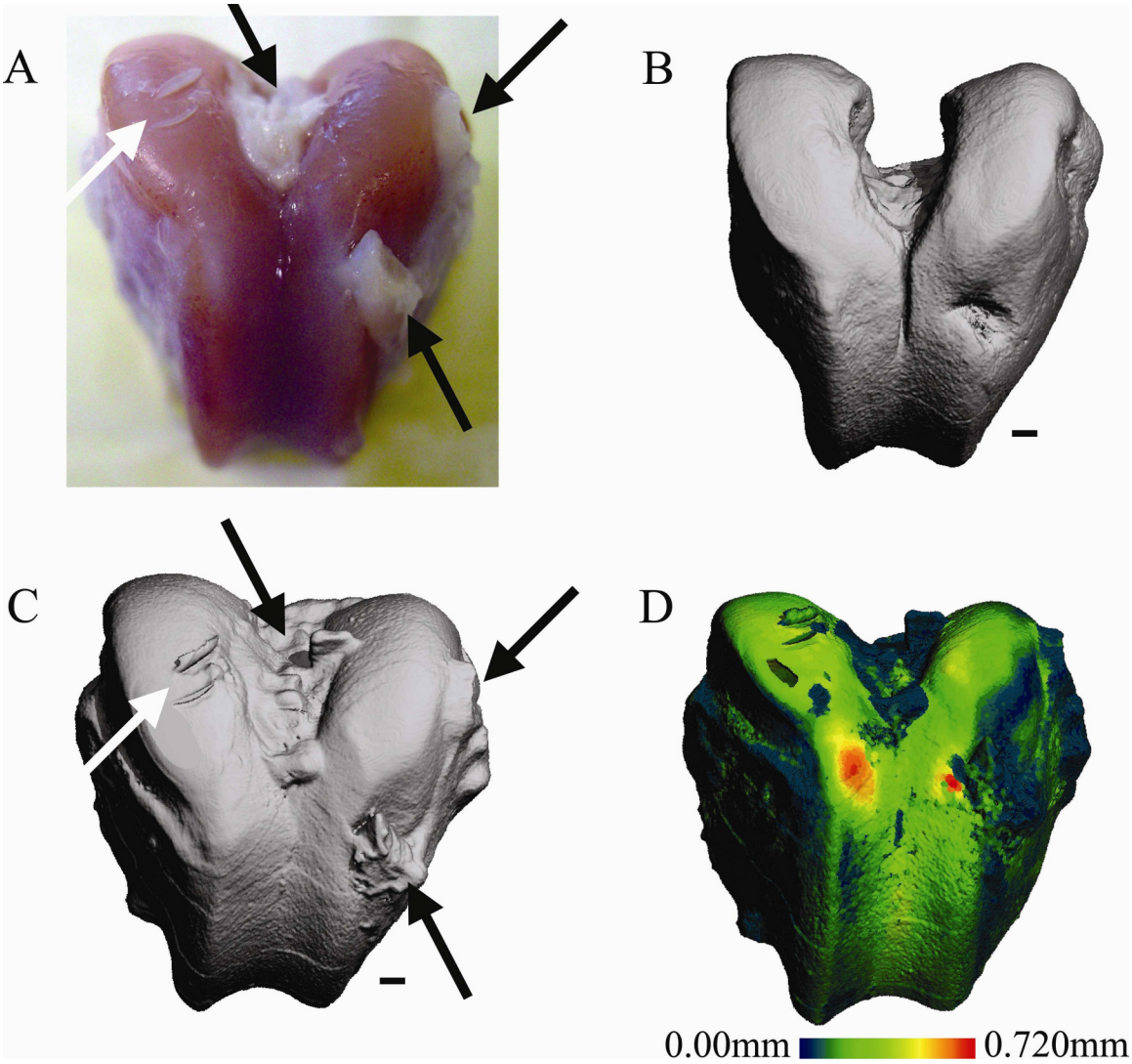

Figure 4.3: In situ imaging of a rabbit femur via EPIC-µCT: (*A*) Color Photograph of a dissected rabbit distal femur. (*B*) µCT scan taken after Hexabrix desorption reveals only the bone geometry. (*C*) µCT scan taken after Hexabrix equilibration demonstrates the ability to visualize the articular surface. Remnants of soft tissues (black arrows) and scalpel cuts to the cartilage (white arrows) can be seen both in the photograph and in the EPIC-µCT image. (*D*) A thickness map generated after segmentation of soft tissue and bone demonstrates the ability to quantitatively analyze soft tissue morphology (scale bars=1 mm).

appropriate threshold (Figure 4.3C). A histogram of the X-ray attenuation values obtained revealed two, partially overlapping peaks corresponding to contrast-enhanced soft tissues and calcified bone (Figure 4.4). The soft tissue peak was isolated from the data set using lower and upper thresholds, and a corresponding soft tissue volume was generated. Using a direct distance transformation algorithm (Scanco), a thickness map of the soft tissue volume was generated (Figure 4.3D). Following desorption of the contrast agent for 1 hr in 0.15M PBS, the femur was rescanned at 21μm and evaluated at the same threshold settings as the control image (Figure 4.3B).

4.2.8 Statistics

Unless otherwise indicated, all results are reported as mean ± SEM. Minitab Release 12.23 (State College, PA) was used for all statistical analyses. Average X-ray attenuation and sGAGs released to the media with time were evaluated using a two factor (treatment and culture time) general linear model and using Tukey's test ($p<0.05$) for pairwise comparisons. The relationship between explant sGAG concentration and average X-ray attenuation was examined via linear regression analysis.

4.3 Results

4.3.1 *In vitro* Cartilage Degeneration Model: EPIC-μCT Images

Three-dimensional images obtained from EPIC-μCT scanning were used to visualize the sGAG distribution in full-thickness control and IL-1-stimulated explants (Figure 4.4). Consistent with the assumed inverse partitioning of the negatively-charged ioxaglate dimer within the ECM of cartilage, low X-ray attenuation corresponded to regions of high sGAG content and high X-ray attenuation indicated regions of low sGAG

content. Control explants showed little visible variation in X-ray attenuation with culture time. In contrast, increases in X-ray attenuation were apparent for IL-1-stimulated explants beginning at day 4. In our full thickness explant model, increases in X-ray attenuation appeared first in the superficial zone, deep zone and on the outer surfaces of the IL-1 stimulated explants and progressed towards the interior with time.

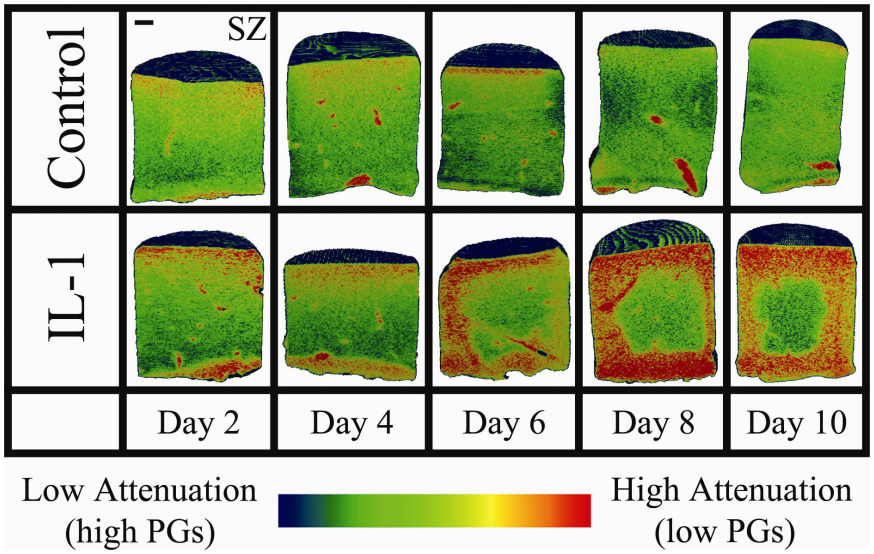

Figure 4.4: Representative 3D EPIC-μCT images of control and IL-1-stimulated explants at 2-day intervals demonstrate progressive increases in attenuation in IL-1-stimulated samples. SZ denotes superficial zone (scale bar=1mm).

4.3.2 *In vitro* Cartilage Degeneration Model: Safranin-O Histology

Histological sections revealed similar patterns of sGAG depletion. In longitudinal sections taken from the center of full-thickness explants, control explants exhibited a dense, uniform distribution of sGAGs (Figure 4.5). In contrast, IL-1-stimulated explants exhibited visible decreases in sGAG staining beginning at day 4 and continuing throughout the culture period. The decreased staining in the IL-1 group consistently

progressed from the superficial zone, deep zone and the outer surfaces inward, consistent with the locations of increased attenuation in the EPIC-μCT images.

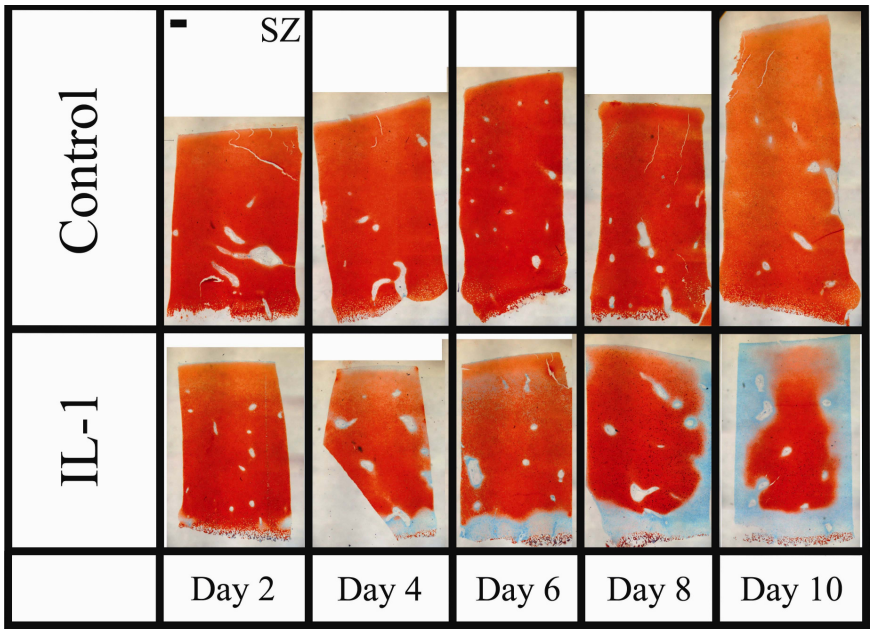

Figure 4.5: Representative safranin-O-stained sections indicate a progressive loss of sGAG content (red staining) in IL-1-stimulated samples, consistent with the EPIC-μCT images. SZ denotes superficial zone (scale bar = 1mm).

4.3.3 *In vitro* Cartilage Degeneration Model: Quantitative Changes in PG Content

Consistent with the EPIC-μCT and histology images, the overall average X-ray attenuation for the full-thickness control explants did not significantly vary with culture time (Figure 4.6). In contrast, the attenuation of IL-1-stimulated explants progressively increased, with levels significantly higher than in control explants beginning at day 6. The increased release of PGs to the media in response to IL-1 treatment was consistent with the increase in X-ray attenuation. Full-thickness control explants released a low

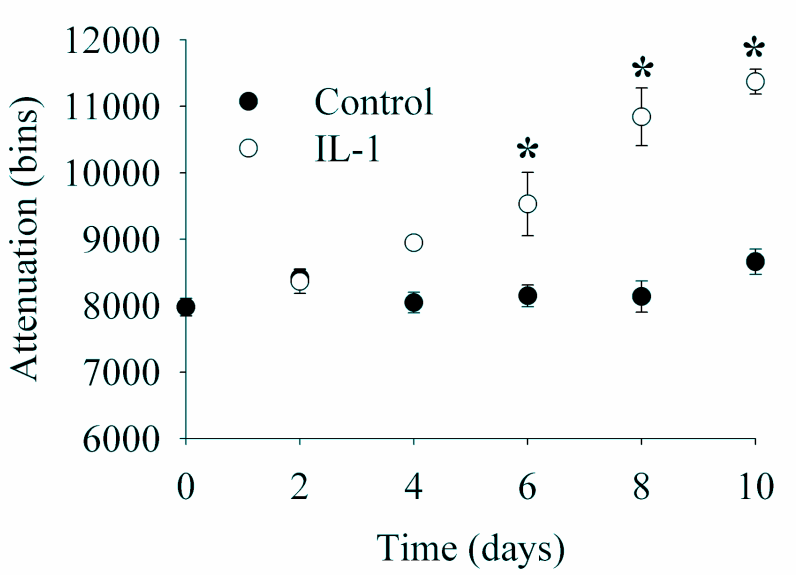

Figure 4.6: Average X-ray attenuation for control and IL-1-stimulated explants over 10 days of culture. * denotes $p<0.05$ between control and IL-1-stimulated explants (n=6, mean±SEM).

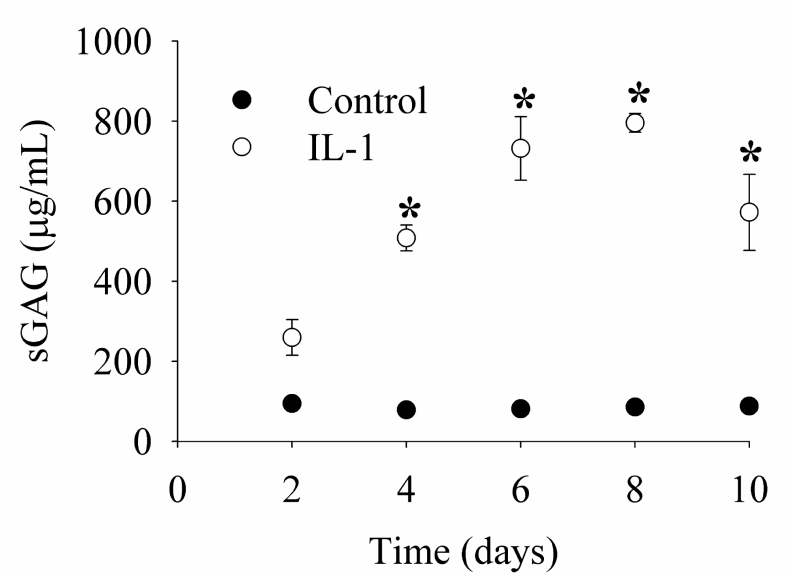

Figure 4.7: sGAG release to the media for control and IL-1-stimulated explants over 10 days of culture. * denotes $p<0.05$ between control and IL-1-stimulated explants (n=6, mean±SEM).

level of sGAGs throughout the 10 day culture (Figure 4.7). In contrast, IL-1-stimulated cartilage showed a characteristic rise in media sGAG levels that peaked at day 8 and was significantly elevated over control explants beginning at day 4. The progressive loss of sGAGs to the media was consistent with both reduced safranin-O staining and increased attenuation in EPIC-μCT analysis.

4.3.4 Correlation of X-ray Attenuation and sGAG concentration

To directly examine the relationship between explant composition and X-ray attenuation, both control and IL-1-stimulated cartilage explants were digested and analyzed for sGAG content following EPIC-μCT scanning. A linear regression analysis revealed a significant correlation (r^2=0.91, $p<0.0005$) between X-ray attenuation and sGAG/H_2O (Figure 4.8). The negative Pearson coefficient, r= -0.95, agreed with the assumed inverse distribution of a negatively charged contrast agent and sGAGs within the ECM.

4.3.5 *In Situ* EPIC-μCT Imaging of a Rabbit Joint

The reconstructed image of an immature rabbit femur after exposure to a 40/60% solution of Hexabrix™/0.15M PBS reveals articular surface topography and soft tissue features (Figure 4.3A and 4.3C) absent from a control image following desorption of the contrast agent (Figure 4.3B). In particular, the EPIC-μCT images demonstrate the ability to distinguish ligament insertion points (black arrows) and a scalpel registration mark in the articular surface (white arrow). Following segmentation of cartilage from bone using thresholds identified from the histogram, a thickness map of the articular cartilage surface

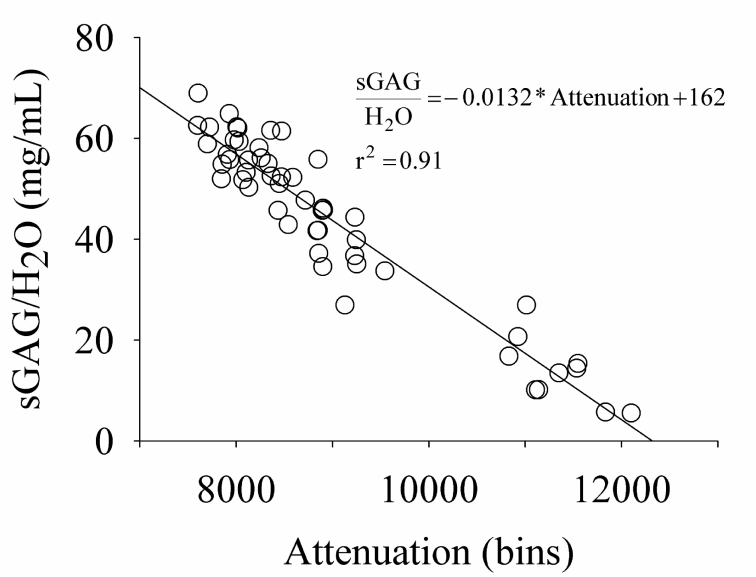

Figure 4.8: Inverse relationship between average X-ray attenuation and the measured sGAG density for combined control and IL-1-stimulated explants ($p<0.0005$).

layer (Figure 4.3D) indicates thickness values that are consistent with the anticipated regional variations in rabbit articular cartilage thickness.

4.4 Discussion

Noninvasive techniques capable of detecting PG content and distribution and tissue morphology could dramatically improve upon existing evaluation options for monitoring the efficacy of osteoarthritis treatments and cartilage repair strategies. This work details the development of EPIC-μCT, a novel technique for the 3D, quantitative imaging of PGs in soft tissues. Using IL-1 stimulation of articular cartilage as an *in vitro* degradation model, the ability of EPIC-μCT to monitor the progressive loss of sGAGs from cartilage explants was demonstrated. In addition, the strong correlation found between X-ray attenuation and sGAG density indicates that this technique can be used not only to monitor relative changes in sGAG content and distribution but also to

quantitatively evaluate sGAG content, a feature that may prove useful for *in vitro* analysis of matrix changes in studies of tissue degeneration and development of tissue engineered constructs. EPIC-μCT also shows the ability to produce 3D images of the articular surface of cartilage *in situ*, illustrating potential applications in monitoring surface contours and engineered construct integration in defect repair studies as well as regional variations in cartilage thickness.

The EPIC-μCT technique is complementary to several other methods that have recently been introduced. Contrast-enhanced MRI techniques including dGEMRIC have shown success in monitoring PG concentration in cartilage *in vitro* and clinically[109,110], but the resolution of current clinical MRI systems (~300μm) and high-powered research MRI systems (~25μm in-plane) may limit their application in small animal models. The use of gadolinium-based contrast agents with μCT has also shown the potential to monitor PG content in cartilage explants[78]. OCT[70] and FT-IRIS[71] may also be useful in the noninvasive monitoring of cartilage ECM changes, potentially providing information on collagen and PG contents. While the later methods provide high resolution planar images, quantitative analyses of 3D distributions and morphology are not currently possible. Although not currently viable as a clinical imaging modality, the ability to simultaneously provide quantitative data regarding tissue composition and morphology makes EPIC-μCT a powerful new research tool.

With the noninvasive, high resolution monitoring capability of μCT, the greatest benefit of this technique may lie in the assessment of ECM changes in rodent models of cartilage degeneration and regeneration. A promising extension of this work is the application of EPIC-μCT for end-stage analysis of intact cartilage surfaces after

dissection of small animal joints. Furthermore, the capability of commercial μCT scanners for *in vivo* analysis raises the exciting possibility of longitudinal monitoring of cartilage matrix changes during disease or treatment progression in individual animals. A critical step in advancing this technique is the development of accurate methodology for segmenting cartilage from bone in 3D data sets, as the X-ray attenuation of bone and Hexabrix™-equilibrated soft tissue can overlap. The overlap in X-ray attenuation is dependent on the mineral content of the subchondral bone as well as the FCD and water content of the cartilage, all of which can vary with age, health, and species. As demonstrated in the present study, one approach is to dilute the contrast agent sufficiently that the attenuation ranges of the soft tissue and bone become distinct, improving the delineation of the cartilage/bone interface and thus the accuracy of cartilage thickness measurements. However, such dilution simultaneously reduces the sensitivity of the contrast agent concentration to FCD, limiting the PG monitoring capabilities of the technique. If intermediate concentrations can not be identified that allow both morphological and compositional analysis, separate scanning after equilibration in dilute and concentrated contrast agent solutions may be required to fully realize the potential of EPIC-μCT. Additionally, *in vivo* imaging raises additional technical issues involving the delivery and retention of a sufficient volume and concentration of the contrast agent. Intraarticular injection offers a simple and direct approach, although clearance of the contrast agent from the joint space could impair adequate equilibration. Distinguishing between apposed cartilage layers, underlying bone and adjacent soft tissues in a small animal joint will be technically challenging and may or may not be resolvable by varying the imaging window and the concentration of Hexabrix™ delivered. Despite these

potential limitations, the present study establishes the basis for a quantitative, high resolution, 3D imaging technique capable of nondestructively monitoring cartilage matrix organization *in vitro* that may become a powerful tool for analyzing small animal models of cartilage degeneration and regeneration.

CHAPTER 5

MONITORING THE DEVELOPMENT OF TISSUE ENGINEERED CARTILAGE CONSTRUCTS VIA EPIC-MICROCOMPUTED TOMOGRAPHY

5.1 Introduction

Tissue engineered articular cartilage represents an attractive alternative to the more than 475,000 total knee replacements performed annually in the United States to ameliorate debilitating conditions including OA[111]. In evaluating the success of cartilage tissue engineering approaches, replacement tissues are commonly benchmarked against the ECM composition and mechanical properties of native articular cartilage. Thus, significant challenges in developing an engineered cartilage tissue are characterizing matrix deposition and scaffold remodeling *in vitro* and *in vivo* in response to different biochemical and mechanical stimuli and monitoring the integration and function of the replacement tissue *in vivo*. Characterization of the ECM and mechanical properties by traditional methods, including biochemical colorimetric assays, histology, scanning and transmission electron microscopy, immunofluorescense, and mechanical testing, necessitate sample destruction or compromise sample sterility. Larger sample numbers are commonly used to compensate for destructive analysis, leading to increased study size and cost and the potential introduction of sample-to-sample variances.

To overcome the disadvantages of destructive characterization techniques, a number of approaches have emerged for use in the nondestructive monitoring of cellular and acellular tissue engineered replacements. Fluorescent labeling of cells (e.g. via Green Fluorescent Protein) and scaffolds has shown promise in monitoring the proliferation and

localization of seeded cells[112,113] and scaffold degradation[112,114], respectively, and the emergence of quantum dot technology with its superior sensitivity and specificity is likely to increase this approach to monitoring cell interactions in engineered tissues[115]. Similarly, 1H NMR spectroscopy has also been used in tissue engineering applications for monitoring cell viability in implanted agarose gel constructs[116].

Noninvasive imaging of cartilage in particular has been the focus of several applications. dGEMRIC relies on the difference in T1 relaxation between control cartilage and cartilage equilibrated in the negatively charged contrast agent Gd-DTPA^{2-} to quantify the amount and distribution of FCD[109,117]. dGEMRIC has demonstrated the ability to longitudinally monitor changes in FCD within the same sample in both degrading cartilage explants[56] and tissue-engineered cartilage constructs[68]. In tissue engineered cartilage, dGEMRIC FCD measurements were significantly correlated with both equilibrium and dynamic compressive moduli but were weaker predictors of mechanical properties than direct biochemical measurement of FCD[118]. OCT and FT-IRIS have also demonstrated recent success in monitoring matrix accumulation in orthopedic replacement tissues[119-121]. Furthermore, optical coherence elastography, a variant of OCT, has recently been reported to noninvasively measure mechanical strains in developing collagen gels[122].

EPIC-μCT has also proven accurate in noninvasively monitoring change in sGAG content in articular cartilage explants[103]. Like dGEMRIC, EPIC-μCT relies on the exclusion of a negatively-charged contrast agent, Hexabrix™, to quantify the amount and distribution of sGAGs in a tissue. To that end, increases in EPIC-μCT attenuation have previously been shown to correspond to decreases in sGAG content in IL-1-stimulated

cartilage explants. The micron-level resolution, *in vivo* monitoring potential, unrestricted penetration depth, fast scan times, and sophisticated 3D morphometric analysis capabilities of EPIC-μCT represent a unique combination of features not readily available with other cartilage imaging techniques. However, the effects of the EPIC-μCT protocol, which includes X-ray scanning and contrast agent exposure, on matrix biochemistry during long-term cell culture have not been investigated. In addition, the sensitivity of the technique to the low levels of sGAGs found in developing matrices and its ability to delineate spatial patterns of matrix deposition have not been characterized. The objectives of this study were to characterize the effects of the EPIC-μCT protocol on sGAG production, cell proliferation, and cell viability in a longitudinal study of chondrocyte-seeded agarose gels and to investigate the ability of EPIC-μCT to monitor the spatial and temporal development of a bilayer chondrocyte/fibrochondrocyte agarose gel.

5.2 Materials and Methods

5.2.1 Tissue Harvest and Cell Isolation

Bovine stifle joints of 1-2 week old calves were obtained within 36 hours of slaughter (Research 87; Boylston, MA) and dissected under aseptic conditions to expose the menisci and articular surface of the distal femora. Throughout the dissection, tissue was kept hydrated with PBS supplemented with 1X antibiotic/antimycotic (Invitrogen; Carlsdbad, CA). The lateral and medial menisci were removed intact from the tibial plateau. Using a scalpel, serial sections (~1cm^2 x 1mm thick) of articular cartilage were removed from the femoral condyles and groove but the deep, vascularized cartilage was avoided. Prior to isolating cells from each tissue type, tissue samples were diced into

smaller sections (~1mm^3) to improve the efficiency and cell viability of the isolation process. The pieces were added to separate T-75 flasks (Becton Dickinson; Franklin Lakes, NJ) containing a digestion solution consisting of DMEM, 1X Penicillin/Streptomycin/Neomycin, 1X Kanamycin Sulfate, 1X Fungizone (Invitrogen), and 0.4% type II collagenase (Sigma; Saint Louis, MO). Digestion of the ECM was allowed to progress for 24-36 hours, or until the tissue was visibly digested. The digest solution was then strained through 37 μm nylon mesh (Small Parts; Miami Lakes, FL) and subjected to 1300 rpm for 7 min in an Allegra 6 Centrifuge (Beckman Coulter; Fullerton, CA) to isolate a cell pellet. The collagenase solution was aspirated and the cell pellet was resuspended in calcium and magnesium free PBS (Invitrogen). A sample of the cell suspension was analyzed in a Vi-CELL analyzer (Beckman Coulter) to determine the total cell number and number of viable cells. Cells were frozen for future use at -80°C at 15E6 cells/mL in a solution of 10% FBS (Hyclone; Logan, UT), 10% DMSO (Fisher; Waltham, MA), and 80% high glucose DMEM.

5.2.2 Gel Preparation

On the day of cell seeding, cells were rapidly thawed, spun down as described above, and the cryopreservation solution was aspirated. Cells were resuspended in calcium and magnesium free PBS and the cell viability was again analyzed by the Vi-CELL analyzer.

5.2.2.1 Homogenous Constructs

Articular chondrocytes (AC) were combined at 15E6 cells/mL with 3% low-melting temperature agarose (Sigma). Gel slabs were created by sandwiching a 3mm-thick U-shaped piece of FDA-approved rubber between glass plates and subsequently

allowing the agarose-AC mixture to gel in the void for 10 minutes at 4°C (Figure 5.1A). A 3mm diameter biopsy punch (Miltex; York, PA) was used to core out cylindrical gels, resulting in a final dimension of 3mm diameter x 3mm thick.

5.2.2.2 Bilayer Constructs

Bilayer constructs consisted of a layer of meniscal fibrochondrocytes (MFC) and a layer of ACs, each seeded at 20E6 cells/mL in 3% low-melting agarose. The combination of MFCs and ACs were chosen to produce an inhomogeneous construct, given the several fold greater production of sGAGs by ACs relative to MFCs[123]. Gel slabs were formed in a two-step process (Figure 5.1A-C). First, the articular chondrocyte layer was formed by sandwiching a 1.5mm-thick U-shaped piece of FDA-approved rubber between glass plates and allowing the agarose-AC mixture to partially gel in the void for 5 minutes at 4°C. Next, one glass plate was carefully removed and a second 1.5mm-thick U-shaped piece of rubber was stacked on the previous spacer. After replacing the glass plate, the agarose-MFC mixture was allowed to gel in the void between the AC layer and the glass plate for 10 minutes at 4°C. Individual gels were then formed using a 3mm diameter biopsy punch, resulting in a final composite dimension of 3mm diameter x 3mm thick.

5.2.3 Culture Conditions and EPIC-μCT Protocol

5.2.3.1 Homogeneous Constructs

To examine the repeated effects of the EPIC-μCT protocol on sGAG production, cell viability, and cell proliferation, fifty gels were longitudinally monitored over 24 days and assigned to one of five groups (n=10/group): control, Hexabrix, Scan, PBS,

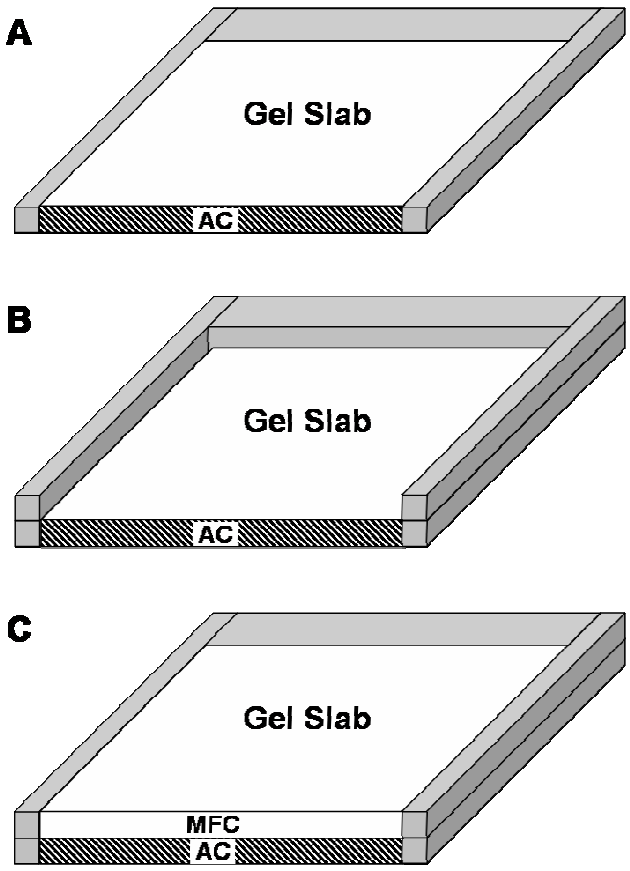

Figure 5.1: Steps in Formation of Homogeneous and Bilayer Agarose Gels: (A) Formation of AC gel slab within U-shaped mold and, for bilayer gels, (B) addition of second spacer, and (C) gelling of MFC gel.

and Hexabrix+Scan. After gelation, gels were place one per well in 24 well plates (Becton Dickinson) in 1.0mL of control medium, which consisted of high glucose DMEM supplemented with 10% FBS, 50μg/mL gentamicin (Invitrogen), 0.1mM non-essential amino acids (Invitrogen), 50μg/mL ascorbate (Sigma), and 1X antibiotic/antimycotic. At days 0, 8, and 16, all gels were subjected to one of five protocols. Gels in the control group were maintained in control medium and saw no additional treatment. The Hexabrix group was removed from control medium and maintained for 2 hours in osmotically-balanced Hexabrix (326 mOsm/kg water, as determined by freeze point osmometry), created by a 1:1 dilution of full strength Hexabrix 320 with sterile distilled water, before being returned to control medium. Gels in the scan group were removed from culture, blotted with a sterile tissue to remove surface fluid, loaded two at a time into custom cassettes (Figure 5.2), and scanned for 17 minutes in a μCT-40 (Scanco Medical; Bassersdorf, Switzerland) before being returned to control medium. The PBS group was removed from culture and exposed for 2 hours to calcium and magnesium free PBS, then blotted and loaded two at a time in custom cassettes and kept at room temp for 17 minutes (to simulate the scanning time) before being returned to culture. Gels in the Hexabrix+Scan group were exposed to the Hexabrix protocol followed by the Scan protocol before being returned to culture. All gels were maintained at 37°C and 5%CO_2 throughout the culture period, except when removed for scanning. Media were collected and replaced every 48 hours, with conditioned media from the protocol period discarded for consistency in the length of time that collected media were exposed to all groups. At the conclusion of the protocol on days 0, 8, and 16, one sample per condition was removed from culture for viability and histological

analysis. At day 24, one sample per condition was removed from culture for cell viability and histology analysis and all remaining samples were exposed to the Hexabris+Scan protocol to determine the endpoint EPIC-μCT attenuation. Following a 2 hour submersion in calcium and magnesium free PBS and protease inhibitors to allow for Hexabrix desorption, gels were frozen in fresh calcium and magnesium free PBS at -20°C until biochemical analysis.

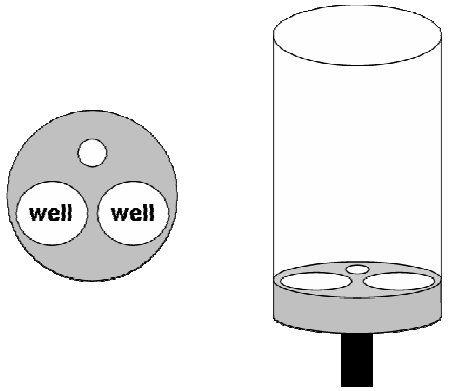

Figure 5.2: Schematic of custom chambers for EPIC-μCT scanning, showing close-up of cassette cross section (left) and cassette in μCT sample tube (right).

5.2.3.2 Bilayer Constructs

To monitor the spatial and temporal development of heterogeneous constructs, forty bilayer gels were cultured for up to 48 days. After gelation, gels were place one per well in 24 well plates (Becton Dickinson) in 1.0mL of control medium, as previously described. At days 0, 8, 16, 32 and 48, eight samples were removed from culture for EPIC-μCT evaluation. Each sample was exposed to a 477 mOsm/kg H_2O solution of Hexabrix, created by a 2:3 dilution with diH2O, for 2 hours at 37°C under gentle agitation. Agarose gels were then blotted, loaded 2 per cassette, 4 cassettes per sample

tube (Figure 5.2) and scanned at a 21μm voxel resolution in a μCT-40 scanner. Following a 2 hour submersion in calcium and magnesium free PBS and protease inhibitors to allow for Hexabrix desorption, gels were frozen in fresh ion-free PBS at -20°C until biochemical analysis.

5.2.4 Biochemical Analysis

Gels were thawed at 37°C. The two layers comprising the bilayer gels were dissected under a magnifying glass, based on the visual difference in ECM opacity, to analyze each layer separately. All gels were weighed wet, lyophilized for 12 hours, and weighed dry. Gels were digested via a sequential proteinase K/β-agarase digestion. First, gels were treated with 0.2-0.4mg/mL proteinase K (Fisher) in 100mM ammonium acetate at 60°C for 18 hours, with periodic vortexing. Proteinase K, which also acts on β-agarase, was then deactivated by incubation of the samples at 100°C for 10 minutes. For agarose digestions, gels were first equilibrated to 45°C. Next, each gel was treated with 2U of β-agarase for 3-4 hours at 45°C. sGAG content in the conditioned media and digests were analyzed on a microtiter plate reader (PowerWave X340; Biotek; Winooski, VT) at 525nm by the 1,9-dimethylmethylene blue assay[90] using shark chondroitin sulfate (Sigma) as standards.

5.2.5 Strain Analysis

At days 32 and 48, gels were shipped on ice in calcium and magnesium free PBS with protease inhibitors to the Cartilage Tissue Engineering Laboratory at the University of California San Diego, where the depth-dependent strain profile of four bilayer constructs was analyzed using the 2D microscopy technique originally developed by

Schinigal et al[28] and refined by others[98,124]. Briefly, gels were exposed to a solution of PBS and protease inhibitors containing ethidium homodimer and calcein AM for 1hour at 4°C to stain cell nuclei. Gels were sectioned along the longitudinal axis to produce two hemi-cylindrical sections. One cylindrical half was placed in a custom chamber (Figure 5.3) A fluorescence image was taken of the sample in the uncompressed state as a reference image (2.9mm x 1.2mm field of view, 8-bit grayscale) for tracking the movement of cell nuclei. After placing the sample between two non-porous platens and applying a small pre-load, a 300μm (nominal 10% of gel thickness) axial compression step was applied at 10μm/s. After a 1 hour stress relaxation period, another image was acquired with the microscope. For each sample, the movements of cell nuclei from the reference to the compressed states were analyzed using a custom image correlation script developed in MATLAB 7.0 (Mathworks; Natick, Massachusetts) to determine the displacement field throughout the construct thickness. Lagrangian strains were calculated for each sample from the gradient of the measured displacement field, where w denotes displacement in the z direction, according to equation 5.1.

$$E_{zz} = \frac{\partial w}{\partial z} \tag{5.1}$$

5.2.6 Cell Viability and Proliferation

To analyze the repeat effects of the EPIC-μCT protocol on cell viability, homogeneous agarose gels from each time point and condition were stained with a commercial fluorescent live/dead kit (Molecular Probes; Eugene, OR). Immediately after removal from culture, one cylindrical half of each sample was exposed to 2μM calcein AM and 4μM ethidium homodimer (Molecular Probes; Eugene, OR) in calcium and

magnesium free PBS at 37°C for 30 minutes under gentle agitation. This was followed by two, sequential washes in calcium and magnesium free PBS for 15 minutes each. Fluorescence images were obtained by dual channel excitation at 488nm and 543nm, with emission captured at 500-530nm and via a long pass filter at 560nm using an LSM 510 confocal microscope (Zeiss; Germany). All images were acquired using a 10X objective and using the same gain settings.

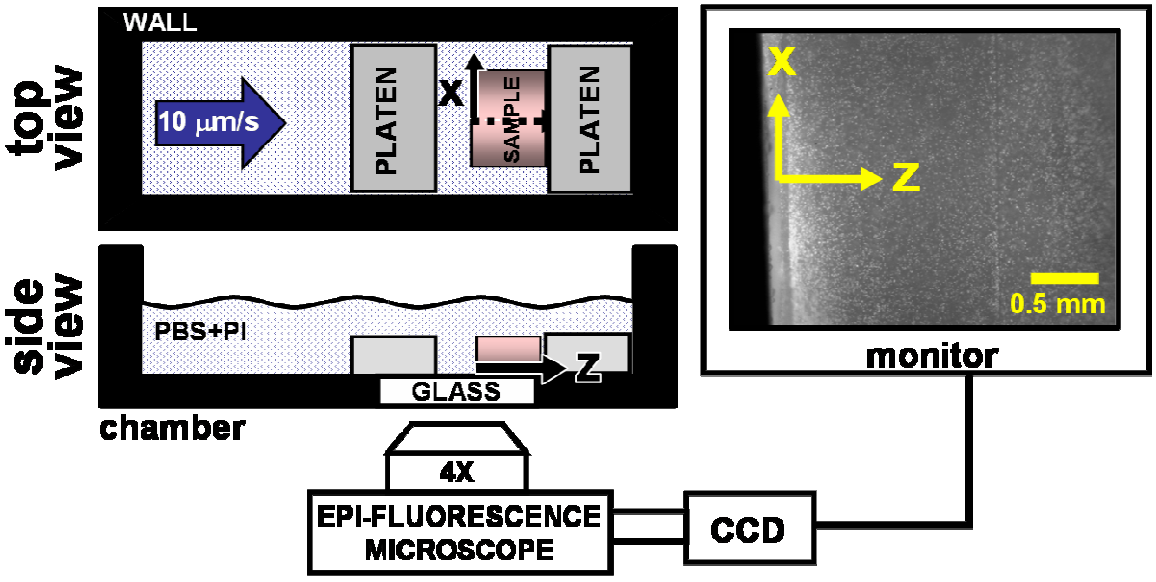

Figure 5.3: Two-dimensional Strain Microscopy Setup illustrating the location of the agarose gel relative to the platens and epi-fluorescence microscope (left) and a representative image of a bilayer construct showing the stained cell nuclei (right) (courtesy of CTEL, UCSD).

As an indication of cell proliferation, all homogeneous agarose gels were exposed to fresh basal media supplemented with 100μL WST-1 quick cell proliferation reagent (Biovision; Mountain View, CA) for two hours prior to EPIC-μCT scanning on day 24. The media were then collected and measured at 440nm and 650nm on a multiwell

colorimetric plate reader. Data are reported as the difference in the readings at 440nm and 650nm (background), normalized to a control sample of WST-1 reagent. The colorimetric assay measures the increase in the formation of formazan dye, which is formed as a byproduct of mitochondrial dehydrogenase activity.

5.2.7 Histology

Safranin-O was used to examine sGAG distribution by histology. After removal from culture, samples for histology were fixed for 12 hours at 4°C in neutral buffered formalin (VWR). Samples were stored at 4°C in 70% ethanol until paraffin processing and embedding. After paraffin embedding, 5μm-thick sections through the entire explant thickness were removed using a HM 355S rotary microtome (Microm; Walldorf, Germany). Sections were stained for sGAGs using a 0.1% safranin-O solution, for cell nuclei using Weigert's Iron Hematoxylin stain, and with a 0.2% aqueous solution of fast green as a counter stain.

5.2.8 Statistics

Minitab Release 14 (State College, PA) was used for all statistical analyses, with $p<0.05$ considered significant. Average X-ray attenuation and overall sGAG content with time were evaluated using a general linear model with Tukey's test for pairwise comparisons. Comparisons between the EPIC-μCT treatment groups at a given time point were evaluated using the general linear model with Dunnett's test for pairwise comparisons to the control group. Differences between AC and MFC zones at a single time point in the bilayer study were compared using a general linear model with Tukey's test for pairwise comparisons between zones.

5.3 Results

5.3.1 Longitudinal Study

5.3.1.1 EPIC-μCT Monitoring

To examine the ability of EPIC-μCT to monitor the progressive accumulation of sGAGs in engineered constructs, the Hexabrix+Scan group was followed throughout the 24 day culture. EPIC-μCT analysis of the Hexabrix+Scan group indicated a progressive decrease in attenuation with time (Figure 5.4), which is indicative of an increase in sGAG content. This trend was also confirmed in representative EPIC-μCT images of the Hexabrix+Scan group cross sections (Figure 5.5), where a progressive, uniform decrease in attenuation was observed with time.

To examine the repeated effect of the EPIC-μCT protocol on matrix composition, gels from all conditions were analyzed by EPIC-μCT at day 24. The Hexabrix+Scan group measured a higher attenuation relative to the control treatment ($p<0.05$), but no other treatment group was significantly different from the control gels (Figure 5.6).

5.3.1.2 Matrix Biochemistry Analysis

To monitor the effect of the EPIC-μCT protocol on sGAG production and retention, sGAGs released to the media and accumulated in the gels were quantified. No differences in the cumulative amount of sGAGs released to the media were seen with treatment at any point during the 24 day culture (Figure 5.7). At the conclusion of the study, the sGAG content in each agarose gel was measured by the DMMB colorimetric

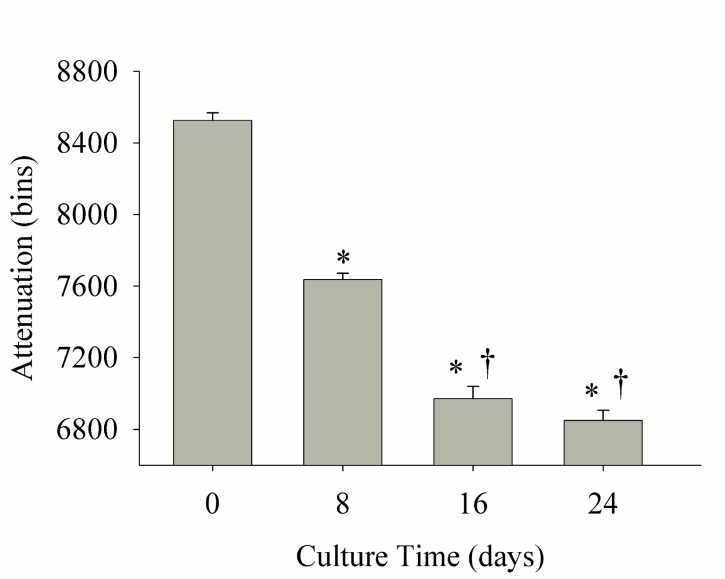

Figure 5.4: EPIC-µCT attenuation decreases with time in longitudinally-monitored homogeneous agarose gels, indicating a progressive increase in sGAG accumulation. * denotes $p<0.05$ versus day 0 and † denotes $p<0.05$ versus day 8 (n=5-6, mean+SEM).

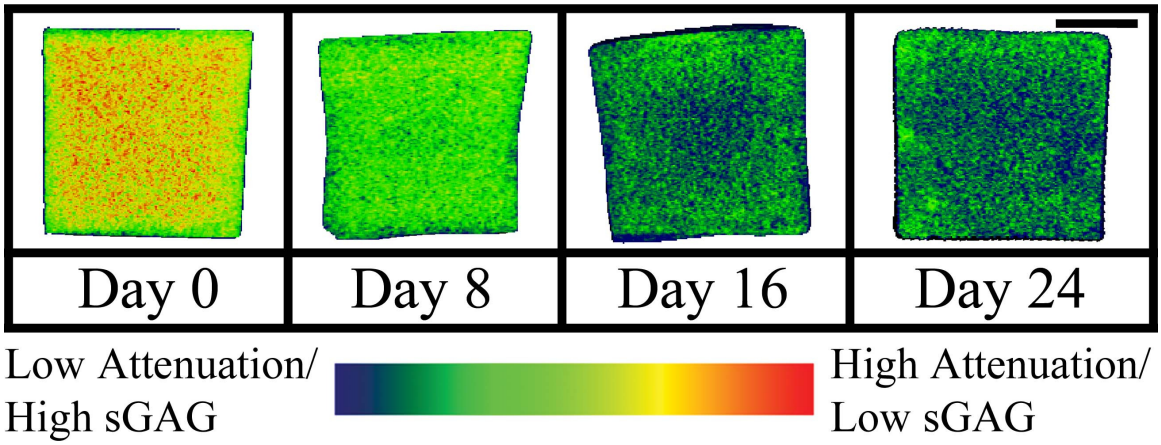

Figure 5.5: Three-Dimensional representative EPIC-µCT images of homogeneous agarose gel constructs illustrating a progressive decrease of attenuation with time. Scale bar=1mm

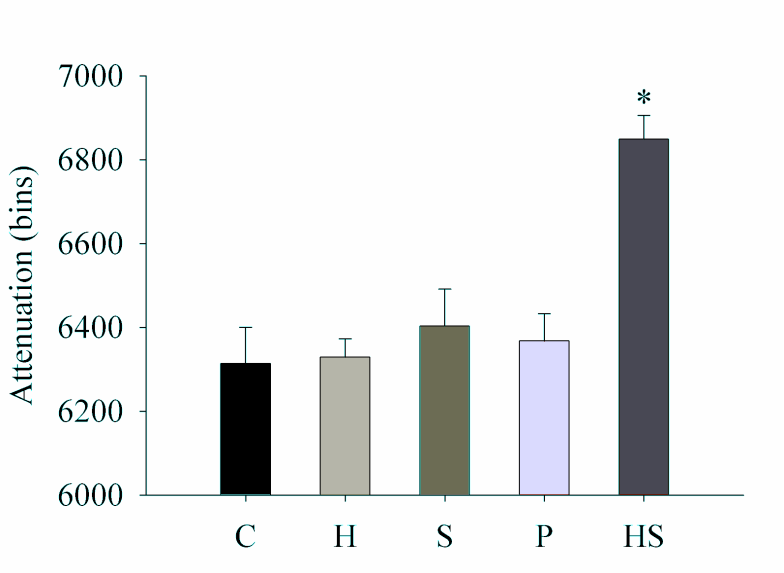

Figure 5.6: EPIC-µCT attenuation for all treatment groups at Day 24. * denotes $p<0.05$ versus C. C=Control, H=Hexabrix, S=Scan, P=PBS, HS=Hexabrix+Scan (n=3-6, mean+SEM). Note the truncated attenuation scale.

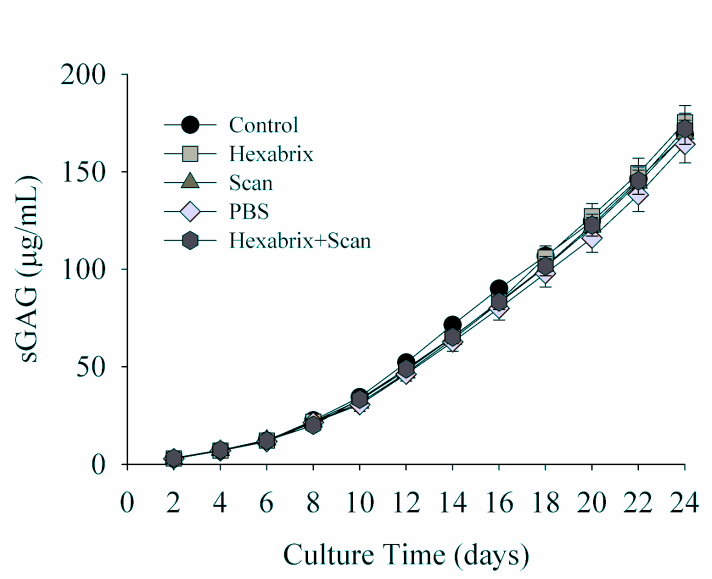

Figure 5.7: Cumulative sGAG released to the media as a function of treatment and culture time (n=6, mean±SEM).

assay. Consistent with the EPIC-µCT attenuation findings at day 24, the Hexabrix+Scan group had significantly lower sGAG content relative to control gels, with no other significant differences from the control group (Figure 5.8). Together with the release data, this suggests that the cells in the Hexabrix+Scan group synthesized fewer sGAGs over the 24 days. Safranin-O histology sections (Figure 5.9) indicate uniform sGAG deposition in the interior of the constructs.

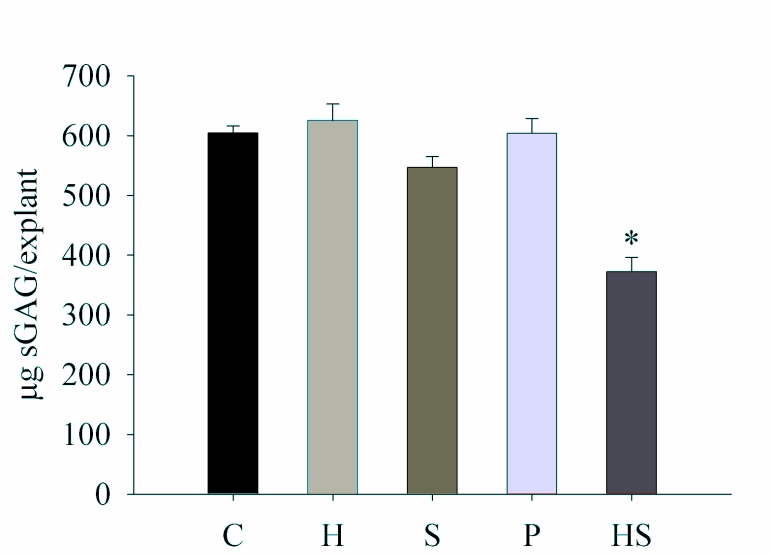

Figure 5.8: Day 24 sGAG content as a function of treatment condition. * denotes $p<0.05$ versus Control. C=Control, H=Hexabrix, S=Scan, P=PBS, HS=Hexabrix+Scan (n=3-6, mean+SEM).

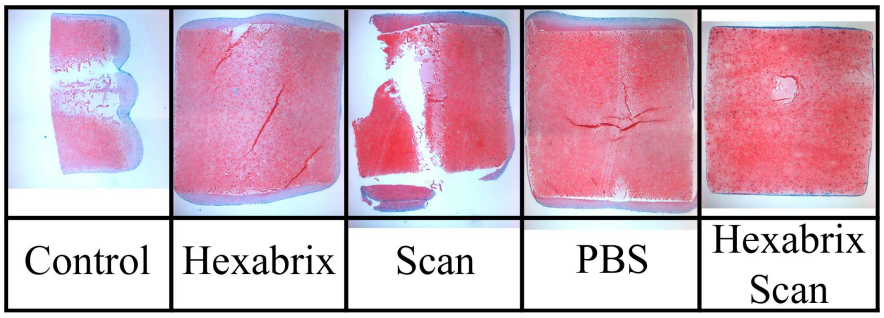

Figure 5.9: Safranin-O stained cross sections of day 24 homogeneous agarose gels illustrate the distribution of sGAGs (red) and non-sGAG-rich ECM (green).

5.3.1.3 Cell Viability and Proliferation

Cell viability and proliferation were measured to assess the potential cytotoxicity of the different treatments on the seeded articular chondrocytes. The WST-1 cell proliferation assay indicated a significant decrease in chondrocyte activity for the Hexabrix+Scan group relative to the control treatment (Figure 5.10). Live/Dead staining of constructs at day 24 were qualitatively consistent with the WST-1 results, with more cell death apparent in the Hexabrix+Scan group, followed by the Scan group, and the other treatments (Figure 5.11).

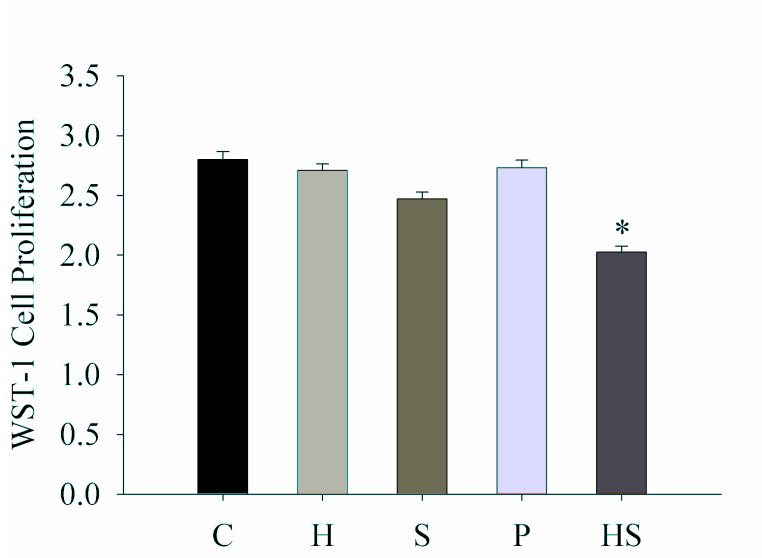

Figure 5.10: WST-1 data for the different treatment conditions at day 24. * denotes $p<0.05$ versus Control. C=Control, H=Hexabrix, S=Scan, P=PBS, HS=Hexabrix+Scan (n=3-6, mean+SEM).

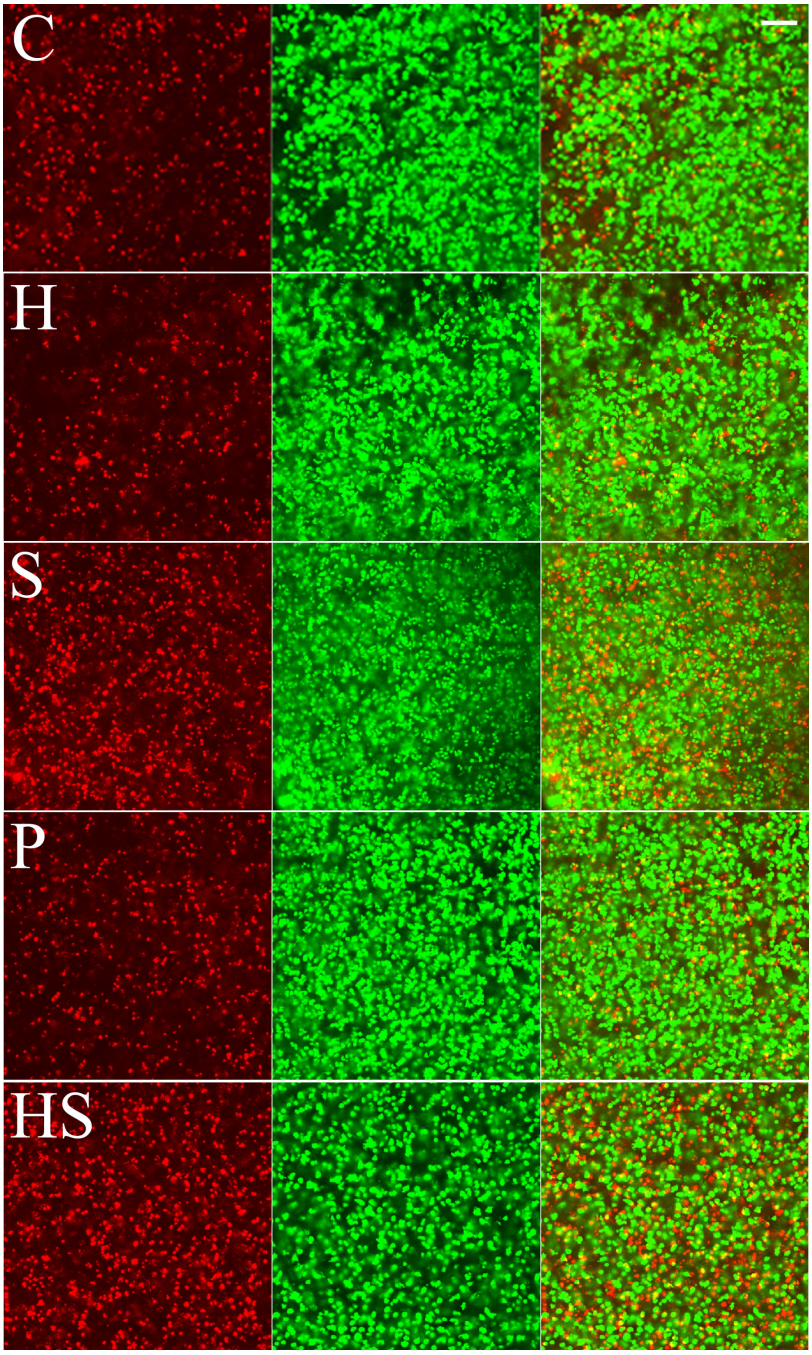

Figure 5.11: Live/Dead Staining of the EPIC-μCT treatment groups at day 24, showing ethidium homodimer staining for dead cells (left), calcein AM staining for live cells (middle), and composite images (right). C=Control, H=Hexabrix, S=Scan, P=PBS, HS=Hexabrix+Scan (scale=100μm).

5.3.2 Bilayer Study

5.3.2.1 EPIC-µCT Attenuation Monitoring

EPIC-µCT analysis showed a progressive decrease in overall attenuation with time, indicative of an increase in sGAG content during construct development (Figure 5.12). EPIC-µCT images of the bilayer gels illustrate a progressive decrease in attenuation with time, as well as regional attenuation differences indicative of differences in the matrix deposition of the AC and MFC layers (Figure 5.13). As early as day 8, the AC layer (bottom) shows a lower attenuation (or higher sGAG content) than the MFC layer (top), which is consistent with the known higher sGAG synthesis rates of ACs relative to MFCs[123] .

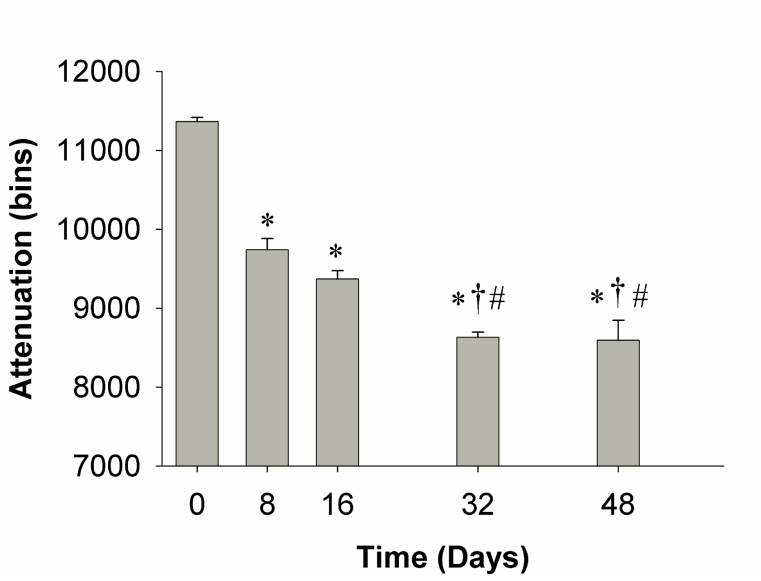

Figure 5.12: Overall EPIC-µCT attenuation of bilayer constructs with time. * denotes $p<0.05$ versus day 0, † denotes $p<0.05$ versus day 8, and # denotes $p<0.05$ versus day 16 (n=8, mean+SEM).

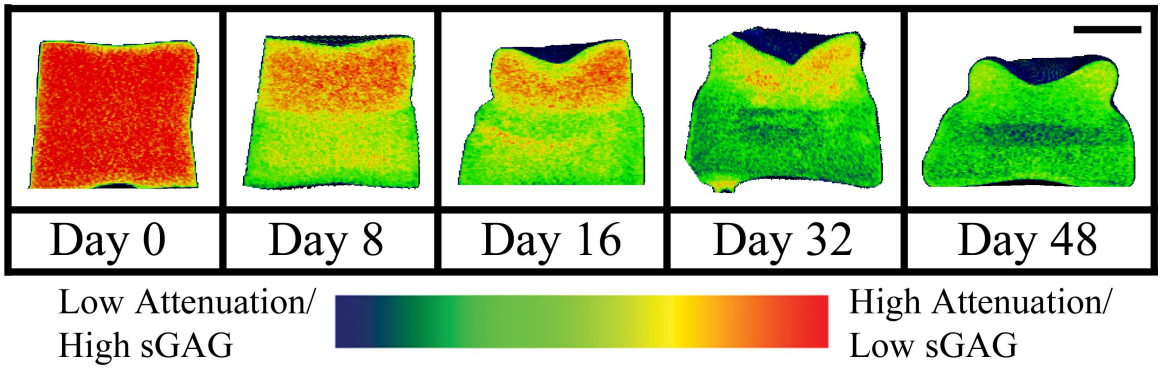

Figure 5.13: Representative 3D EPIC-µCT images illustrating the developing patterns of attenuation in bilayer constructs. MFC layer is on top of AC layer (scale=1mm).

5.3.2.2 Matrix Biochemistry

sGAG contents of the individual layers comprising the bilayer gels were analyzed by the DMMB assay (Figure 5.14A). Significant differences in sGAG/H_2O were noted between layers, with the AC layers possessing significantly higher sGAG contents at days 8, 16, and 32. This pattern is consistent with both the EPIC-µCT images and the higher sGAG synthesis rate of ACs. When analyzed as total constructs, the bilayer gels showed a progressive increase in sGAG/H_2O content with time (Figure 5.14B), or the expected inverse trend of the overall attenuation. Note that the volume fraction of the MFC layer was significantly smaller than the AC layer, resulting in an overall construct sGAG content that is weighted more heavily by the content of the AC layer.

Safranin-O staining for sGAGs supported the EPIC-µCT images and matrix biochemistry results (Figure 5.15). Clear delineations of the MFC layer (top) and AC layer (bottom) were apparent by the distribution and intensity of sGAGs. The histology images also support a general increase in sGAG content with time.

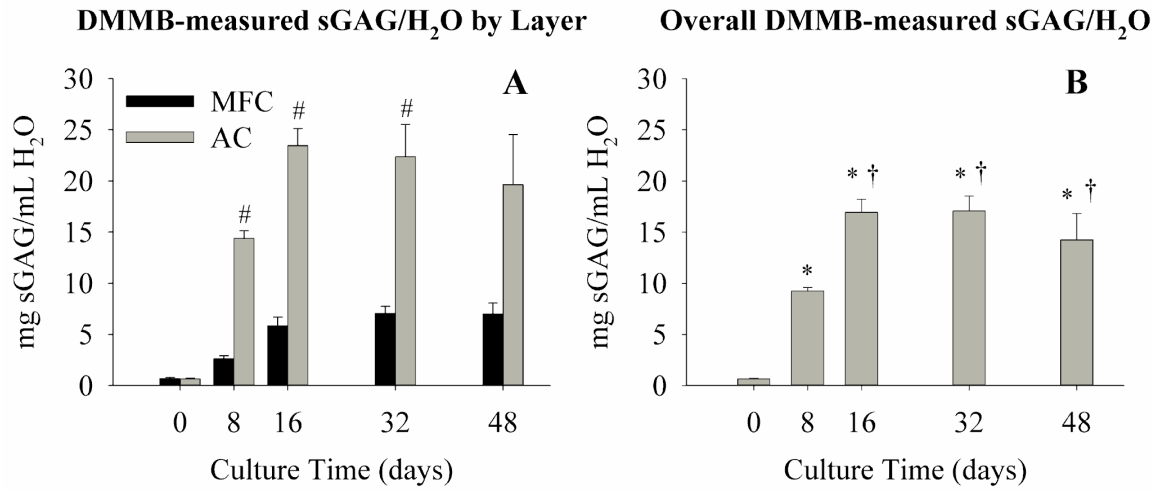

Figure 5.14: DMMB-measured sGAG content in bilayer constructs (A) within MFC and AC layers and (B) over the total construct. # denotes $p<0.05$ between MFC and AC layer, * denotes $p<0.05$ versus day 0, and † denotes $p<0.05$ versus day 8 (n=3-7, mean+SEM).

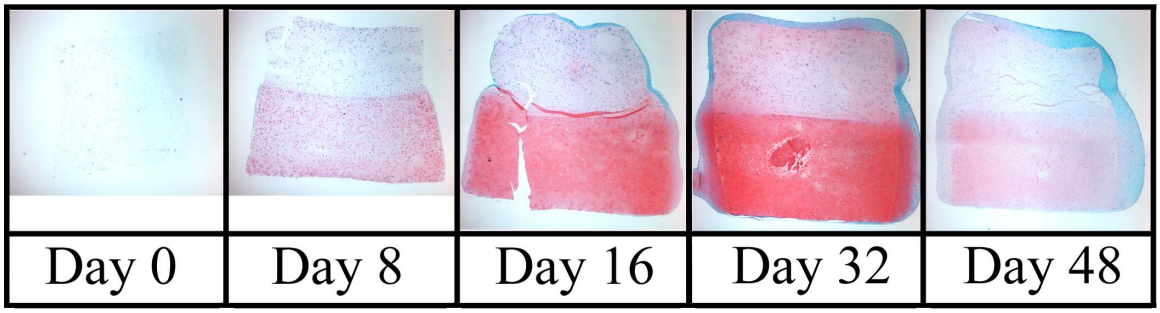

Figure 5.15: Safranin-O-stained bilayer gels illustrate sGAG distribution (red) in the MFC (top) and AFC (bottom) layers with time.

5.3.2.3 sGAG content by EPIC-μCT

To relate EPIC-μCT attenuation to gel sGAG content, a regression analysis between the overall DMMB-measured sGAG/H_2O (Figure 5.14B) and the corresponding EPIC-μCT measurements (Figure 5.12) was performed. A significant, linear regression was found, indicating that gel attenuation readings were a strong predictor of sGAG

content (Figure 5.16). Using this calibration, EPIC-μCT attenuation measurements throughout the depth of the construct were converted to sGAG/H_2O. The overall EPIC-μCT sGAG measurements (Figure 5.17B) were consistent with the DMMB-based measurements, as expected, although the EPIC-μCT analysis predicted a higher sGAG content in the MFC layer (Figure 5.17A).

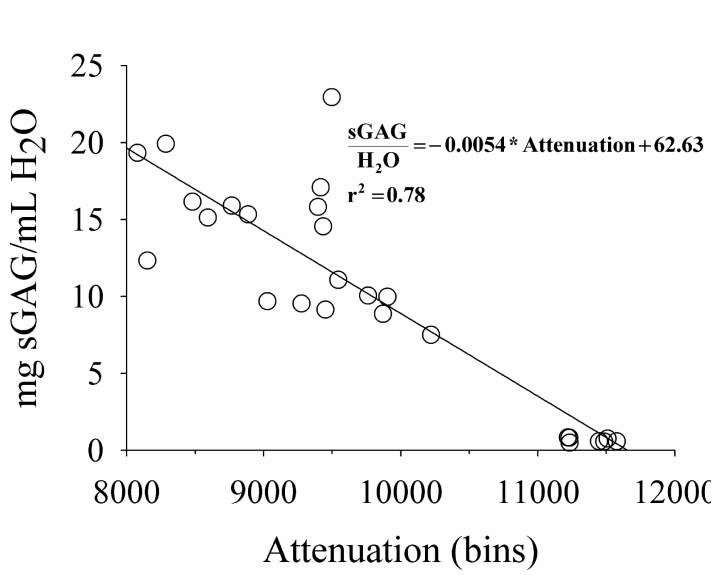

Figure 5.16: Linear relationship between EPIC-μCT attenuation and sGAG/H_2O in bilayer 3% agarose gels at a 1.5:1 Hexabrix:diH20 dilution ($p<0.0005$)

5.3.2.3 Strain and sGAG Inhomogeneity

Image analysis of the displacements of labeled cell nuclei following compression of the gels along the thickness provided a map of the local strain as a function of depth within the construct (Figure 5.18A). The data are reported as the local strain $E_{zz}(z)$ normalized to the overall construct strain E'_{zz}. No differences in the average strain of the AC and MFC layers were observed between days 32 and 48, consistent with the plateau

in sGAG content at the same time points. However, strains at the interface of the two gels appear to exhibit a smoother transition at day 48. Significant differences in strain were noted between the MFC layer (0-1.5mm) and AC layer (1.5-3.0mm) at days 32 and 48. Over days 32 and 48, the MFC layer had an average strain of 2.01 compared with 0.17 for the AC layer, indicating the MFC layer absorbed the majority of the imposed deformation.

The local EPIC-μCT sGAG measurements also showed variation throughout the construct (Figure 5.18B). At day 32 in the MFC layer (subvolumes 0-12), higher sGAG contents were localized to the periphery of the layer. By day 48, the sGAG accumulation in the MFC layer was more uniform throughout its depth. In contrast, sGAG accumulation in the AC layer was uniform throughout its depth at both days 32 and 48.

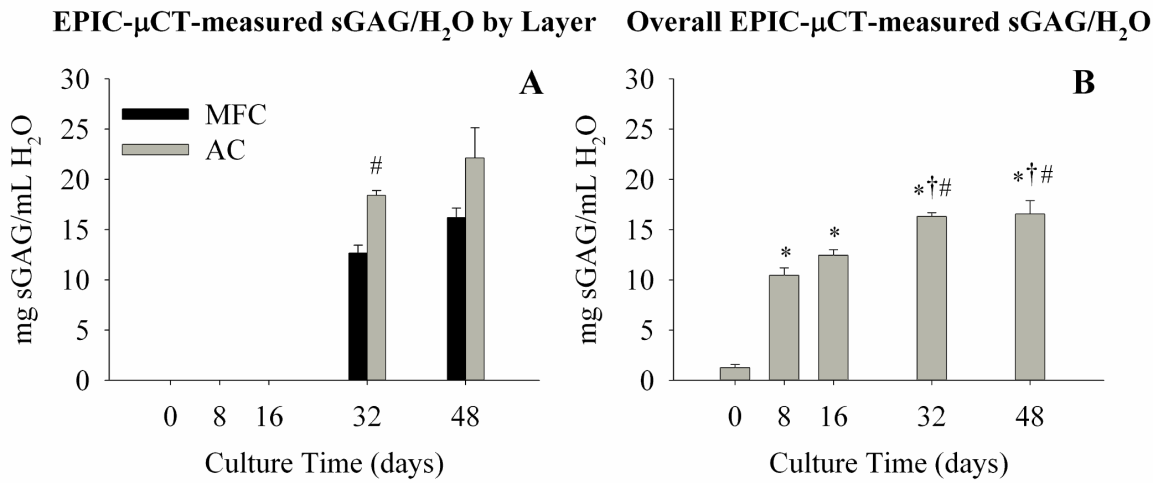

Figure 5.17: EPIC-μCT-measured sGAG content in bilayer constructs (A) within MFC and AC layers and (B) over the total construct. # denotes $p<0.05$ between MFC and AC layer, * denotes $p<0.05$ versus day 0, † denotes $p<0.05$ versus day 8, and # denotes $p<0.05$ versus day 16 (n=4-8, mean+SEM)

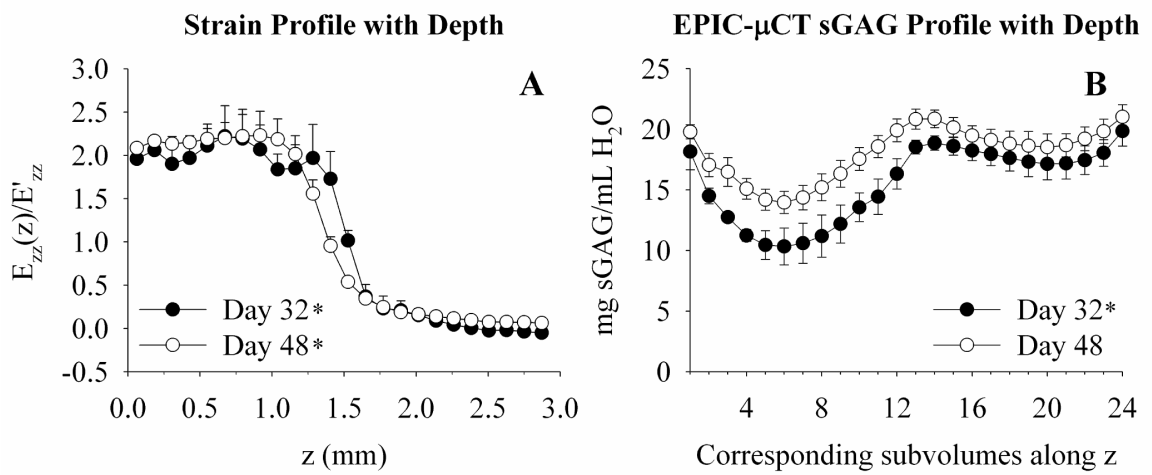

Figure 5.18: Strain (A) and (B) EPIC-µCT sGAG profiles as a function of depth illustrate inhomogeneity in bilayer gels. * denotes $p<0.05$ between AC and MFC layers (n=4, mean+SEM).

5.4 Discussion

These studies investigated the use of EPIC-µCT to longitudinally monitor engineered cartilage constructs and to characterize the spatial and temporal changes in matrix composition and mechanical properties in developing constructs. Consistent with previous EPIC-µCT studies[103], EPIC-µCT was a strong predictor of sGAG content in agarose gels and exhibited sensitivity to changes in sGAG accumulation with time in both homogeneous and heterogeneous agarose constructs. At the intervals examined, the combined effects of the EPIC-µCT protocol resulted in gels with lower sGAG content, although Hexabrix exposure or scanning alone did not affect sGAG content. In bilayer agarose gels, EPIC-µCT identified an inhomogeneous sGAG distribution that indicated differences with zone.

EPIC-µCT demonstrated high sensitivity to sGAG content in agarose gels. Previously, EPIC-µCT had been characterized only in sGAG-rich cartilage explants and

joints, so the suitability of EPIC-μCT for detecting low levels of sGAG in developing matrices was unknown. In this study, the technique measured significant differences in attenuation at eight days, which represented 53.0% of the total change in attenuation over the culture period, and continued to measure significant decreases in attenuation through day 16.

While EPIC-μCT was sensitive to matrix accumulation in developing constructs, the protocol did have a significant effect on matrix production. Though there were no differences in the amount of sGAG released to the media among treatments, significantly lower sGAG was found in the Hexabrix+Scan group at day 24. The Hexabrix+Scan group also showed lower proliferation levels, as indicated by the WST-1 assay, and higher levels of cell death were present in live/dead images of the group. Given that the Hexabrix and Scan groups did not vary from the control treatment, the interaction of the Scan and Hexabrix protocols is likely responsible for the reduced matrix activity. X-ray exposure at the doses delivered by the Scanco CT system (~0.67Gy) has not previously shown significant effects on sGAG incorporation or sGAG content in 3D chondrocyte cultures, though decreased cell proliferation has been noted with exposure to 2Gy[125]. One potential explanation for the results is that build up of heat during X-ray scanning could lead to dehydration of the sample, which could be exacerbated in the presence of salts contained in the Hexabrix formulation. This problem could be addressed through better designed closed systems for housing the constructs, or if changes in temperature during scanning are significant, by regulating the temperature or humidity within the CT chamber. For *in vitro* studies, less frequent or fewer scanning increments are likely to reduce the effects of the protocol on sGAG accumulation. While the effect of the EPIC-

μCT protocol *in vivo* has not been characterized, the low cytotoxicity of the Hexabrix formulation *in vitro* suggests there would be minimal effect on sGAG accumulation *in vivo*.

In addition to EPIC-μCT's ability to monitor changes in sGAG accumulation in engineered constructs, the results of the bilayer study demonstrate the use of the technique to resolve spatial differences in developing constructs. For example, a subtle change in sGAG density at the interface of the two layers is apparent between days 32 and 48 (Figure 5.18B). This change is reflected in the increased sGAG content in the MFC layer relative to the AC layer between days 32 and 48 (Figure 5.17A). Differences in the relative amount of sGAG in the MFC and AC zones were noted in the DMMB and EPIC-μCT analyses, though the techniques reported similar total sGAG content. These differences may reflect analysis of slightly different layer regions between the two techniques, due in part to variances associated with the physical dissection of the MFC and AC layers. To that end, EPIC-μCT's micron-level resolution and ability to precisely define the analysis region may be particularly advantageous when working with small samples. Furthermore, the ability to characterize spatial patterns of ECM deposition is critical to studies where an understanding of matrix responses to local stimuli (e.g. release of growth factors, degrading scaffolds) or the ability to observe matrix development and remodeling (e.g. stratified construct, cell co-cultures) is sought.

The inhomogeneous patterns of strain and sGAG content present in the bilayer gels suggest the importance of analyzing local composition-function relationships. Previous work characterizing the depth-dependent mechanical properties in stratified agarose layers and immature cartilage emphasized the contribution of regional

differences in matrix composition to the local modulus[126,127]. Similarly, a composition-function analysis combining indentation measurements of tibial plateaus with site-matched dGEMRIC measurements of sGAG content demonstrated that the Pearson correlation coefficient between the measured stiffness and sGAG concentration decreased substantially with depth, further emphasizing the significance of local changes in tissue composition to mechanical properties[102].

The sensitivity of EPIC-μCT to low levels of sGAG, its ability to analyze spatial patterns of matrix deposition, and its potential to predict mechanical properties makes EPIC-μCT a power tool for investigating temporal and spatial changes in cartilaginous tissues. Additional work is necessary to resolve concerns with the EPIC-μCT protocol regarding matrix biochemistry and to fully characterize the relationships between EPIC-μCT measurements and mechanical properties. However, the findings of this study encourage future use of EPIC-μCT in tissue engineering studies and composition-function analyses.

CHAPTER 6

CONCLUSIONS AND RECOMMENDATIONS

6.1 Summary

The goals of this dissertation research were to investigate composition-function relationships in healthy, degraded, and engineered articular cartilage using EPIC-μCT and mechanical testing to characterize these relationships. By analyzing differences in the composition and distribution of ECM components and the corresponding mechanical properties under anabolic, catabolic, and homeostatic conditions, it may be possible to identify or eliminate factors (e.g. ECM content, distribution, and structure) which are most critical to mechanical function. This approach is particularly applicable in developing strategies to halt or reverse cartilage degeneration or to engineer replacement cartilage. In the studies presented here, ECM composition and distribution were significant regulators of the mechanical properties of all types of articular cartilage. In particular, sGAG content was a significant predictor of compressive and shear properties in healthy and IL-1-stimulated (degraded) cartilage, and differences in GAG content and distribution in engineered cartilage were reflected in its strain profile. The development of EPIC-μCT, with its ability to monitor sGAG content and distribution in cartilaginous tissues, thus provides a versatile tool for investigating composition-function relationships. Furthermore, the results of this work emphasize the importance of sGAG content and distribution in the development of therapeutic strategies for treating cartilage degeneration and suggest that monitoring changes in sGAG content and distribution via

EPIC-μCT may be an excellent indicator of the success of therapeutic strategies and a useful surrogate for direct mechanical assessment.

The studies in Chapter 3 revealed differences in the composition-function relationships in normal and IL-1-stimulated (degraded) cartilage explants. Consistent with previous studies[1,9,20], the mechanical properties of healthy articular cartilage explants were significantly dependent on collagen and sGAG content for both compressive and shear moduli. sGAG content was a stronger predictor than collagen content of E_{equil} and $|G^*_{dynl}$. However, collagen content was a much stronger predictor of $|E^*_{dyn}|$, indicating the importance of collagen fibers in resisting dynamic compressive loading[18]. In contrast, IL-1-stimulated explants showed no dependence on collagen content for compressive properties, with a weak dependence on collagen for the shear modulus. This finding suggests that decreases in sGAG content in articular cartilage may be accurate indicators of deteriorating mechanical function. Measurements of the mechanical properties of cartilage explants with progressive degradation also suggested differences in the sensitivity of the compressive and shear moduli. In IL-1-stimulated explants, the dynamic compressive and shear moduli were measurable at days 24 and 20, respectively, after nearly complete sGAG depletion but prior to significant collagen depletion, suggesting these measurements were sensitive to changes in both collagen and sGAG content. In contrast, the equilibrium modulus reached the detection limit of the mechanical test at day 16. Finally, the strength of the correlations between the equilibrium and dynamic compressive moduli ($0.877<r<0.929$) suggest they reflect similar trends in their assessment of mechanical function.

The studies in Chapter 4 reported the development and validation of EPIC-μCT, a μCT-based tool for the assessment of cartilage composition, morphology, and function. Using the ionic contrast agent Hexabrix, EPIC-μCT attenuation was found to be a strong predictor (R^2=0.91, $p<0.0005$) of sGAG content over a broad range of densities. EPIC-μCT monitoring of changes in sGAG content in IL-1-stimulated cartilage explants was consistent with biochemical and histological assessments of sGAG content and distribution. IL-1 stimulation resulted in loss of sGAGs first in the deep zone of full-thickness explants, followed by decreases in PG content throughout the explant thickness. In studies with a dissected rabbit femur, articular surface morphology (e.g. scalpel cuts, ligaments) was visible with EPIC-μCT that was not visible with conventional μCT. Analytical methods were also developed to segment cartilage from other tissues and measure its thickness, highlighting EPIC-μCT's ability to provide information on sGAG content as well as cartilage morphology.

The studies in Chapter 5 examined the potential of EPIC-μCT to monitor the development of engineered cartilage. The effects of the EPIC-μCT protocol on sGAG production were examined. Over a 24 day culture with 4 equally-spaced evaluations using EPIC-μCT, significant decreases in sGAG accumulation and mitochondrial activity and high levels of cell death were noted in the Hexabrix+Scan group. Effects on sGAG accumulation and cell proliferation and viability were not noted with the Hexabrix only and Scan only treatments, indicating that the results may represent an interactive effect. Dehydration from elevated temperatures during scanning may account for the noted differences, but additional characterization is needed. In studies using bilayer agarose gels, differences in sGAG deposition in the distinct layers were detected using

biochemical analysis, histological assessment, and EPIC-μCT. Higher levels of sGAG content were found in the AC layer, consistent with the higher rate of sGAG incorporation reported for ACs over MFCs[123]. The patterns of sGAG accumulation resulted in an inhomogeneous profile through the thickness of the construct. Strain microscopy analysis through the construct depth indicated significantly lower strains were localized in the AC layer than the MFC layer, indicating the AC layer was much stiffer. The higher level of sGAG content in the AC layer and the greater stiffness of the AC layer suggested by the strain analysis indicate the importance of sGAG content and distribution in the mechanical properties of engineered cartilage.

6.2 Conclusions

One of the most significant findings of this work relates to the versatility of EPIC-μCT. In studies with cartilage explants and engineered cartilage, EPIC-μCT was accurate over a broad range of sGAG/H_2O (~5-70mg/mL) and sensitive to low levels of sGAG accumulation in agarose gels (~17μg/mg wet weight). In addition, EPIC-μCT images also revealed soft tissue morphology (e.g. articular surface cuts, ligaments) not visible with traditional μCT. The analytical capabilities of μCT also allowed for the segmentation or isolation of articular cartilage from other tissues *in situ* in a rabbit joint and the spatial assessment of inhomogeneous sGAG content in engineered cartilage. Furthermore, the results of the EPIC-μCT-estimated sGAG measurements and strain analysis of the AC and MFC layers in Chapter 5 together suggest that EPIC-μCT sGAG measurements may also be predictive of mechanical function in engineered cartilage.

EPIC-μCT and dGEMRIC have been shown to be excellent predictors of sGAG content in healthy, degraded, and engineered cartilage and have also demonstrated the

ability to quantify the distribution of sGAG content. The later capability is especially critical for monitoring the local effects of tissue engineering and other interventional strategies. As demonstrated in chapter 5, this approach can illustrate regional differences in sGAG accumulation during development of stratified tissue engineered constructs. In addition, these techniques may prove useful in monitoring the integration and maturation of constructs in cartilage defect repair models. μCT has previously been used to characterize the porosity and anisotropy of polymer scaffolds[128], suggesting the use of EPIC-μCT to simultaneously monitor both the remodeling of tissue engineering scaffolds and the matrix accumulation within the constructs. EPIC-μCT's ability to segment materials of differing radiopacity for analysis epitomizes its versatility and analytical power. Furthermore, EPIC-μCT may also be useful in monitoring the effects of local therapies (e.g. growth factors, gene delivery, drug treatments) on sGAG composition in adjacent orthopedic soft tissues *in vivo*. Though the ability to noninvasively visualize soft tissues is not unique to EPIC-μCT, its ability to isolate and quantify regional differences in sGAG composition and tissue morphology encourages its use in a number of applications.

Analysis of composition-function relationships underscores the importance of bulk ECM content to the mechanical properties of cartilaginous tissues, but the contributions of ECM distribution and organization should not be overlooked in assessing cartilage function. The challenge lies in isolating the roles of ECM molecules in a tissue like cartilage which exhibits both macroscopic inhomogeneity and anisotropy. The composition-function analyses in Chapter 3 were performed on middle zone cartilage, which while relatively uniform in composition (Figure 2.3), still exhibits anisotropy,

primarily due to the orientation of collagen fibers. In those studies with degraded cartilage, collagen content was not a significant predictor of compressive properties yet sGAG content alone could not completely account for the measured properties. This observation suggests the role of additional parameters other than bulk ECM content in regulating cartilage mechanical properties. This argument is supported by composition-function analyses of enzymatically-degraded, full-thickness cartilage explants, which indicated that spatial or zonal differences related to the inhomogeneity of the cartilage ECM and the anisotropy of its structure were significant predictors of the Young's modulus[54]. In addition, increases in pyridinoline crosslinks with maturation were significant predictors of increases in tensile moduli strength in bovine cartilage explants[29], indicating that the structural organization of collagen fiber bundles also regulates the mechanical properties. Changes to the collagen fiber birefringence in the superficial zone have also been noted prior to macroscopic ECM changes in experimental OA models[18,129], adding further evidence that bulk mechanical properties (and sGAG, in particular) may not provide the earliest indication of degeneration or fully predict mechanical function. As previously stated, it is difficult to isolate the effects of bulk ECM content from the role of cartilage inhomogeneity and anisotropy, but these factors should be considered when using bulk sGAG-based diagnostics, such as EPIC-μCT and dGEMRIC, in monitoring cartilage degeneration or assessing mechanical function.

In evaluating the success of interventional strategies aimed at reversing degeneration and engineering strategies aimed at developing replacement cartilage, comparisons are often made to the composition and mechanical properties of the native tissue. Composition-function analyses support these comparisons by emphasizing the

importance of ECM components, particularly sGAG and collagen, to articular cartilage mechanics. An important observation that has been given more recent attention in the tissue engineering community is that the exact composition of native cartilage may not be necessary to achieve equivalent mechanical function. This is evident in a study examining the recovery of sGAG content and mechanical properties in cartilage explants following a brief period of IL-1-induced catabolism, where compressive moduli recovered to control levels despite significantly lower levels of sGAG content in IL-1-stimulated explants[130]. This finding suggests the importance of other factors (e.g. ECM distribution and organization) in regulating mechanical properties and implies that targeting native levels of ECM composition may not be necessary or even worthwhile given the remodeling that will occur *in vivo*.

Given the limited success of clinical regenerative therapies, preservation of existing cartilage function by protecting the ECM may be the best strategy for managing degeneration in the short term. The importance of sGAG content in the loss of mechanical properties in IL-1-stimulated cartilage suggests it may be an appropriate target for interventional strategies. To that end, Pratta *et al.* have suggested that the PG aggrecan may afford protection to the collagen network in articular cartilage, as evidenced by the preservation of collagen content when IL-1-stimulated articular cartilage was treated with an aggrecanase inhibitor[89]. This protection however appears to be transient, only delaying depletion of the ECM and the loss of mechanical properties[95]. These and other studies indicate that the ECM may be degraded by a combination of MMPs, aggrecanases, and other enzymes. Thus, until the mechanisms responsible for

ECM degradation are identified, it will be difficult to prevent degeneration despite improved understandings of composition-function relationships.

6.3 Future Recommendations

This dissertation research reinforced the importance of sGAG content to the mechanical properties of healthy, degrading, and engineered cartilage and introduced EPIC-μCT as a powerful technique for the assessment of changes in PG content and morphology *in vitro* and *in situ*. The most obvious extensions of this work are in the continued development and application of EPIC-μCT. There are a number of possible areas of research related to studying the progression of OA, evaluating the success of tissue engineering strategies, investigating more basic cartilage mechanics problems, and potentially, developing EPIC-μCT as a clinical diagnostic.

EPIC-μCT is a particularly attractive technique for assessing composition and morphology changes in small animal models of degeneration and regeneration. In rodents, in particular, the articular cartilage is on the order of 100μm at its thickness point, making assessment of changes in sGAG content difficult with the spatial resolution currently offered by existing techniques (e.g. dGEMRIC). As outlined in Chapter 4, a number of technical hurdles must be addressed to realize *in vivo* potential in small animals. Briefly, these include experimental validation of the *in situ* thickness measurements presented in Chapter 4, determining optimal Hexabrix dilution for sGAG and thickness measurements, evaluating Hexabrix delivery options (e.g. systemic versus intraarticular injection), and characterizing the optimal scanning window.

A number of opportunities to apply EPIC-μCT also exist in the tissue engineering community. The results of Chapter 5 suggest that additional evaluation is needed to use

EPIC-μCT in the longitudinal monitoring of tissue engineered constructs *in vitro*. It may also be of interest to use the technique in characterizing the development of osteochondral constructs *in vitro* and their subsequent integration following implantation *in vivo.* The ability to characterize both cartilage composition and bone architecture would make excellent use of the powerful analytical capabilities of EPIC-μCT.

EPIC-μCT may also be of interest in studies related to basic cartilage mechanics. Work presented in Appendix A outlines the development of a micro indentation device that allows for the controlled compression of cartilaginous tissues and subsequent EPIC-μCT analysis of changes in matrix composition and structure. This system, with the inclusion of a load cell, can be used to monitor stress relaxation of tissues. It may be useful to studies investigating the effects of compression on changes in local FCD and indentation studies characterizing deformations to different probe tip geometries.

APPENDIX A

DEVELOPMENT OF AN EPIC-MICROCOMPUTED TOMOGRAPHY-COMPATIBLE MICROINDENTATION DEVICE AND PRELIMINARY CHARACTERIZATIONS OF COMPRESSION-INDUCED CHANGES IN ARTICULAR CARTILAGE FCD

A.1 Introduction

Physiologic loading of joints deforms the 3D structure of articular cartilage, resulting in complex changes in the local strain field and the inhomogeneous FCD. Changes in the mechanical environment induced by mechanical loading have previously been reported to regulate cell matrix synthesis[123,131,132]. In addition, local changes in the FCD and strain field due to applied deformations are germane to accurate design and interpretation of indentation measurements of articular cartilage stiffness[88,124] and to the development of accurate models relating tissue composition to mechanical properties. Characterizing these changes has proven challenging due to the need to analyze changes in ECM distribution and local deformation in the deformed state. 2D video microscopy techniques capable of measuring the continuous depth-dependent strain and FCD of full-thickness articular cartilage explants have increased our understanding of these changes [28,133]. However, a technique capable of 3D mapping is necessary to fully characterize changes in FCD and deformation. EPIC-μCT, a contrast-enhanced microcomputed tomography technique that has been used to quantitatively monitor *in vitro* FCD decreases during cartilage degeneration[103] and FCD increases during development of

engineered cartilage, represents a viable alternative to existing approaches with its high resolution, 3D assessment capabilities.

This work was initiated to explore the use of EPIC-μCT to monitor changes in FCD and local deformation due to compression. Initial work focused on the development and validation of an EPIC-μCT-compatible microindentation device to apply controlled deformations. Subsequent work focused on characterizing compression-induced changes in FCD in full-thickness articular cartilage explants and in visualizing changes in deformation due to indentation. While proof of principle was established, difficulty was encountered when trying to characterize the time necessary to reach contrast agent chemical equilibrium following compression. Additional characterization of the system is necessary to resolve this issue.

A.2 Development and Validation of the Microindentation Device

A.2.1 Design Considerations

There were a number of design constraints, imposed primarily by the EPIC-μCT protocol and the μCT scanner. First, the EPIC-μCT protocol necessitated that the device include a well around the sample to be filled with Hexabrix during chemical equilibration, both before and after compression. Since the samples in the EPIC-μCT protocol (Appendix B) are scanned in air rather than liquid, it was also necessary to be able to drain the Hexabrix from the device and to have access to the free surfaces of the sample to blot surface fluid that would produce scanning artifacts. In addition, materials used in constructing the device could not interfere with the X-ray signal (i.e. the materials needed to be of low radiopacity). The device also needed to include a calibrated,

controlled system for applying uniaxial compression. To ensure the versatility of the device for characterization of a wide range of sample geometries, the device also needed to accommodate samples with thicknesses ranging from 2mm to 6mm. Finally, to facilitate imaging at a spatial resolution of 21μm, the device needed to fit within a space of 20mm diameter by 80mm.

A.2.2 First Generation Microindentation Device

The frame of the microindentation device consists of two delrin platforms connected by two threaded delrin rods (Figure A.1A). The rods allow for gross positioning of the platforms to account for a range of sample thicknesses. A digital micrometer is used in positioning the platforms to ensure that they are parallel. A rotating spindle micrometer head (Mitutoyo Model 148-203) with a range of 0-6.5mm is secured to the top platform by a lock nut. A micrometer head with a non-rotating spindle with this range and meeting the size constraints of the μCT chamber could not be located, so a coupler was designed to absorb the rotation of the micrometer spindle while delivering the intended axial translation. This coupler, also made of delrin, was machined to include the 4mm diameter flat indentor at its base (Figure A.1B). A 0.25in diameter hole bored into the top of the coupler held a stainless steel ball bearing (OD 0.25in, ID 0.125in) that was press fit into the bore space. The 0.125in diameter spindle shaft of the micrometer head was press fit into the ball bearing. Rotation of the coupler assembler was prevented by fixing it via two 1mm diameter stainless steel shafts to the top platform. The collective design of the coupler assembly transferred all of the spindle rotation to the ball bearings but permitted uniaxial translation of the indentor. The outer diameter of the bottom platform was externally threaded to mate with a threaded cylindrical shell, forming a well

to hydrate the sample. A keyed post was fixed to the bottom platform for interfacing the microindentation device with the Scanco CT systems.

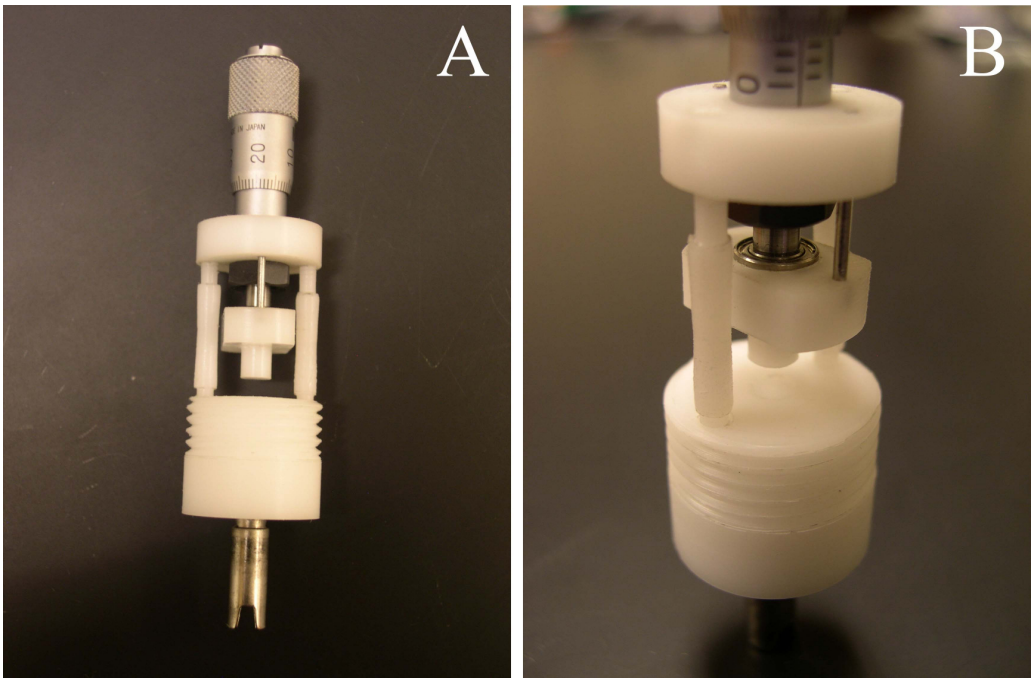

Figure A.1: Color photographs of the first generation microindentation device depicting the (A) overall view and (B) close up of the coupler,

A.2.3 Second Generation Microindentation Device

A load cell was incorporated into a second version of the device in order to measure the resultant stress arising from compression (Figure A.2). The load cell was required to have a diameter less than 10mm and an interface that could be modified to serve as an 8mm diameter rigid, flat platen. A 10lb male threaded load button (Futek Model LLB 210) met these requirements, and an 8mm diameter flat stainless steel platen was machined to interface with the threaded rod of the load button. The bottom platform of the microindentation device was redesigned to accommodate the load cell.

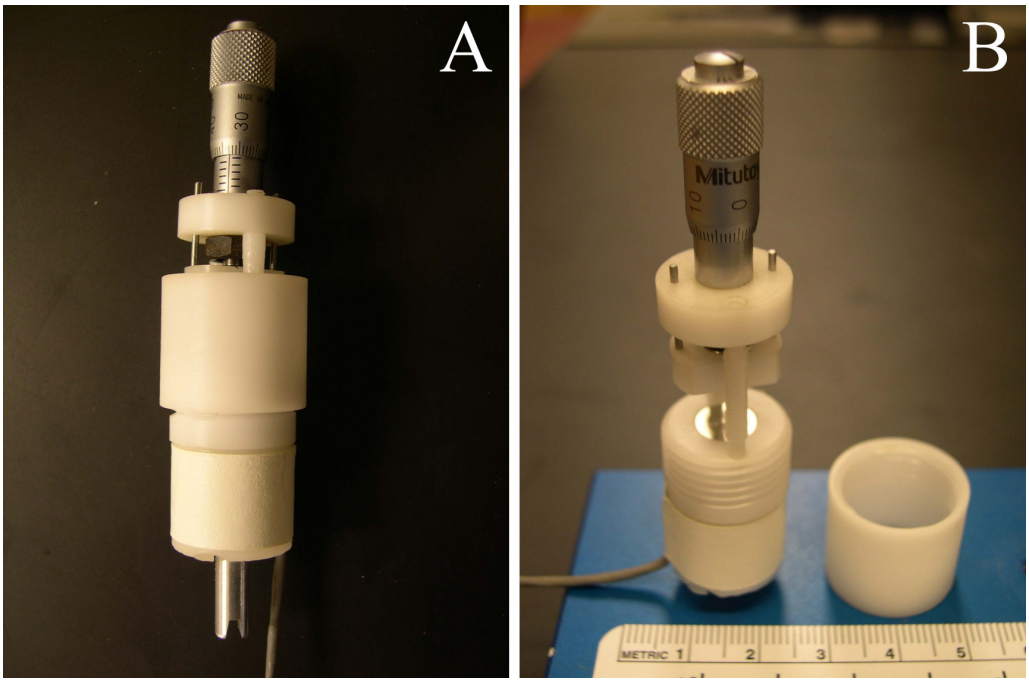

Figure A.2: Color photographs of the second generation microindentation device showing the (A) assembled device and (B) the cylindrical shell removed to expose the load cell button in the bottom platen.

Briefly, the bottom was machined as two pieces. A bore was drilled through the top half of the new bottom platform to accommodate the diameter of the load cell and button. The load cell was sandwiched between the two halves, which were secured together by delrin screws. The load cell cable exited via a channel cut along the outer diameter of the bottom platform, preventing any interference with the X-ray detector as the device was moved along the cylindrical bore of the scanner. A disconnect attachment was wired to the cable, allowing the cable to be separated from the data acquisition system during scanning. The signal of the load cell was amplified by a custom amplifier with a 1000X gain, which was connected to a data acquisition card (National Instruments PCI-6229) and a local PC. Data acquisition was performed using LabView 7.1. Unfortunately, the

load cell was damaged after testing of initial samples, preventing complete validation of the design.

A.2.4 Validation of Applied Uniaxial Compression

To determine the differences between the requested compressive displacement and the displacement felt by the sample, the translation of the system was characterized. The system was characterized using a LX300 laser micrometer with a 1μm resolution, with data acquired using TestWorks software (MTS; Eden Prairie, MN). The laser micrometer works by tracking motion of markings on reflective tape relative to a fixed point of reference. In this setup (Figure A.3), reflective tape was placed on the moving top platen and the base of the microindentation device. The micrometer head was translated approximately 100μm (rotated approximately 72°), as indicated by its 10μm graduated markings, and the movement of the top platen was tracked by the laser.

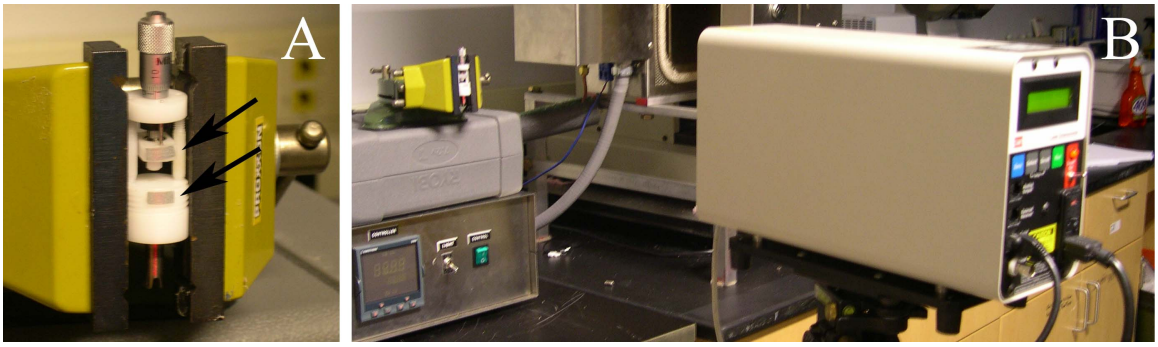

Figure A.3: Color photographs of the validation experiment showing (A) close up of laser beam spanning reflective tape (black arrows) and (B) overview of laser micrometer relative to indentation device.

A.2.5 CAD Drawings of Second-Generation Microindentation Device

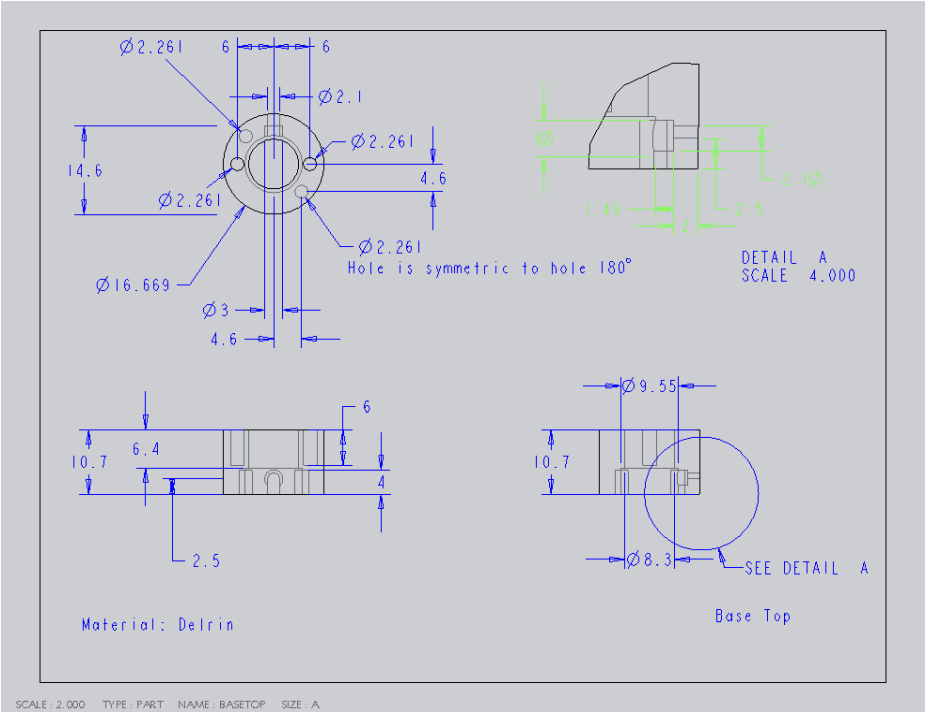

Figure A.4: CAD Drawing of Top Half of Bottom Platen

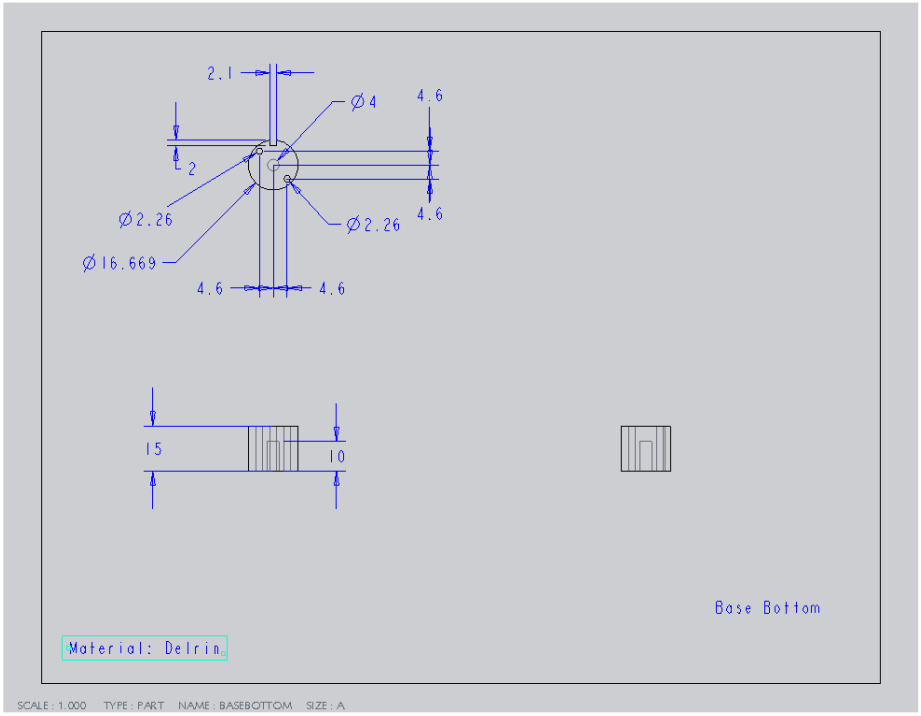

Figure A.5: CAD drawing of bottom half of base platen

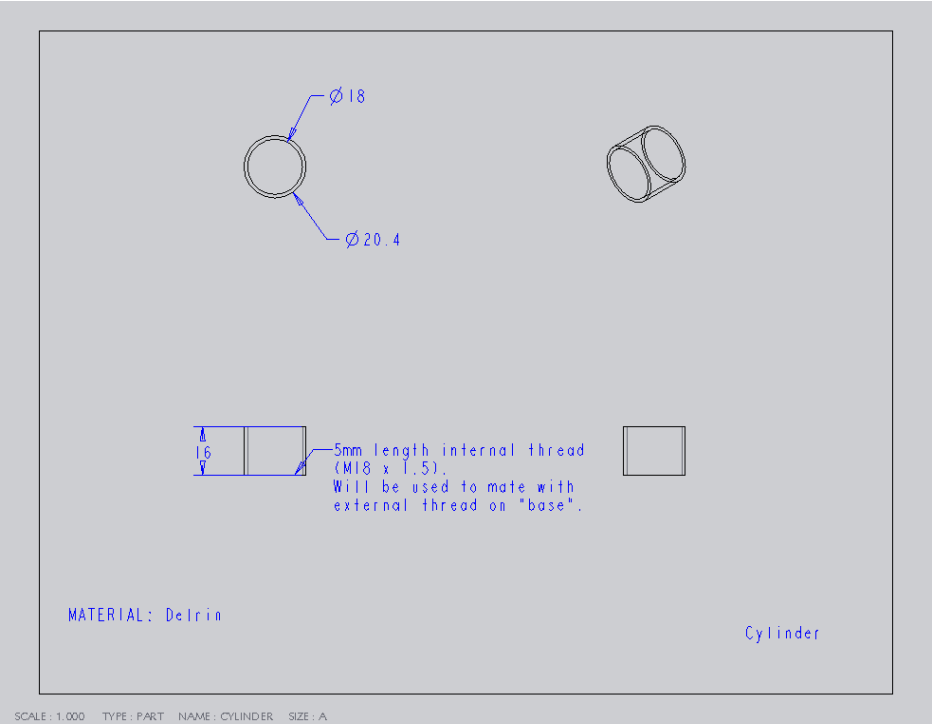

Figure A.6: CAD Drawing of Cylinder

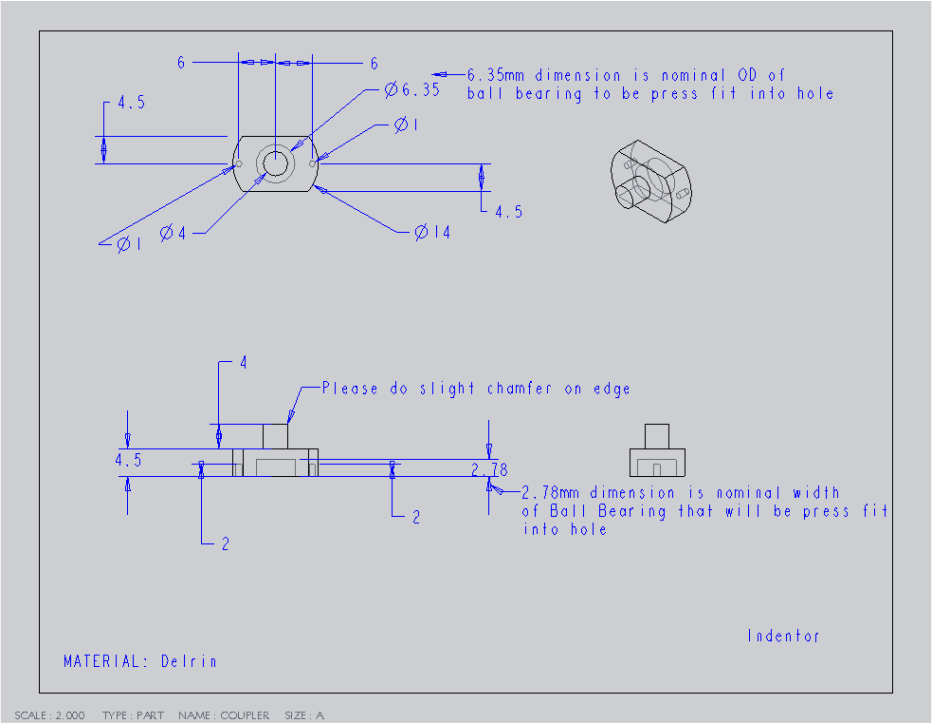

Figure A.7: CAD drawing of indentor/coupler

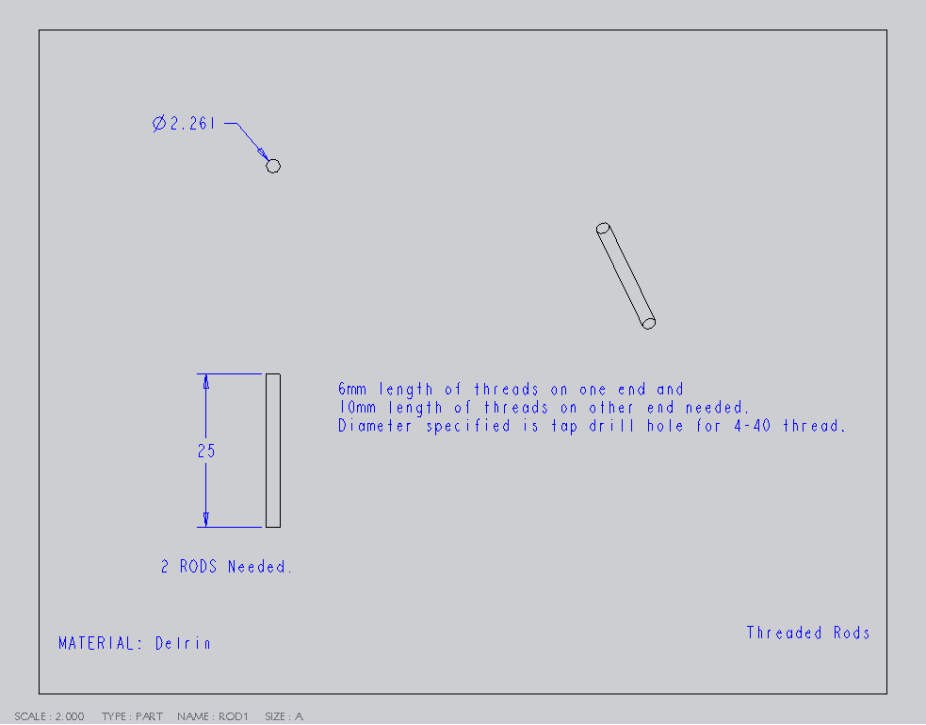

Figure A.8: CAD drawing of threaded rods to connect top and bottom platforms

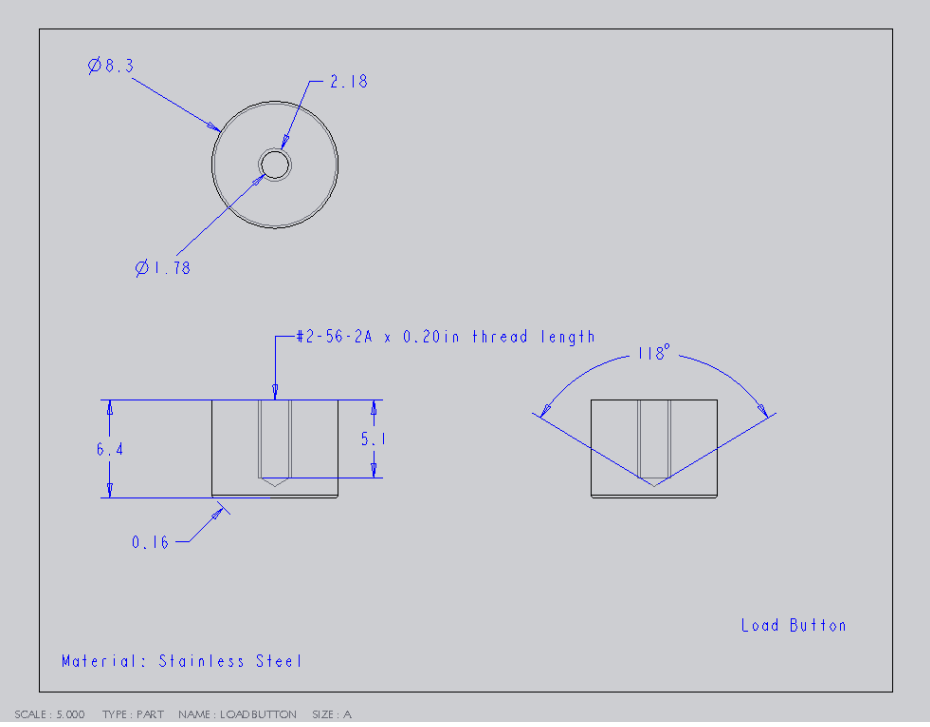

Figure A.9: CAD drawing of platen attaching to load cell

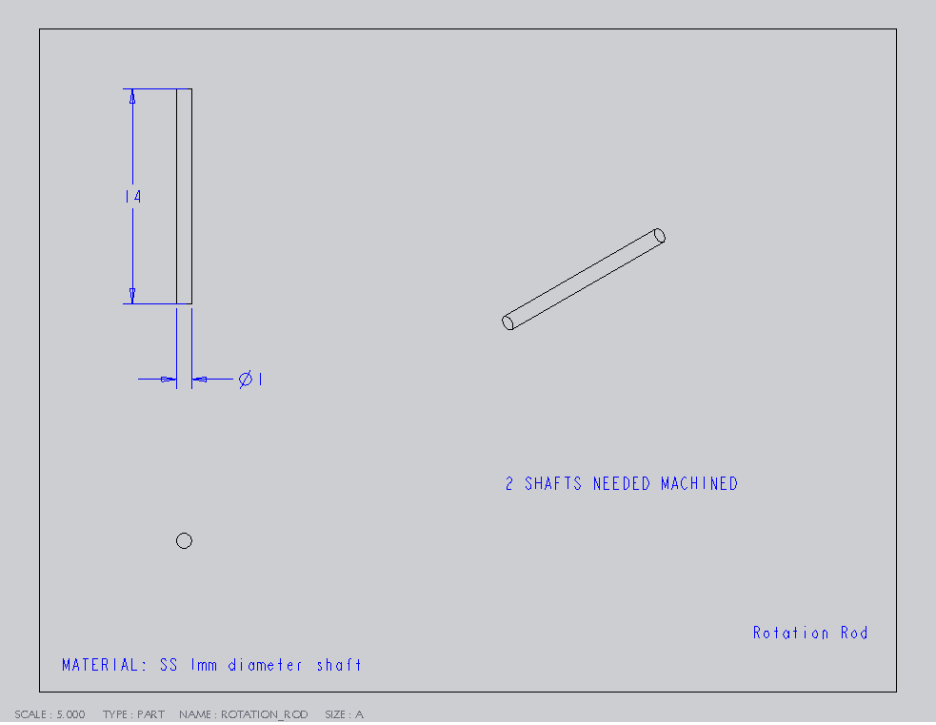

Figure A.10: CAD drawing of shafts to connect indentor/coupler to top platform

A.3 Preliminary Characterization of Changes in FCD and Deformation with Uniaxial Compression

A.3.1 Methods

A.3.1.1 Sample Preparation

Four 4mm diameter and one 8mm diameter, full thickness cartilage explants were harvested aseptically from the femoral condyles and femoral groove of a 1-2 week old calf. The samples were trimmed of any visible subchondral bone using a custom cutting device and stored in PBS with protease inhibitors at -20°C until testing.

A.3.1.2 EPIC-μCT Scanning

After thawing, each explant was allowed to equilibrate in full strength Hexabrix™ (Mallinckrodt) for 24 hours at 37°C under gentle agitation. Prior to scanning, each sample was blotted to remove excess surface fluid. All samples were scanned in air at a 21μm voxel resolution in a Scanco VivaCT 40. Between scans, the well formed by the base of the indentation device and a removable cylindrical shell was filled with Hexabrix™, the opening was sealed with parafilm, and the device was maintained at 37°C.

A.3.1.3 Unconfined Compression and Indentation

A custom, EPIC-μCT-compatible microindentation device with a 4mm diameter flat, impermeable platen (Figure A.1) was used to apply axial compressive strains to full-thickness explants. For unconfined compression experiments, the platen was lowered until contact was made with the articular surface. This position represents the uncompressed sample. The sample was subsequently compressed by 10% and 20% of the uncompressed height at ~10μm/s with a 2hr relaxation period between each step. EPIC-μCT scans were made of the uncompressed state and at each compression level.

A.3.2 Results

Using the EPIC-μCT calibration curve previously determined for articular cartilage (Figure 4.8), EPIC-μCT attenuation measurements as a function of depth were converted to sGAG/H_2O and then to FCD (mEq/mL), assuming all sGAGs were chondroitin sulfate with a molecular weight of 458 g/mol. Consistent with reported values[133], the EPIC-μCT-estimated FCD of uncompressed explants ranged from a

minimum of 0.065 mEq/mL in the most superficial 10% of the explant thickness to a maximum of 0.19 mEq/mL in the deepest zone (Figure A.11). To analyze differences in the effects of compression on EPIC-μCT-estimated FCD as a function of depth, the average EPIC-μCT-estimated FCD at each subvolume was normalized to the maximum value measured in the explant. Unconfined axial compression increased the EPIC-μCT-estimated FCD of the explants, with the greatest increase appearing during the 10% relaxation step and in the superficial zone, where the greatest local strain would be expected (Figure A.12). The increase in EPIC-μCT-estimated FCD in the superficial zone as well as the compaction of the superficial zone was also apparent in longitudinal slices taken from the center of a representative explant (Figure A.13). Analysis of the non-normalized EPIC-μCT-estimated FCD (not shown) indicated no significant increase in FCD for the entire explant, suggesting that chemical equilibration of Hexabrix following compression might be incomplete.

EPIC-μCT images of a 4mm flat indentor pre and post 10% compression of an 8mm diameter sample identified the deformation pattern in the cartilage samples (Figure A.14). The sharp edges of the indentor geometry were clear visible, as were complex changes in the matrix composition under the indentor.

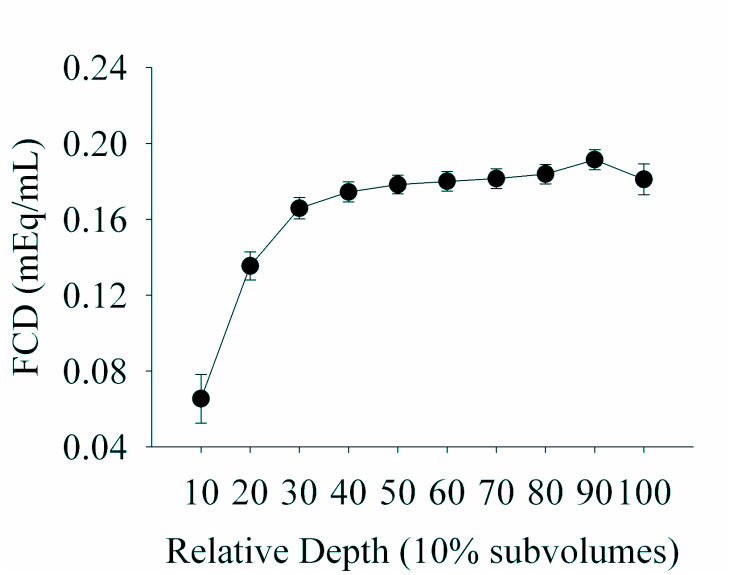

Figure A.11: EPIC-µCT measurements of FCD as a function of depth in uncompressed full-thickness cartilage explants (n=4, mean±SEM).

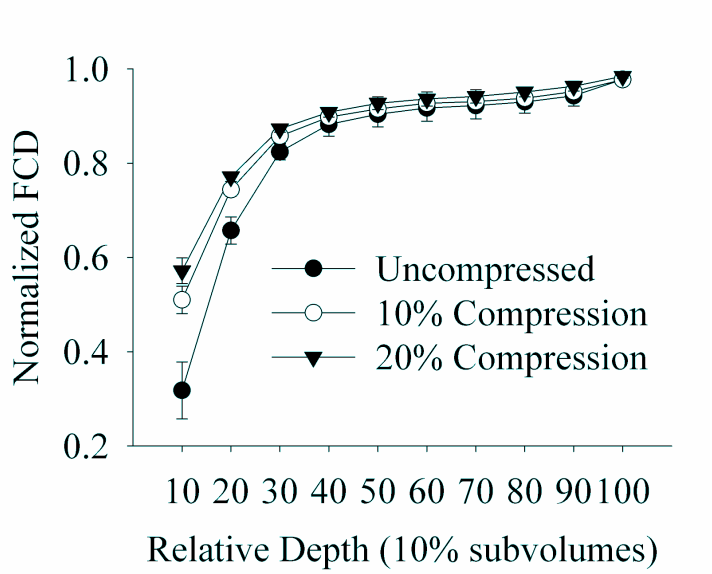

Figure A.12: EPIC-µCT measurements of normalized FCD illustrate zonal differences in response to 10% and 20% uniaxial compression in full-thickness cartilage explants (n=4, mean±SEM).

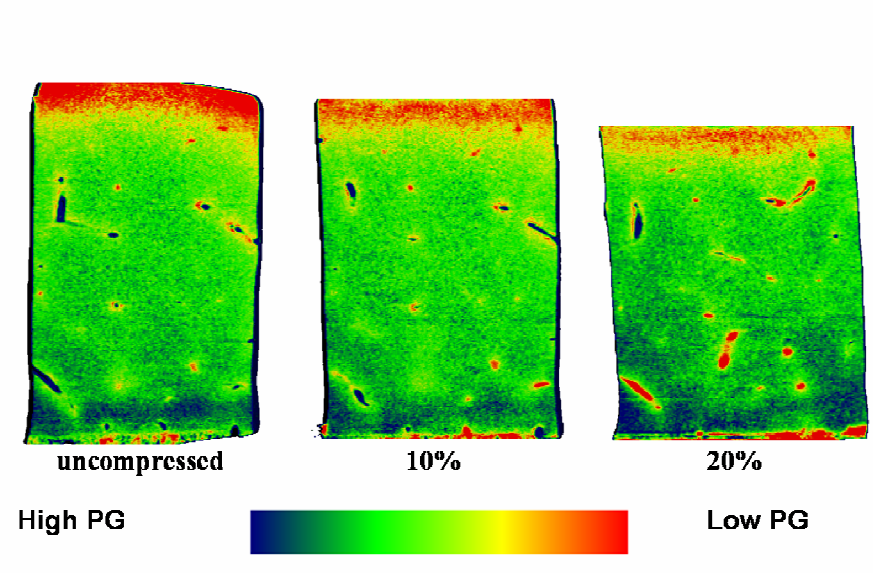

Figure A.13: EPIC-μCT images of the FCD of a representative sample indicate local differences in the FCD with unconfined compression. Superficial zone is at top of image.

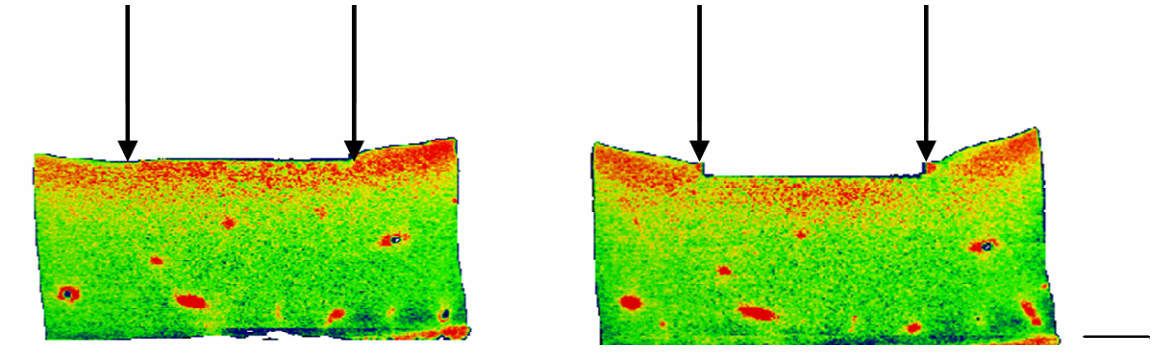

Figure A.14: EPIC-μCT images of an 8mm full-thickness cartilage explant before (left) and after (right) 10% compression by a 4mm flat indentor. The arrows indicate the location of the edges of the indentor (scale=2mm).

A.4 Characterization of Chemical Equilibrium

A.4.1 Introduction

Before proceeding with additional studies, it was necessary to characterize the time needed for the contrast agent to reach chemical equilibrium. This is a legitimate concern with articular cartilage, where static compression has been shown to reduce tissue permeability and increase diffusion time of solutes[134]. Given that 18 hours was needed to reach chemical equilibrium in full thickness articular cartilage explants (Figure 4.2), it may require more than the 2 hours given in the preliminary study to again reach equilibrium, despite the much shorter re-equilibration anticipated in the redistribution of Hexabrix™ following a 10% compression step.

A.4.2 Chemical Equilibration

The goal of this experiment was to characterize the amount of time required to reach chemical equilibrium for an explant following 10% uniaxial static compression. Full-thickness articular cartilage explants were harvested from the femoral condyles of 1-2 week old femurs, trimmed of subchondral bone, and frozen at -20°C in PBS with protease inhibitors until the day of testing. After thawing at 37°C, the sample was equilibrated for 24 hours at 37°C under gentle agitation in full-strength Hexabrix supplemented with protease inhibitors. The sample was then blotted and scanned at its uncompressed state in a μCT 40 (Scanco). After scanning, the indentation device was filled with Hexabrix™ and the sample was compressed by 10% of its height. The sample was allowed to relax in its compressed state at 37°C. At periodic intervals (2, 4, and 19 hours), the device was drained of Hexabrix, the sample was blotted, and the samples was imaged by EPIC-μCT. Attenuation measurements were converted to FCD (mEq/mL) as

previously described. With time, samples showed either no change or decreases in EPIC-μCT-estimated FCD (Figure A.15), which contradicts conventional theory.

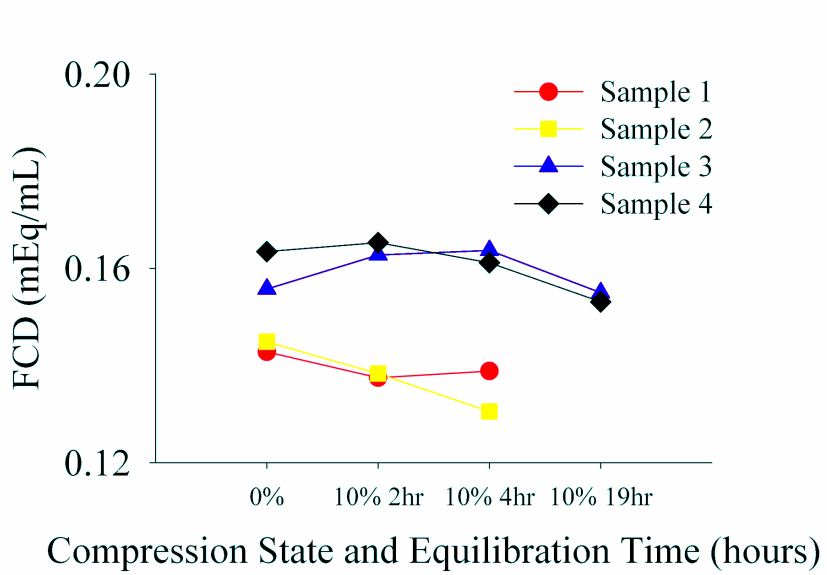

Figure A.15: Changes in FCD with compression state and equilibration time for full thickness articular cartilage explants.

A.4.3 Active Exudation of sGAGs

One potential explanation for the observed decreases in FCD during chemical equilibrium was stress-induced exudation of sGAGs from the ECM due to the applied deformation. To test this theory, untested samples were placed in the indentation device with 1.5mL PBS and compressed by 10% of their sample height. The PBS was collected and replaced at periodic intervals (1, 2, 3, and 4 hours post-compression). A subset of samples (Samples 1 and 2) were unloaded at the end of 4 hours, allowed to recover to their original height over 1 hour in PBS, and recompressed to 10% thickness. PBS collections were made at 1 and 2 hours post-recompression (1r, 2r) to see if a second

compression would exude sGAGs disrupted by the initial compression. The PBS collections were subsequently analyzed for sGAG content by the DMMB assay. Note that Hexabrix was not used for these experiments as it might interfere with the DMMB assay, which relies on the ionic binding of the dye with negatively-charged species (i.e. Hexabrix and sGAGs). The results of this study, presented in Figure A.16, indicate that ~16µg of sGAGs per explant were released over the 4 hours post-compression and that repeated compression had little additional effect.

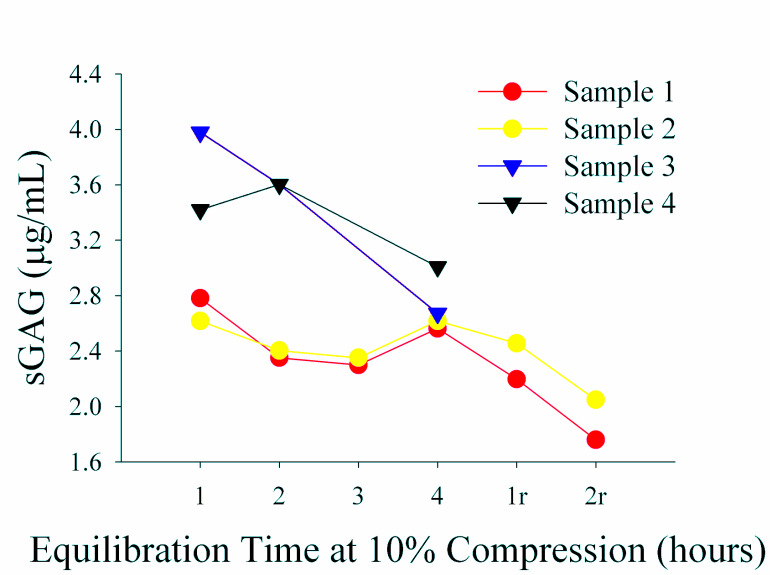

Figure A.16: sGAG released during a 10% static compression as a function of time. 1r and 2r indicate 1 hour and 2 hours after a repeated 10% compression.

A.5 Summary

After being unable to reach chemical equilibrium over a 19 hour period, which was previously sufficient for uncompressed explants, and being unable to account for the observed decreases in EPIC-µCT-estimated FCD, these studies were halted. One possible

explanation that may account for the noted decrease in EPIC-μCT-estimated FCD is explant swelling, which could result in an effective dilution of the EPIC-μCT-estimated FCD. Cartilage explants in culture are known to swell with time, due in part to decreased ability of cut collagen fibers at the free surface of the explants to prevent swelling of the entrapped PGs. Theoretical calculations of the amount of water needed to dilute the FCD of an explant of this geometry suggest it would be on the order of 10μL, which would be difficult to measure experimentally. If it is not possible to resolve this issue, this approach to characterizing deformation-induced changes in EPIC-μCT-estimated FCD may still be useful in characterizing the relative changes between zones.

APPENDIX B

EPIC-MICROCOMPUTED TOMOGRAPHY PROTOCOL

B.1 Hexabrix Equilibration and Sample Preparation

This protocol is appropriate for bovine cartilage explants up to 4mm diameter and 6 mm thick and for agarose gels up to 3mm diameter and 3mm thick. The Hexabrix equilibration time should be increased for larger diameter and thicker samples, and the design of larger sample cassettes may be necessary. NOTE: Hexabrix is light sensitive and should be stored appropriately.

1. The experiment should be timed such that scanning is performed immediately after sample equilibration is complete.

2. Equilibrate 1 explant in 1mL of full strength Hexabrix 320 (Mallinckrodt) for 24 hours or 1 agarose gel in 1mL of a solution of 1:1 Hexabrix 320:diH2O for 2 hours in a sealed microcentrifuge tube at 37°C under gentle agitation using a shaker plate.

3. Remove the sample from Hexabrix and blot surface fluid using a KimWipe.

4. Using tweezers or a “scoop”, carefully place the sample in a well of the custom CT cassette. Stretch parafilm over the cassette to seal the well and prevent sample dehydration. Place the cassette into the sample tube, pushing it to the bottom of the tube. Stretch parafilm over the sample tube to seal the tube.

5. Secure sample tube in CT chamber and initiate scanning. The scan and evaluation parameters of B.2 should serve as a guide.

B.2 CT Scan and Evaluation Parameters

B.2.1 CT Settings

B.2.1.1 VIVA CT

Table B.1: VIVA CT Settings for EPIC-µCT

Parameter	Value
Current	133 µA
Voltage	45 kVp
Integration Time	200ms
Voxel Size/Sample Tube Diameter	20.5µm nominal (adjust as appropriate)
Resolution	Medium (adjust as appropriate)

B.2.1.2 µCT 40

Table B.2: µCT 40 Settings for EPIC-µCT

Parameter	Value
Current	177 µA
Voltage	45 kVp
Integration Time	200ms
Voxel Size/Sample Tube Diameter	20.5µm nominal (adjust as appropriate)
Resolution	Medium (adjust as appropriate)

B.2.2 Evaluation Settings

Table B.3: 3D Evaluation settings for the experiments presented in chapters 4 and 5. NOTE: The choice of threshold will change with the strength of Hexabrix used.

Parameter	Cartilage	3% Agarose
Sigma	1.2	1.2
Support	2	2
Threshold	102	150

REFERENCES

[1] Mow VC, Ratcliffe A. Structure and Function of Articular Cartilage and Meniscus. In: Mow VC, Hayes WC, eds. *Basic Orthopaedic Biomechanics*. 2nd ed. Philadelphia: Lippincott-Raven; 1997:113-177.

[2] Kempson GE, Muir H, Pollard C, Tuke M. The tensile properties of the cartilage of human femoral condyles related to the content of collagen and glycosaminoglycans. *Biochim Biophys Acta.* Feb 28 1973;297(2):456-472.

[3] Bader DL, Kempson GE. The short-term compressive properties of adult human articular cartilage. *Biomed Mater Eng.* 1994;4(3):245-256.

[4] Setton LA, Mow VC, Muller FJ, Pita JC, Howell DS. Altered structure-function relationships for articular cartilage in human osteoarthritis and an experimental canine model. *Agents Actions Suppl.* 1993;39:27-48.

[5] Front P, Aprile F, Mitrovic DR, Swann DA. Age-related changes in the synthesis of matrix macromolecules by bovine articular cartilage. *Connect Tissue Res.* 1989;19(2-4):121-133.

[6] LeRoux MA, Arokoski J, Vail TP, Guilak F, Hyttinen MM, Kiviranta I, Setton LA. Simultaneous changes in the mechanical properties, quantitative collagen organization, and proteoglycan concentration of articular cartilage following canine meniscectomy. *J Orthop Res.* May 2000;18(3):383-392.

[7] Roughley PJ. Age-associated changes in cartilage matrix: implications for tissue repair. *Clin Orthop Relat Res.* Oct 2001(391 Suppl):S153-160.

[8] Kempson GE. Age-related changes in the tensile properties of human articular cartilage: a comparative study between the femoral head of the hip joint and the talus of the ankle joint. *Biochim Biophys Acta.* Oct 31 1991;1075(3):223-230.

[9] Williamson AK, Chen AC, Sah RL. Compressive properties and function-composition relationships of developing bovine articular cartilage. *J Orthop Res.* Nov 2001;19(6):1113-1121.

[10] Buckwalter JA, Mankin HJ. Articular cartilage: tissue design and chondrocyte-matrix interactions. *Instr Course Lect.* 1998;47:477-486.

[11] Muir H. The chondrocyte, architect of cartilage. Biomechanics, structure, function and molecular biology of cartilage matrix macromolecules. *Bioessays.* Dec 1995;17(12):1039-1048.

[12] Poole AR, Kojima T, Yasuda T, Mwale F, Kobayashi M, Laverty S. Composition and structure of articular cartilage: a template for tissue repair. *Clin Orthop.* Oct 2001(391 Suppl):S26-33.

[13] Silver FH, Bradica G, Tria A. Relationship among biomechanical, biochemical, and cellular changes associated with osteoarthritis. *Crit Rev Biomed Eng.* 2001;29(4):373-391.

[14] Brama PA, Tekoppele JM, Bank RA, Barneveld A, van Weeren PR. Functional adaptation of equine articular cartilage: the formation of regional biochemical characteristics up to age one year. *Equine Vet J.* May 2000;32(3):217-221.

[15] Brown MP, West LA, Merritt KA, Plaas AH. Changes in sulfation patterns of chondroitin sulfate in equine articular cartilage and synovial fluid in response to aging and osteoarthritis. *Am J Vet Res.* Jun 1998;59(6):786-791.

[16] Bayliss MT, Osborne D, Woodhouse S, Davidson C. Sulfation of chondroitin sulfate in human articular cartilage. The effect of age, topographical position, and zone of cartilage on tissue composition. *J Biol Chem.* May 28 1999;274(22):15892-15900.

[17] Ng L, Grodzinsky AJ, Patwari P, Sandy J, Plaas A, Ortiz C. Individual cartilage aggrecan macromolecules and their constituent glycosaminoglycans visualized via atomic force microscopy. *J Struct Biol.* Sep 2003;143(3):242-257.

[18] Appleyard RC, Burkhardt D, Ghosh P, Read R, Cake M, Swain MV, Murrell GA. Topographical analysis of the structural, biochemical and dynamic biomechanical properties of cartilage in an ovine model of osteoarthritis. *Osteoarthritis Cartilage.* Jan 2003;11(1):65-77.

[19] Setton LA, Mow VC, Muller FJ, Pita JC, Howell DS. Mechanical properties of canine articular cartilage are significantly altered following transection of the anterior cruciate ligament. *J Orthop Res.* Jul 1994;12(4):451-463.

[20] Zhu W, Mow VC, Koob TJ, Eyre DR. Viscoelastic shear properties of articular cartilage and the effects of glycosidase treatments. *J Orthop Res.* Nov 1993;11(6):771-781.

[21] Legare A, Garon M, Guardo R, Savard P, Poole AR, Buschmann MD. Detection and analysis of cartilage degeneration by spatially resolved streaming potentials. *J Orthop Res.* Jul 2002;20(4):819-826.

[22] Ding M. Age variations in the properties of human tibial trabecular bone and cartilage. *Acta Orthop Scand Suppl.* Jun 2000;292:1-45.

[23] Ding M, Dalstra M, Linde F, Hvid I. Mechanical properties of the normal human tibial cartilage-bone complex in relation to age. *Clin Biomech (Bristol, Avon).* Jun 1998;13(4-5):351-358.

[24] Hudelmaier M, Glaser C, Hohe J, Englmeier KH, Reiser M, Putz R, Eckstein F. Age-related changes in the morphology and deformational behavior of knee joint cartilage. *Arthritis Rheum.* Nov 2001;44(11):2556-2561.

[25] Charlebois M, McKee MD, Buschmann MD. Nonlinear tensile properties of bovine articular cartilage and their variation with age and depth. *J Biomech Eng.* Apr 2004;126(2):129-137.

[26] Laasanen MS, Toyras J, Korhonen RK, Rieppo J, Saarakkala S, Nieminen MT, Hirvonen J, Jurvelin JS. Biomechanical properties of knee articular cartilage. *Biorheology.* 2003;40(1-3):133-140.

[27] Jurvelin JS, Arokoski JP, Hunziker EB, Helminen HJ. Topographical variation of the elastic properties of articular cartilage in the canine knee. *J Biomech.* Jun 2000;33(6):669-675.

[28] Schinagl RM, Gurskis D, Chen AC, Sah RL. Depth-dependent confined compression modulus of full-thickness bovine articular cartilage. *J Orthop Res.* Jul 1997;15(4):499-506.

[29] Williamson AK, Chen AC, Masuda K, Thonar EJ, Sah RL. Tensile mechanical properties of bovine articular cartilage: variations with growth and relationships to collagen network components. *J Orthop Res.* Sep 2003;21(5):872-880.

[30] Vunjak-Novakovic G, Martin I, Obradovic B, Treppo S, Grodzinsky AJ, Langer R, Freed LE. Bioreactor cultivation conditions modulate the composition and mechanical properties of tissue-engineered cartilage. *J Orthop Res.* Jan 1999;17(1):130-138.

[31] Rivers PA, Rosenwasser MP, Mow VC, Pawluk RJ, Strauch RJ, Sugalski MT, Ateshian GA. Osteoarthritic changes in the biochemical composition of thumb carpometacarpal joint cartilage and correlation with biomechanical properties. *J Hand Surg [Am].* Sep 2000;25(5):889-898.

[32] Bank RA, Bayliss MT, Lafeber FP, Maroudas A, Tekoppele JM. Ageing and zonal variation in post-translational modification of collagen in normal human articular cartilage. The age-related increase in non-enzymatic glycation affects biomechanical properties of cartilage. *Biochem J.* Feb 15 1998;330 (Pt 1):345-351.

[33] Hickery MS, Bayliss MT, Dudhia J, Lewthwaite JC, Edwards JC, Pitsillides AA. Age-related changes in the response of human articular cartilage to IL-1alpha and transforming growth factor-beta (TGF-beta): chondrocytes exhibit a diminished sensitivity to TGF-beta. *J Biol Chem.* Dec 26 2003;278(52):53063-53071.

[34] Barone-Varelas J, Schnitzer TJ, Meng Q, Otten L, Thonar EJ. Age-related differences in the metabolism of proteoglycans in bovine articular cartilage explants maintained in the presence of insulin-like growth factor I. *Connect Tissue Res.* 1991;26(1-2):101-120.

[35] Guilak F, Ratcliffe A, Lane N, Rosenwasser MP, Mow VC. Mechanical and biochemical changes in the superficial zone of articular cartilage in canine experimental osteoarthritis. *J Orthop Res.* Jul 1994;12(4):474-484.

[36] Ewers BJ, Weaver BT, Sevensma ET, Haut RC. Chronic changes in rabbit retro-patellar cartilage and subchondral bone after blunt impact loading of the patellofemoral joint. *J Orthop Res.* May 2002;20(3):545-550.

[37] Ewers BJ, Jayaraman VM, Banglmaier RF, Haut RC. Rate of blunt impact loading affects changes in retropatellar cartilage and underlying bone in the rabbit patella. *J Biomech.* Jun 2002;35(6):747-755.

[38] DiMicco MA, Patwari P, Siparsky PN, Kumar S, Pratta MA, Lark MW, Kim YJ, Grodzinsky AJ. Mechanisms and kinetics of glycosaminoglycan release following in vitro cartilage injury. *Arthritis Rheum.* Mar 2004;50(3):840-848.

[39] Kurz B, Jin M, Patwari P, Cheng DM, Lark MW, Grodzinsky AJ. Biosynthetic response and mechanical properties of articular cartilage after injurious compression. *J Orthop Res.* Nov 2001;19(6):1140-1146.

[40] Jeffrey JE, Thomson LA, Aspden RM. Matrix loss and synthesis following a single impact load on articular cartilage in vitro. *Biochim Biophys Acta.* Mar 15 1997;1334(2-3):223-232.

[41] Patwari P, Cook MN, DiMicco MA, Blake SM, James IE, Kumar S, Cole AA, Lark MW, Grodzinsky AJ. Proteoglycan degradation after injurious compression of bovine and human articular cartilage in vitro: interaction with exogenous cytokines. *Arthritis Rheum.* May 2003;48:1292-1301.

[42] Thibault M, Poole AR, Buschmann MD. Cyclic compression of cartilage/bone explants in vitro leads to physical weakening, mechanical breakdown of collagen and release of matrix fragments. *J Orthop Res.* Nov 2002;20(6):1265-1273.

[43] Chen CT, Burton-Wurster N, Lust G, Bank RA, Tekoppele JM. Compositional and metabolic changes in damaged cartilage are peak-stress, stress-rate, and loading-duration dependent. *J Orthop Res.* Nov 1999;17(6):870-879.

[44] Loening AM, James IE, Levenston ME, Badger AM, Frank EH, Kurz B, Nuttall ME, Hung HH, Blake SM, Grodzinsky AJ, Lark MW. Injurious mechanical compression of bovine articular cartilage induces chondrocyte apoptosis. *Arch Biochem Biophys.* Sep 15 2000;381(2):205-212.

[45] Stanton H, Ung L, Fosang AJ. The 45 kDa collagen-binding fragment of fibronectin induces matrix metalloproteinase-13 synthesis by chondrocytes and aggrecan degradation by aggrecanases. *Biochem J.* May 15 2002;364(Pt 1):181-190.

[46] Yasuda T, Poole AR. A fibronectin fragment induces type II collagen degradation by collagenase through an interleukin-1-mediated pathway. *Arthritis Rheum.* Jan 2002;46(1):138-148.

[47] Williams JM, Zhang J, Kang H, Ummadi V, Homandberg GA. The effects of hyaluronic acid on fibronectin fragment mediated cartilage chondrolysis in skeletally mature rabbits. *Osteoarthritis Cartilage.* Jan 2003;11(1):44-49.

[48] Saito S, Yamaji N, Yasunaga K, Saito T, Matsumoto S, Katoh M, Kobayashi S, Masuho Y. The fibronectin extra domain A activates matrix metalloproteinase gene expression by an interleukin-1-dependent mechanism. *J Biol Chem.* Oct 22 1999;274(43):30756-30763.

[49] Bonassar LJ, Sandy JD, Lark MW, Plaas AH, Frank EH, Grodzinsky AJ. Inhibition of cartilage degradation and changes in physical properties induced by IL-1beta and retinoic acid using matrix metalloproteinase inhibitors. *Arch Biochem Biophys.* Aug 15 1997;344(2):404-412.

[50] Campbell MA, Handley CJ. The effect of retinoic acid on proteoglycan biosynthesis in bovine articular cartilage cultures. *Arch Biochem Biophys.* Mar 1987;253(2):462-474.

[51] Von den Hoff HW, de Koning MH, van Kampen GP, van der Korst JK. Transforming growth factor-beta stimulates retinoic acid-induced proteoglycan depletion in intact articular cartilage. *Arch Biochem Biophys.* Sep 1994;313(2):241-247.

[52] Pratta MA, Di Meo TM, Ruhl DM, Arner EC. Effect of interleukin-1-beta and tumor necrosis factor-alpha on cartilage proteoglycan metabolism in vitro. *Agents Actions.* Jun 1989;27:250-253.

[53] Arner EC, Hughes CE, Decicco CP, Caterson B, Tortorella MD. Cytokine-induced cartilage proteoglycan degradation is mediated by aggrecanase. *Osteoarthritis and Cartilage.* May 1998;6:214-228.

[54] Rieppo J, Toyras J, Nieminen MT, Kovanen V, Hyttinen MM, Korhonen RK, Jurvelin JS, Helminen HJ. Structure-function relationships in enzymatically modified articular cartilage. *Cells Tissues Organs.* 2003;175(3):121-132.

[55] Kozaci LD, Buttle DJ, Hollander AP. Degradation of type II collagen, but not proteoglycan, correlates with matrix metalloproteinase activity in cartilage explant cultures. *Arthritis Rheum.* Jan 1997;40(1):164-174.

[56] Williams A, Oppenheimer RA, Gray ML, Burstein D. Differential recovery of glycosaminoglycan after IL-1-induced degradation of bovine articular cartilage depends on degree of degradation. *Arthritis Res Ther.* 2003;5(2):R97-105.

[57] Arner EC, Pratta MA. Independent effects of interleukin-1 on proteoglycan breakdown, proteoglycan synthesis, and prostaglandin E2 release from cartilage in organ culture. *Arthritis Rheum.* Mar 1989;32(3):288-297.

[58] Tyler JA, Benton HP. Synthesis of type II collagen is decreased in cartilage cultured with interleukin 1 while the rate of intracellular degradation remains unchanged. *Coll Relat Res.* Sep 1988;8(5):393-405.

[59] Smith RJ, Rohloff NA, Sam LM, Justen JM, Deibel MR, Cornette JC. Recombinant human interleukin-1 alpha and recombinant human interleukin-1 beta stimulate cartilage matrix degradation and inhibit glycosaminoglycan synthesis. *Inflammation.* Aug 1989;13(4):367-382.

[60] Neidel J, Zeidler U. Independent effects of interleukin 1 on proteoglycan synthesis and proteoglycan breakdown of bovine articular cartilage in vitro. *Agents Actions.* May 1993;39(1-2):82-90.

[61] Goldring MB. Control of collagen synthesis in human chondrocyte cultures by immune interferon and interleukin-1. *J Rheumatol.* May 1987;14 Spec No:64-66.

[62] Goldring MB, Krane SM. Modulation by recombinant interleukin 1 of synthesis of types I and III collagens and associated procollagen mRNA levels in cultured human cells. *J Biol Chem.* Dec 5 1987;262(34):16724-16729.

[63] Morales TI, Roberts AB. Transforming growth factor beta regulates the metabolism of proteoglycans in bovine cartilage organ cultures. *J Biol Chem.* Sep 15 1988;263(26):12828-12831.

[64] Redini F, Galera P, Mauviel A, Loyau G, Pujol JP. Transforming growth factor beta stimulates collagen and glycosaminoglycan biosynthesis in cultured rabbit articular chondrocytes. *FEBS Lett.* Jul 4 1988;234(1):172-176.

[65] Rayan V, Hardingham T. The recovery of articular cartilage in explant culture from interleukin-1 alpha: effects on proteoglycan synthesis and degradation. *Matrix Biol.* Apr 1994;14(3):263-271.

[66] Neidel J, Schulze M, Sova L. Insulin-like growth factor I accelerates recovery of articular cartilage proteoglycan synthesis in culture after inhibition by interleukin 1. *Arch Orthop Trauma Surg.* 1994;114(1):43-48.

[67] Manaster BJ, Johnson T, Narahari U. Imaging of cartilage in the athlete. *Clin Sports Med.* Jan 2005;24(1):13-37.

[68] Seidel JO, Pei M, Gray ML, Langer R, Freed LE, Vunjak-Novakovic G. Long-term culture of tissue engineered cartilage in a perfused chamber with mechanical stimulation. *Biorheology.* 2004;41(3-4):445-458.

[69] Li X, Martin S, Pitris C, Ghanta R, Stamper DL, Harman M, Fujimoto JG, Brezinski ME. High-resolution optical coherence tomographic imaging of osteoarthritic cartilage during open knee surgery. *Arthritis Res Ther.* 2005;7(2):R318-323.

[70] Patel NA, Zoeller J, Stamper DL, Fujimoto JG, Brezinski ME. Monitoring osteoarthritis in the rat model using optical coherence tomography. *IEEE Trans Med Imaging.* Feb 2005;24(2):155-159.

[71] Camacho NP, West P, Torzilli PA, Mendelsohn R. FTIR microscopic imaging of collagen and proteoglycan in bovine cartilage. *Biopolymers.* 2001;62(1):1-8.

[72] Sell CA, Masi JN, Burghardt A, Newitt D, Link TM, Majumdar S. Quantification of Trabecular Bone Structure Using Magnetic Resonance Imaging at 3 Tesla-Calibration Studies Using Microcomputed Tomography as a Standard of Reference. *Calcif Tissue Int.* May 5 2005.

[73] Dong XN, Yeni YN, Zhang B, Les CM, Gibson GJ, Fyhrie DP. Matrix Concentration of Insulin-like Growth Factor I (IGF-I) is Negatively Associated with Biomechanical Properties of Human Tibial Cancellous Bone Within Individual Subjects. *Calcif Tissue Int.* May 26 2005.

[74] Qiu S, Sudhaker Rao D, Fyhrie DP, Palnitkar S, Parfitt AM. The morphological association between microcracks and osteocyte lacunae in human cortical bone. *Bone.* May 4 2005.

[75] Yeni YN, Christopherson GT, Dong XN, Kim DG, Fyhrie DP. Effect of microcomputed tomography voxel size on the finite element model accuracy for human cancellous bone. *J Biomech Eng.* Feb 2005;127(1):1-8.

[76] Schmidt C, Priemel M, Kohler T, Weusten A, Muller R, Amling M, Eckstein F. Precision and accuracy of peripheral quantitative computed tomography (pQCT) in

the mouse skeleton compared with histology and microcomputed tomography (microCT). *J Bone Miner Res.* Aug 2003;18(8):1486-1496.

[77] Duvall CL, Robert Taylor W, Weiss D, Guldberg RE. Quantitative microcomputed tomography analysis of collateral vessel development after ischemic injury. *Am J Physiol Heart Circ Physiol.* Jul 2004;287(1):H302-310.

[78] Cockman MD, Blanton CA, Chmielewski PA, Dong L, Dufresne TE, Hookfin EB, Karb MJ, Liu S, Wehmeyer KR. Quantitative imaging of proteoglycan in cartilage using a gadolinium probe and microCT. *Osteoarthritis Cartilage.* Mar 2006;14(3):210-214.

[79] Park S, Krishnan R, Nicoll SB, Ateshian GA. Cartilage interstitial fluid load support in unconfined compression. *J Biomech.* Dec 2003;36(12):1785-1796.

[80] Basser PJ, Schneiderman R, Bank RA, Wachtel E, Maroudas A. Mechanical properties of the collagen network in human articular cartilage as measured by osmotic stress technique. *Arch Biochem Biophys.* Mar 15 1998;351(2):207-219.

[81] Kuettner KE. Biochemistry of articular cartilage in health and disease. *Clin Biochem.* Jun 1992;25(3):155-163.

[82] Williamson AK, Masuda K, Thonar EJ, Sah RL. Growth of immature articular cartilage in vitro: correlated variation in tensile biomechanical and collagen network properties. *Tissue Eng.* Aug 2003;9(4):625-634.

[83] Bank RA, Soudry M, Maroudas A, Mizrahi J, TeKoppele JM. The increased swelling and instantaneous deformation of osteoarthritic cartilage is highly correlated with collagen degradation. *Arthritis Rheum.* Oct 2000;43(10):2202-2210.

[84] Narmoneva DA, Wang JY, Setton LA. A noncontacting method for material property determination for articular cartilage from osmotic loading. *Biophys J.* Dec 2001;81(6):3066-3076.

[85] Armstrong CG, Lai WM, Mow VC. An analysis of the unconfined compression of articular cartilage. *J Biomech Eng.* May 1984;106(2):165-173.

[86] Park S, Hung CT, Ateshian GA. Mechanical response of bovine articular cartilage under dynamic unconfined compression loading at physiological stress levels. *Osteoarthritis Cartilage.* Jan 2004;12(1):65-73.

[87] Korhonen RK, Laasanen MS, Toyras J, Rieppo J, Hirvonen J, Helminen HJ, Jurvelin JS. Comparison of the equilibrium response of articular cartilage in unconfined compression, confined compression and indentation. *J Biomech.* Jul 2002;35(7):903-909.

[88] Lu XL, Sun DD, Guo XE, Chen FH, Lai WM, Mow VC. Indentation determined mechanoelectrochemical properties and fixed charge density of articular cartilage. *Ann Biomed Eng.* Mar 2004;32(3):370-379.

[89] Pratta MA, Yao W, Decicco C, Tortorella MD, Liu RQ, Copeland RA, Magolda R, Newton RC, Trzaskos JM, Arner EC. Aggrecan protects cartilage collagen from proteolytic cleavage. *J Biol Chem.* Nov 14 2003;278(46):45539-45545.

[90] Farndale RW, Sayers CA, Barrett AJ. A direct spectrophotometric microassay for sulfated glycosaminoglycans in cartilage cultures. *Connect Tissue Res.* 1982;9(4):247-248.

[91] Woessner JF, Jr. The determination of hydroxyproline in tissue and protein samples containing small proportions of this imino acid. *Arch Biochem Biophys.* May 1961;93:440-447.

[92] Zar JH. *Biostatistical Analysis*. 2nd ed. Englewood Cliffs, NJ: Prentice Hall; 1984.

[93] Billinghurst RC, Wu W, Ionescu M, Reiner A, Dahlberg L, Chen J, van Wart H, Poole AR. Comparison of the degradation of type II collagen and proteoglycan in nasal and articular cartilages induced by interleukin-1 and the selective inhibition of type II collagen cleavage by collagenase. *Arthritis Rheum.* Mar 2000;43(3):664-672.

[94] Stabellini G, De Mattei M, Calastrini C, Gagliano N, Moscheni C, Pasello M, Pellati A, Bellucci C, Gioia M. Effects of interleukin-1beta on chondroblast viability and extracellular matrix changes in bovine articular cartilage explants. *Biomed Pharmacother.* Sep 2003;57(7):314-319.

[95] Wilson CG, Palmer AW, Zuo F, Eugui E, Wilson S, Mackenzie R, Sandy JD, Levenston ME. Selective and non-selective metalloproteinase inhibitors reduce IL-1-induced cartilage degradation and loss of mechanical properties. *Matrix Biol.* Nov 11 2006.

[96] Treppo S, Koepp H, Quan EC, Cole AA, Kuettner KE, Grodzinsky AJ. Comparison of biomechanical and biochemical properties of cartilage from human knee and ankle pairs. *J Orthop Res.* Sep 2000;18(5):739-748.

[97] Jadin KD, Wong BL, Bae WC, Li KW, Williamson AK, Schumacher BL, Price JH, Sah RL. Depth-varying Density and Organization of Chondrocytes in Immature and Mature Bovine Articular Cartilage Assessed by 3D Imaging and Analysis. *J Histochem Cytochem.* Sep 2005;53(9):1109-1119.

[98] Chen AC, Bae WC, Schinagl RM, Sah RL. Depth- and strain-dependent mechanical and electromechanical properties of full-thickness bovine articular cartilage in confined compression. *J Biomech.* Jan 2001;34(1):1-12.

[99] Buschmann MD, Grodzinsky AJ. A molecular model of proteoglycan-associated electrostatic forces in cartilage mechanics. *J Biomech Eng.* May 1995;117(2):179-192.

[100] Maroudas A. Physio-chemical Properties of Articular Cartilage. In: Freeman MAR, ed. *Adult Articular Cartilage*. 2nd ed. Tunbridge Wells, England: Pitman; 1979:215-290.

[101] Guilak F, Meyer BC, Ratcliffe A, Mow VC. The effects of matrix compression on proteoglycan metabolism in articular cartilage explants. *Osteoarthritis Cartilage.* Jun 1994;2(2):91-101.

[102] Samosky JT, Burstein D, Eric Grimson W, Howe R, Martin S, Gray ML. Spatially-localized correlation of dGEMRIC-measured GAG distribution and mechanical stiffness in the human tibial plateau. *J Orthop Res.* Jan 2005;23(1):93-101.

[103] Palmer AW, Guldberg RE, Levenston ME. Analysis of cartilage matrix fixed charge density and three-dimensional morphology via contrast-enhanced microcomputed tomography. *Proc Natl Acad Sci U S A.* Dec 19 2006;103(51):19255-19260.

[104] Maroudas A, Bannon C. Measurement of swelling pressure in cartilage and comparison with the osmotic pressure of constituent proteoglycans. *Biorheology.* 1981;18(3-6):619-632.

[105] Sandy JD, Verscharen C. Analysis of aggrecan in human knee cartilage and synovial fluid indicates that aggrecanase (ADAMTS) activity is responsible for the catabolic turnover and loss of whole aggrecan whereas other protease activity is required for C-terminal processing in vivo. *Biochem J.* Sep 15 2001;358(Pt 3):615-626.

[106] Plaas AH, West LA, Wong-Palms S, Nelson FR. Glycosaminoglycan sulfation in human osteoarthritis. Disease-related alterations at the non-reducing termini of chondroitin and dermatan sulfate. *J Biol Chem.* May 15 1998;273(20):12642-12649.

[107] Rupprecht M, Pogoda P, Mumme M, Rueger JM, Puschel K, Amling M. Bone microarchitecture of the calcaneus and its changes in aging: a histomorphometric analysis of 60 human specimens. *J Orthop Res.* Apr 2006;24(4):664-674.

[108] Jiang Y, Zhao J, Liao EY, Dai RC, Wu XP, Genant HK. Application of micro-CT assessment of 3-D bone microstructure in preclinical and clinical studies. *J Bone Miner Metab.* 2005;23 Suppl:122-131.

[109] Bashir A, Gray ML, Burstein D. Gd-DTPA2- as a measure of cartilage degradation. *Magn Reson Med.* Nov 1996;36(5):665-673.

[110] Kim YJ, Jaramillo D, Millis MB, Gray ML, Burstein D. Assessment of early osteoarthritis in hip dysplasia with delayed gadolinium-enhanced magnetic resonance imaging of cartilage. *J Bone Joint Surg Am.* Oct 2003;85-A(10):1987-1992.

[111] Kozak LJ DC, Hall MJ. *National Hospital Discharge Survey: 2004 Annual Summary with Detailed Diagnosis and Procedure Data* 2006.

[112] Lee HS, Teng SW, Chen HC, Lo W, Sun Y, Lin TY, Chiou LL, Jiang CC, Dong CY. Imaging Human Bone Marrow Stem Cell Morphogenesis in Polyglycolic Acid Scaffold by Multiphoton Microscopy. *Tissue Eng.* Sep 1 2006.

[113] Powers MJ, Domansky K, Kaazempur-Mofrad MR, Kalezi A, Capitano A, Upadhyaya A, Kurzawski P, Wack KE, Stolz DB, Kamm R, Griffith LG. A microfabricated array bioreactor for perfused 3D liver culture. *Biotechnol Bioeng.* May 5 2002;78(3):257-269.

[114] Yang Y, Yiu HH, El Haj AJ. On-line fluorescent monitoring of the degradation of polymeric scaffolds for tissue engineering. *Analyst.* Nov 2005;130(11):1502-1506.

[115] Stroh M, Zimmer JP, Duda DG, Levchenko TS, Cohen KS, Brown EB, Scadden DT, Torchilin VP, Bawendi MG, Fukumura D, Jain RK. Quantum dots spectrally distinguish multiple species within the tumor milieu in vivo. *Nat Med.* Jun 2005;11(6):678-682.

[116] Stabler CL, Long RC, Jr., Constantinidis I, Sambanis A. In vivo noninvasive monitoring of a tissue engineered construct using 1H NMR spectroscopy. *Cell Transplant.* 2005;14(2-3):139-149.

[117] Bashir A, Gray ML, Hartke J, Burstein D. Nondestructive imaging of human cartilage glycosaminoglycan concentration by MRI. *Magn Reson Med.* May 1999;41(5):857-865.

[118] Chen CT, Fishbein KW, Torzilli PA, Hilger A, Spencer RG, Horton WE, Jr. Matrix fixed-charge density as determined by magnetic resonance microscopy of bioreactor-derived hyaline cartilage correlates with biochemical and biomechanical properties. *Arthritis Rheum.* Apr 2003;48(4):1047-1056.

[119] Bagnaninchi PO, Yang Y, Zghoul N, Maffulli N, Wang RK, Haj AJ. Chitosan Micro-Channel Scaffolds for Tendon Tissue Engineering Characterized Using Optical Coherence Tomography. *Tissue Eng.* Jan 1 2007.

[120] Yang Y, Dubois A, Qin XP, Li J, El Haj A, Wang RK. Investigation of optical coherence tomography as an imaging modality in tissue engineering. *Phys Med Biol.* Apr 7 2006;51(7):1649-1659.

[121] Kim M, Bi X, Horton WE, Spencer RG, Camacho NP. Fourier transform infrared imaging spectroscopic analysis of tissue engineered cartilage: histologic and biochemical correlations. *J Biomed Opt.* May-Jun 2005;10(3):031105.

[122] Ko HJ, Tan W, Stack R, Boppart SA. Optical coherence elastography of engineered and developing tissue. *Tissue Eng.* Jan 2006;12(1):63-73.

[123] Vanderploeg EJ, Imler SM, Brodkin KR, Garcia AJ, Levenston ME. Oscillatory tension differentially modulates matrix metabolism and cytoskeletal organization in chondrocytes and fibrochondrocytes. *J Biomech.* Dec 2004;37(12):1941-1952.

[124] Bae WC, Lewis CW, Levenston ME, Sah RL. Indentation testing of human articular cartilage: effects of probe tip geometry and indentation depth on intra-tissue strain. *J Biomech.* 2006;39(6):1039-1047.

[125] Matsumoto T, Iwasaki K, Sugihara H. Effects of radiation on chondrocytes in culture. *Bone.* Jan-Feb 1994;15(1):97-100.

[126] Kelly TA, Ng KW, Wang CC, Ateshian GA, Hung CT. Spatial and temporal development of chondrocyte-seeded agarose constructs in free-swelling and dynamically loaded cultures. *J Biomech.* 2006;39(8):1489-1497.

[127] Klein TJ, Chaudhry M, Bae WC, Sah RL. Depth-dependent biomechanical and biochemical properties of fetal, newborn, and tissue-engineered articular cartilage. *J Biomech.* 2007;40(1):182-190.

[128] Lin AS, Barrows TH, Cartmell SH, Guldberg RE. Microarchitectural and mechanical characterization of oriented porous polymer scaffolds. *Biomaterials.* Feb 2003;24(3):481-489.

[129] Panula HE, Hyttinen MM, Arokoski JP, Langsjo TK, Pelttari A, Kiviranta I, Helminen HJ. Articular cartilage superficial zone collagen birefringence reduced and cartilage thickness increased before surface fibrillation in experimental osteoarthritis. *Ann Rheum Dis.* Apr 1998;57(4):237-245.

[130] Baum EJ, Wilson, C. W., Levenston, M. E. Recovery of Cartilage Material Properties After IL-1 Challenge. Paper presented at: 51st Annual Meeting of the Orthopaedic Research Society February 20 - 23, 2005, 2005; Washington, D.C.

[131] Hunter CJ, Imler SM, Malaviya P, Nerem RM, Levenston ME. Mechanical compression alters gene expression and extracellular matrix synthesis by chondrocytes cultured in collagen I gels. *Biomaterials.* Feb 2002;23(4):1249-1259.

[132] Sah RL, Kim YJ, Doong JY, Grodzinsky AJ, Plaas AH, Sandy JD. Biosynthetic response of cartilage explants to dynamic compression. *J Orthop Res.* 1989;7(5):619-636.

[133] Wang CC, Guo XE, Sun D, Mow VC, Ateshian GA, Hung CT. The functional environment of chondrocytes within cartilage subjected to compressive loading: a theoretical and experimental approach. *Biorheology.* 2002;39(1-2):11-25.

[134] Quinn TM, Morel V, Meister JJ. Static compression of articular cartilage can reduce solute diffusivity and partitioning: implications for the chondrocyte biological response. *J Biomech.* Nov 2001;34(11):1463-1469.

VITA

ASHLEY WELLS PALMER

Ashley Wells Palmer was born in Birmingham, AL in the winter of 1977 to Kenneth and Marjorie Palmer. She was raised in Tuscaloosa, Alabama, where she grew up cheering on the Alabama Crimson Tide at football and basketball games. Ashley attended public schools in Tuscaloosa, graduating valedictorian from Central High School in 1996. Ashley enrolled at Duke University in Durham, North Carolina in the fall of 1996. There, she was involved in numerous activities, including the Duke club tennis team, the Chi Omega fraternity, and undergraduate research. Ashley graduated *cum laude* from Duke with a double major in biomedical engineering and mechanical engineering in the spring of 2000. After graduating from Duke, Ashley accepted an engineering position with Cordis Corporation in Warren, NJ, where she was involved in the design and development of cardiovascular and endovascular stents. In the fall of 2001, she left the medical device industry to enroll in the mechanical engineering PhD program at Georgia Institute of Technology in Atlanta, GA and pursue her interests in orthopedic bioengineering. At Georgia Tech, she was active in the student council of the Georgia Tech/Emory Center for the Engineering of Living Tissues, co-chairing the Education and Outreach committee. While in Atlanta, Ashley played on a number of women's and mixed doubles teams through ALTA, the Atlanta Lawn Tennis Association. After completing her PhD, Ashley will join Becton Dickinson in Franklin Lakes, New Jersey, where she will be involved in market and technology opportunity assessment for the Medical Surgical Systems R&D group.